NTNU
Det skapende universitet

Dynamisk modellering og analyse av flytebruer

Axel Wullf Wathne

Bygg- og miljøteknikk
Innlevert: Juni 2012
Hovedveileder: Svein N Remseth, KT
Medveileder: Ragnar Sigbjörnsson, KT

Norges teknisk-naturvitenskapelige universitet
Institutt for konstruksjonsteknikk

ACCESSIBILITY

DEPARTMENT OF STRUCTURAL ENGINEERING

Faculty of Engineering Science and Technology

NTNU- Norwegian University of Science and Technology

MASTER THESIS 2012

SUBJECT AREA:	DATE: 11.06.2012	NO. OF PAGES:
Marine Civil Engineering		

TITLE:

Dynamic modelling and analysis of floating bridges

Dynamisk modellering og analyse av flytebruer

BY:

Axel Wullf Wathne

SUMMARY:

The thesis is concerned with the evaluation of the dynamic characteristics of floating bridges.

A generic floating bridge model is proposed within a finite element format, inspired by an already-built floating bridge located in Norway.

The dynamic response of the floating bridge from wave action is assessed, with emphasis on vertical modes of motion. The dynamic response analysis is performed in frequency-domain.

The environmental loading on the bridge is evaluated and formulations for determining the hydrostatic and hydrodynamic restoring forces, as well as the wave loading on the floating bridge is presented.

The dynamic response analysis of the floating bridge is conducted by an initial Eigenvalue analysis, followed by a method for development of frequency response functions and finalized by a probabilistic response analysis.

The hydrostatic and hydrodynamic restoring forces are considered to greatly influence the response of the floating bridge for low frequencies of motion.

In addition, the accuracy of the modelled sea state, which forms the basis for the wave loading on the floating bridge, is seen to greatly affect the computed response of the bridge.

RESPONSIBLE TEACHER: Svein Remseth

SUPERVISOR(S) Ragnar Sigbjörnsson and Svein Remseth

CARRIED OUT AT: Department of Structural Engineering

PREFACE AND ACKNOWLEDGMENTS

This thesis is conducted during the spring of 2012 at the Department of Structural Engineering, at the Norwegian University of Science and Technology.

The work constitutes 30 credits and is submitted as a fulfilment of the degree of Master of Science.

The author has a background from structural engineering and the thesis is written as to pursue a newfound interest in the interdisciplinary field of marine civil engineering.

The author wishes to thank the responsible teacher Professor Svein Remseth for valuable input and guidance throughout the work. A large thanks is in addition given to Dr. Ragnar Sigbjörnsson for his invaluable guidance and for sharing his vast expertise within the field of dynamic analysis of marine structures.

ABSTRACT

This thesis is concerned with the evaluation of the dynamic behaviour of a generic pontoon-separated floating bridge from wave action, with emphasis on the vertical response. The dynamic analyses are performed in the frequency-domain, which allows for convenient inclusion of the frequency dependent hydrodynamic effects. The structural model of the generic floating bridge is inspired by the outer geometry of the Bergsøysund floating bridge, located on the west coast of Norway. This is to ensure reasonable dimensions and structural properties of the generic bridge model.

An evaluation of the concept of floating bridges and the applicability of such structures initiate the thesis. Followed by a discussion of the environmental effects that are considered relevant in the design of a floating bridge.

The environmental loads and fluid-structure interaction effects are introduced, and procedures for the determination of the hydrostatic and hydrodynamic forces on a floating body are proposed. The determination of the hydrostatic and hydrodynamic coefficients forms the basis for the hydrodynamic model developed to describe the properties of the dynamic fluid-structure system.

The floating bridge is further modelled in a finite element format. Hydro-elastic elements are developed for the parts of the model being in contact with the surrounding fluid, incorporating the hydrostatic and hydrodynamic effects. As a result, the properties of the fluid-structure system are completely included in the finite element formulation of the floating bridge model.

The dynamic evaluation of the floating bridge model is performed through various methods of analysis. Eigenvalue analyses of both the fluid-structure properties and the purely structural parts of the model are conducted in order to assess the effects of the hydrostatic and hydrodynamic restoring forces on the free response of the system. A frequency response function method of analysis is further proposed to include the hydrodynamic damping of the system. A probabilistic response analysis concludes the dynamic evaluation of the floating bridge structure. In the analyses, different idealizations are introduced for the description of the sea surface, and the resulting loading situation on the floating bridge. The validity of the computed responses from the various methods of approach is evaluated in light of the assumptions and restrictions within the theories applied in establishing the wave-loading situation.

The hydrostatic and hydrodynamic restoring forces are found to dictate the response characteristics at low frequencies of motion, whereas the structural properties governs to a larger extent the response of the bridge at higher frequencies. A wave load situation on a floating bridge is assumed to mainly excite the structure at low frequencies of motion. This is supported by the

computed responses, and the hydro-effects are considered to be of great significance to the actual response of the floating bridge.

Additionally, the discretization of the wave field is found to be of great significance to the computed responses of the floating bridge. The responses computed for a wave loading consistent with long-crested waves, exciting every point on the structure simultaneously, is found to be unrealistically large. As the wave field model is refined to express an irregular, short-crested sea state, corresponding better with sea states experienced in nature, the computed results are dramatically reduced. The proper modelling of an actual sea state is thus considered vital in the safe and economic design of a floating bridge.

SAMMENDRAG

Denne oppgaven tar for seg evalueringen av den dynamiske oppførselen til en generisk pontoon-separert flytende bru fra bølgelast, hvor det legges vekt på vertikale svingninger. De dynamiske analysene er utført i frekvens-planet, som er gunstig for praktisk inkludering av de frekvensavhengige hydrodynamiske effektene. Den strukturelle modellen for den generiske flytebrua er inspirert av den ytre geometrien til Bergsøysund flytebru, som bygget på vestkysten av Norge. Dette er for å sikre rimelige dimensjoner og egenskaper for den generisk brumodellen. Oppgaven er innlededet med en konseptevaluering av flytenbruer og deres anvendelsesområder. En påfølgende diskusjon tar for seg aktuelle miljølaster som vurderes i utformingen av en flytende bru. Miljølaster og interaksjonseffekter mellom fluid og konstruksjon er innført, og prosedyrer for bestemmelse av de hydrostatiske og hydrodynamiske krefter på et flytende legeme blir introdusert. Bestemmelsen av de hydrostatiske og hydrodynamiske koeffisientene danner grunnlaget for den hydrodynamiske modellen utviklet for å beskrive egenskapene til den dynamiske systemet. Den flytende brua er videre modellert i et elementmetoden format. Hydro-elastiske elementer er utviklet for de deler av modellen som er i kontakt med vannet. De hydrostatiske og hydrodynamiske effecter er inkludert i elementformuleringen. Som et resultat, er egenskapene til det kombinerte system fullstendig inkludert i utformingen av modellen av flytebrua, i henhold til elementmetodeteori.

Den dynamiske evaluering av flytebrumodellen utføres gjennom ulike analysemetoder. Egenverdiproblemer er etablert for analyser av både de "våte" egenskapene og de "tørre", rent strukturelle egenskapene for å vurdere effekten av de hydrostatiske og hydrodynamiske tilbakeføringskreftene for frie responsen av systemet. En analysemetode ved etablering av frekvens-respons-funksjoner er videre foreslått for å inkludere den hydrodynamiske dempingen av systemet. En probabilistisk responsanalyse avslutter den dynamisk evalueringen av flytebrumodellen. I analysene er forskjellige idealisering introdusert for beskrivelse av havoverflaten, og den resulterende lastsituasjonen på flytebrua. Gyldigheten av de kalkulerte responsene, fra de ulike tilnærmingsmåtene, blir vurdert i lys av de forutsetninger og begrensninger forutsatt av teoriene som benyttes i etableringen av bølgelast situasjonen. De hydrostatiske og hydrodynamiske tilbakeføringskreftene er funnet å i stor grad diktere flutebrua sine egenskaper ved lavfrekvent response, mens de strukturelle egenskapene i større grad bestemmer responsen av brua ved høyere frekvenser. En virkelig lastsituasjon på en flytende bru antas å hovedsakelig påvirke konstruksjonen for lave frekvenser. Dette støttes av resultatene funnet i denne oppgaven, og de hydrostatiske og hydrodynamiske effekter vurderes å være av stor betydning for den faktiske responsen av flytebrua. I tillegg er tilnærmingsmetoden for modellering av bølgefeltet funnet å være av stor betydning for responsen til en

flytende bru. Responsen som ble beregnet for en bølgelast forbundet med langkammede bølger er vurdert som urealistiske. Dette er begrunnet med at en langkammet bølge vil vise en stor grad av korrelasjon over bruspennet og påvirke alle punkter over konstruksjonen med en samtidig og likt rettet last. Ettersom bølgefeltet er modellert mer i tråd med en virkelig havoverflate, som uregelmessig og kortkammete, blir responsen til flytebrua dramatisk redusert. En tilstrekkelig nøyaktig modelleringen av havoverflaten betraktes således som særdeles viktig for å oppnå en sikker og økonomisk gunstig flytebrukonstruksjon.

LIST OF TABLES

LIST OF FIGURES

1. INTRODUCTION

1.1 MOTIVATION AND PURPOSE

The dynamic modelling and analysis of slender bridge structures are important aspects within the field of structural dynamics. Long, slender bridge structures are generally exposed to environmental loadings of various kinds, and the interaction effects are regarded as integral parts of the dynamic modelling. Generally, the dynamic analysis of a structure may be performed in either time- or frequency-domain, depending on the purpose of the analysis. This report is concerned with the dynamic behaviour of a generic floating bridge. The dynamic analyses are performed in frequency-domain consistent with a finite element format, and with emphasis on the vertical modes of motion.

The main source of environmental loading on a floating bridge is considered to arise from the surrounding water mass, with the wave load exerted on the bridge regarded as the governing dynamic load situation. Hydrostatic and hydrodynamic restoring forces arise as to oppose the motion of the floating body, and the hydrodynamic damping is considered significant. These are effects of the fluid-structure interaction that is considered necessary to address properly to ensure a realistic dynamic behaviour of the floating bridge. Traditionally, the description of a wave field has been to consider the waves as random and unidirectional when approaching a marine structure. The waves are assumed as long-crested and to show a high degree of spatial correlation. For dynamic analyses of structures and floating bodies that are considered of small dimensions relative to the wavelengths of the incident waves, this application has been regarded acceptable. The dynamic analysis of larger structure does however result in overly conservative estimates of the response. The reason being, that a long-crested wave is modelled to excite the structure equally and simultaneously en every point. In order to properly evaluate the dynamic response of large floating structures, it is necessary to assess the sea state more similar to what is encountered in nature. A true sea state is not seen to display a particularly long-crested behaviour. A wave field consists of various waves of different frequencies, amplitudes and directions of approach, superposed to form the sea state we normally see with finite, random crest lengths. Consequently, a proper modelling of the sea state is considered vital in order to obtain a reasonable dynamic response of a floating bridge, and to allow for a secure and economic design, which in turn adds to the feasibility of construction.

The main goals of the report is to gain an increased understanding of the environmental effects and their importance in the dynamic modelling of marine structures, and to evaluate the dynamic vertical response of the generic bridge model from different load situations. The hydrostatic and hydrodynamic effects

of the fluid-structure interactions are considered in the development of a hydrodynamic model to properly describe the dynamic behaviour. Different idealizations of the external wave loading are proposed, and the validity of the response calculations are viewed in light of the assumptions and restraints associated with the theories applied. The argumentation for the validity will mainly be concerned with the modelling of the sea state, as the structural properties and the hydrodynamic coefficients are introduced similarly in the dynamic analyses performed throughout the report.

1.2 THE STRUCTURE OF THE REPORT

The report sets out to investigate the concept and application of floating bridges, and the environmental effects that are regarded necessary for a proper evaluation of the dynamic behaviour. Research within the fields of coastal and naval engineering is considered for their applicability to a floating bridge construction. The design of the generic floating bridge model is inspired by the Bergsøysund pontoon-separated floating bridge, located near Kristiansund on the west coast of Norway. The structural model employed is a simplified version of this bridge, with similar dimensions and geometry to ensure realistic structural properties.

The theories employed for wave modelling are presented together with procedures for determination of sea state parameters and the fluid-structure interaction, and their validity to real life situations is considered. The wave theories presented form the basis for the development of the hydrodynamic model of the fluid-structure system, and the various wave loading situations applied to the model.

The generic floating bridge model is discretized within a finite element format. The hydrostatic and hydrodynamic restoring forces are conveniently incorporated in the finite element formulation by the development of hydro-elastic elements. Resulting in a finite element bridge model that effectively includes the fluid-structure interaction effects for the submerged parts of the bridge structure.

The dynamic analyses are performed in frequency-domain, which allows for convenient inclusion of the frequency dependent hydrodynamic effects. The methods employed for the dynamic analyses of the floating bridge structure are outlined, with emphasis on the description of the sea surface. The wave load situation on the floating bridge arises due to the spatial structure of the surrounding wave field, and is considered of outmost importance in dictating the dynamic response of the bridge. An Eigenvalue analysis is initially performed to evaluate the natural frequencies and corresponding mode shapes of both the

fluid-structure model, and a purely structural model for comparison. The analysis continues by employing frequency response functions for evaluation of the vertical response of the floating bridge model as function of frequency. A probabilistic response analysis concludes the dynamic modelling and incorporates the wave spectral density of a given sea state and extreme value statistics are employed for response estimations.

2. THE CONCEPT OF FLOATING BRIDGES

The concept of floating bridges is not new to mankind. The use of such structures has been applied for both military and civil purposes; the earlier attempts dating centuries back in time. The earliest registered approaches to construct floating bridges dates back to the 11th century China and these were believed to address the need for temporary crossings for military personnel during times of war [1]. The early floating bridge structures were constructed by means of available equipment at the time and typically consisted of moored boats or rafts tied together, with planks across to provide a walkway.

The floating bridge structures have evolved throughout the years, and are today seen to serve as more permanent installations of a country's infrastructure. At present, there are about twenty permanent floating bridges in use throughout the world. Two of which are located along the west coast of Norway. The applicability of a floating bridge construction depends to a great extent on the local environment at the site of construction as well as human activities and interests in the area.

Different designs have been applied for the pontoons and the superstructures of recent permanent floating bridge structures. The first types of modern floating bridges were constructed by use of continuous pontoons moored to the seabed for lateral support. This type of construction is prevailing for the floating bridges located in the pacific north part of North America. This is an area were floating bridges were included as permanent features of the infrastructure rather early. The Washington Lake Bridge opened as early as in 1940 to become the largest floating structure ever built at the time. The continuous pontoon construction provides vertical hydrostatic buoyancy support along the entire span of the structure. The early attempts to scientifically assess the dynamic behaviour of continuous floating bridges were by experiments on horizontal floating cylinders [2]. The continuous pontoon floating bridge design is attractive by its simplicity. The hydrostatic and hydrodynamic contributions may readily be included over the continuous bridge span. And it allows for a favourable assembly of the bridge as the individual bridge sections are provided with sufficient buoyancy to be self-supported. The continuous-pontoon floating bridge structure will, however, interfere greatly with the local wave climate at the site. Attracting wave forces along the entire bridge span, and possibly changing the marine environment due to alteration of the original water circulation at the site. The Nordhordaland floating bridge located in Norway is designed by use of continuous pontoons for the floating bridge part of the structure. This bridge has an additional high-span part, which is constructed as a traditional suspension bridge.

An alternative type of design was introduced by the pontoon-separated floating bridge. The vertical loads are in this case supported by individual pontoons, which are located some distance apart along the bridge span. A pontoon-separated floating bridge construction interferes to a lesser extent with the local wave climate at the site and may allow for the marine environment to remain rather unaffected. Certain structures of this type may also allow for the passage of smaller recreational boats between the pontoons. The pontoon-separated bridge construction will put greater demands on the superstructure supported by the pontoons, as well as complicating the hydrodynamic interaction of the fluid-structure system, as compared to a continuous-pontoon floating bridge. The second floating bridge located in Norway, the Bergsøysund floating bridge, applies a pontoon-separated bridge design.

Both of the floating bridges built in Norway are designed with a horizontal arch to provide lateral support through a geometric stiffness contribution. The horizontal forces are thus transferred to the end supports through arch action. The horizontal arch design replaces the need for mooring cables anchored to the seabed, which is a great advantage when constructing floating bridges across deep waters. However, the application of such an arch design puts demands on the landside foundation conditions as greater forces are supported at these connections.

Another aspect of the floating bridge design to consider is the need for waterway passage of larger ships. Some floating bridge designs provide a solution to this problem by introducing a draw-span or a swing-span. A drawback of such a solution is the obvious outcome that the vehicles on the bridge need to pause as the ship traffic passes. To avoid this, other floating bridges have been designed with a high span. Such a design leaves the vehicles crossing the bridge unaffected by the passage of ship traffic. A high span is seen to be most favourably located near one of the landsides. This allows for the high span part of the bridge to be supported as a more traditional bridge structure in shallower water conditions, with the possibility of installing piers that are supported by the seabed. In certain cases a floating bridge may be designed with both a high span and a draw-span, which is seen for the Governor Albert D. Rosellini Bridge crossing Lake Washington in Seattle, USA. The high span is then expected to cope with the regular waterway traffic, while the draw-span is to be used for the occasional passage of very large ships or as to relieve the floating bridge of wave forces during extreme storm events.

A floating bridge structure utilizes the buoyancy of water to provide support for the vertical loads. This concept seems both simple and ingenious. Poor geotechnical conditions of the seabed or great water depths may provide the installation of bridge piers uneconomical or even impossible to conduct. A floating bridge, on the other hand, may be designed to be independent of the

bottom characteristics of the water basin. Furthermore, Zhang [3] has investigated the dynamic behaviour of both the continuous-pontoon design and the pontoon-separated design for floating bridges at different water depths. The report states that the water depth has little influence on the dynamic responses of both types of floating bridges, so that the effect of water depth may be neglected during the course of design. Thus, a floating bridge design may prove as a favourable choice at many locations. In addition, a floating bridge design may in many cases prove as a comparatively low cost project compared to more traditional bridge constructions.

The abovementioned advantages may lead to expectations of floating bridge constructions to be highly represented in many countries' infrastructure. This is clearly not the case as traditional bridge designs are seen to prevail over floating bridge alternatives, even at sites where a floating bridge may prove as a more functional and economical choice of construction. It seems likely that the traditional bridge designs are preferred by the industry due to a high level of experience and competence in modelling, analysing and construction of such structures. This effect may be further fuelled by the lack of experience and knowledge of floating structures within departments of bridge analysis throughout the industry. Further research on the hydrodynamic fluid-structure interaction and the environmental loading on floating structures, along with an increasing will to invest in and execute ambitious projects of this character, will hopefully contribute to increased understanding and competence in the field. Knowledge obtained through such projects and relevant research may also contribute greatly to the development of other types of marine constructions. The rapid growing interest in the field of submerged floating tunnels may be viewed as an example. The research and understanding developed in this field may be improved by, as well as contribute to, the knowledge and competence in the design of floating bridges.

3. THE FLOATING BRIDGE AND ITS ENVIRONMENT

The external effects on a floating bridge may be assigned to various sources within the surrounding environment of the construction. The floating bridge will be subject to dead loads from self-weight, and wind and traffic actions similarly as for a regular bridge construction. In addition, the hydro-effects from the surrounding water are considered of great significance. At some locations, a floating bridge may also be subject to ice action. A discussion of the effects from the surrounding water and wind field, and their significance to the dynamic response evaluation of a floating bridge is presented in this section. Dead loads from self-weight are not discussed further herein as these are assumed included satisfactorily in the development of the floating bridge model. Neither is the traffic loading, which is assumed governed by appropriate design codes and not regarded within the scope of this thesis. The effect of ice action is merely mentioned for the sake of completeness and not pursued further.

3.1. HYDRO LOADING

The loading situation on a floating bridge resulting from hydro-effects is considered to be significant, and to a large extent govern the total loading situation on the bridge. The hydro loading may be attributed to different characteristics of the fluid domain. The discussion herein is limited to loading from tidal effects and from the local wave climate at the site of construction.

It is necessary to address the tidal variations at a construction site of interest to evaluate the feasibility of a floating bridge structure. On a local scale, tides are associated with the rise and fall of the sea level. Tides are regular and predictable as they are created mainly by the attraction from the moon and the sun, along with the rotation of the earth around the common centre of gravity of the moon-earth system. Most areas around the world experience a semi-diurnal tidal range, which means that high tide and low tide occur twice for a period of approximately 24 hours. However, some places experience a diurnal tide, which is associated with a single high and a single low water level during the same period. The magnitude of the tidal fluctuations will depend on the location and local bathymetry at the site. The relative magnitude between the highest high, and lowest low tidal levels will determine whether a floating bridge is a possible alternative for the bridge design. The possibility of additional raised sea levels due to storm surge should be included in the evaluation. A floating bridge is vertically supported by the fluid, and will attempt to follow the sea surface elevation. If the bridge span is restrained from following the tidal fluctuations, large forces will occur over the bridge span and at the end-connections. Consequently, for a floating bridge design to be considered feasible, the local tidal variations will have to be within a reasonable range so that the end

supports may be designed as hinged and allow for vertical displacement of the bridge span within the range of the tidal variation. A second effect of the tidal variation is tidal currents. As the water mass is deformed over the earth's surface, the fluid is set in motion as to travel from high levels to lower levels. The tidal current may be significant at narrow estuaries and in fjords and will generally act in the transverse-horizontal direction of the bridge span.

The hydrodynamic loading from oncoming waves is a more intuitive loading situation. A wave passing the floating bridge will generally excite the bridge span in multiple modes of motion. The raised surface elevation will exert vertical forces along the bridge, the propagating waves will contribute with horizontal loading in the transverse direction, and moment loading about the length-axis of the bridge span occurs from combined effects of the vertical and horizontal loadings. It is considered crucial to address the local wave climate at the site of construction in order to evaluate the dynamic response of a floating bridge structure properly.

Within a relatively short time window, from half an hour to a couple of hours, some of the wave loading components may be considered as quasi-static [4]. The tidal variations are slowly varying effects, and with a proper end-connection-design the sea level alterations from tidal effects may be disregarded in the loading situation. The tidal currents are nevertheless present and can be considered quasi-static throughout the course of a dynamic analysis. Waves are continuously fluctuating of nature, but may be separated into a quasi-static slowly varying drift component and an unsteady fluctuating component. Consequently, within a relatively short time-window, the hydro loading on a floating bridge may be expressed by two quasi-static terms and one time-dependent term.

$$W(t) = W_{tidal\ current} + W_{drift\ force} + W_{waves}(t)$$

3.2. WIND LOADING

Forces from wind actions will undoubtedly be present on a floating bridge. How much the wind action comes in to play depends on the location of the bridge and the local wind characteristics, as well as the length and shape of the bridge span.

A wind field is acting in a three-dimensional space and varies with time. This makes the wind properties at a single point in space dependent on four parameters. The fluctuating wind induced loading may be idealized as a stationary process, and the loading on the structure may be split into a time-invariant part, U_s, and a fluctuating time-dependent part, U_f, for the relatively short time-window of the dynamic analysis [5].

$$U(t) = U_s + U_f$$

The time-invariant part is thus applied as a quasi-static loading situation while the fluctuating part of the wind load contributes to the dynamic response of the floating bridge.

Wind loading can result in different response patterns of a bridge span, depending on the geometry of the structure and the intensity of the wind. The static response of a line-like structure from the time-invariant wind component, acting normal to the bridge span, is regarded proportional to the square of the mean wind velocity within the theory of bridge aerodynamics.

The dynamic response of a line-like bridge structure is more complicated. At relatively low and steady wind velocities a phenomenon called vortex shedding may occur. This is due to separation of the wind field as it passes the structure. The separation will induce pressure differences above and below the cross-section, resulting in a vertical and rotational motion of the bridge cross-section. This type of wind-induced motion may become quite large for a long slender structure, and in some cases be fatal, as the increased motion of the structure is further amplified by a reduction in the wind-structure system damping properties. This effect is referred to as lock-in. Vortex shedding response is heavily dependent on the damping of the system, and is normally self-destructive. Resulting in narrow banded response peaks located in the vicinity of the natural frequencies associated with vortex shedding modes of motion. As the wind velocity increases, a bridge span is seen to be less prone to vortex shedding response. At intermediate wind velocities, the motion of the structure is dominated by the fluctuating wind component. This response is referred to as buffeting response. The buffeting response is mainly in the horizontal direction as this is assumed as the governing design wind direction for a bridge structure. At relatively high wind velocities the dominating dynamic response of a slender bridge span is seen to be due to motion-induced forces. These forces arise due to the relative motion of the structure and the wind field. The effect of motion-induced forces is to reduce the wind-structure damping and stiffness properties. Hence, a stability limit is approached as the wind velocity increases towards very high velocities.

Throughout the remainder of the thesis, the wind-induced dynamic response is considered negligible to the hydro-induced response of the floating bridge. The motivation for this is the large hydrodynamic influence on the system. The critical dynamic responses arising from the oncoming wind field, as discussed above, are mainly due to a reduction in the system damping. This may be the governing design criterion for a long slender bridge span of a traditional bridge structure, as the structural damping is considered low. The bridge span of a floating bridge is however subject to hydrodynamic effects transferred from the pontoons, which are interacting with the surrounding fluid. The fluid-structure interaction is considered to result in a significant hydrodynamic damping of the

system, as to oppose the motion of the pontoons. Consequently, the fluctuating part of the wind field is not considered to exert sufficient loading on the bridge span to produce any major dynamic response, and any contributions from the wind field to the dynamic response of the floating bridge will be disregarded.

4. STRUCTURAL MODEL

The aim of the report is to investigate the dynamic behaviour of a generic floating bridge structure. It is nevertheless considered necessary to evaluate a bridge model with dimensions that may apply to a real floating bridge construction. This is to avoid unrealistic results in the dynamic analyses. As a result, the dimensions of an already-built floating bridge have formed the basis in the development of the generic model. The geometry of the generic floating bridge model is inspired by the Bergsøysund floating bridge situated near Kristiansund on the west coast of Norway. The bridge is constructed as a horizontally curved truss girder steel superstructure supported on seven floating high-strength-concrete pontoons. The radius of the horizontal arch is $R = 1300m$. There is no vertical curvature of the bridge. The roadway is placed on top of a steel box-section, which constitutes the top flange of the superstructure. A top view of the bridge is illustrated below [6].

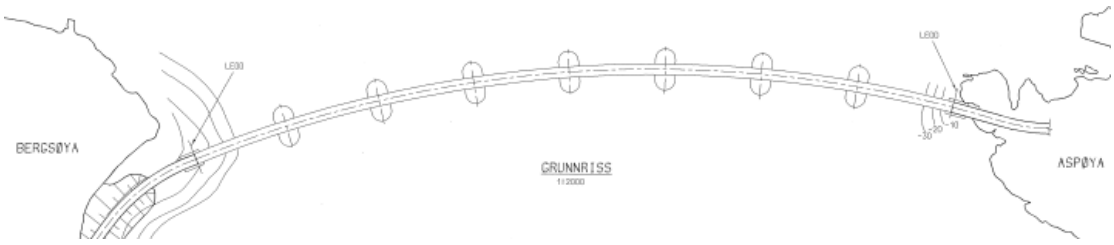

FIGURE 1 TOP VIEW OF THE BERGSØYSUND FLOATING BRIDGE [6]

The oval pontoons are idealized as rectangular, and the truss girder is idealized as an equivalent box cross-section. The connection between the pontoons and the superstructure is idealized as a single circular hollow steel rod. The end-connections are assumed simply supported in the vertical plane, and fixed with respect to the to transverse horizontal displacement, rotation in the horizontal plane and torsional rotation. The properties applied to the different parts of the floating bridge model are tabulated below.

Superstructure box-cross section	
Width, B_s	11.20 [m]
Height, h_s	7.00 [m]
Thickness top deck, t_p	0.08 [m]
Thickness bottom deck, t_b	0.04 [m]
Thickness walls, t_w	0.01 [m]
Cross-section area, A_s	1.4816 [m^2]
Moment of inertia, $I_{s,y}$	15.0981 [m^4]
Moment of inertia, $I_{s,z}$	16.2030 [m^4]
Torsional moment of inertia, I_x	13.5089 [m^4]
Mass density, ρ_s	7500 [kg/m^3]
Modulus of elasticity, E	200×10^9 [N/m^2]
Shear modulus, G	76.9×10^9 [N/m^2]
Poisson's ratio, ν	0.3

TABLE 1 PROPERTIES OF SUPERSTRUCTURE BOX CROSS SECTION

Rectangular pontoons	
Length, L_p	30.00 [m]
Width, B_p	20.00 [m]
Thickness top deck, t_p	0.35 [m]
Thickness bottom deck, t_b	0.35 [m]
Thickness walls, t_w	0.55 [m]
Cross-section area, A_p	20.93 [m^2]
Width/draft ratio, B_p/d	4.48 [m]
Moment of inertia, $I_{p,y}$	177.84 [m^4]
Moment of inertia, $I_{p,z}$	1122.30 [m^4]
Torsional moment of inertia, I_x	561.04 [m^4]
Mass density, ρ_c	2500 [kg/m^3]
Modulus of elasticity, E	30×10^9 [N/m^2]
Shear modulus, G	12.5×10^9 [N/m^2]
Poisson's ratio, ν	0.2

TABLE 2 PROPERTIES OF RECTANGULAR PONTOONS

Circular hollow connector rod	
Length, L_c	1.20 [m]
Radius, r_c	1.00 [m]
Wall thickness, t_c	0.05 [m]
Cross-section area, A_c	1.2252 [m^2]
Moment of inertia, $I_{c,y}$	0.5827 [m^4]
Moment of inertia, $I_{c,z}$	0.5827 [m^4]
Torsional moment of inertia, I_x	190.8265 [m^4]
Mass density, ρ_s	7500 [kg/m^3]
Modulus of elasticity, E	200×10^9 [N/m^2]
Shear modulus, G	76.9×10^9 [N/m^2]
Poisson's ratio, ν	0.3

TABLE 3 PROPERTIES OF CONNECTOR ROD

5. MOTION OF A FLOATING BRIDGE

The response of a general bridge span section may be considered as a three-degrees-of-freedom (3-DOF) response in every point along the bridge. The DOF's are referred to as displacements in the vertical direction, horizontal direction and in a rotational direction about the shear-centre axis of the bridge cross-section. The environmental loading on a bridge section is effectively divided into components corresponding to these degrees-of-freedom.

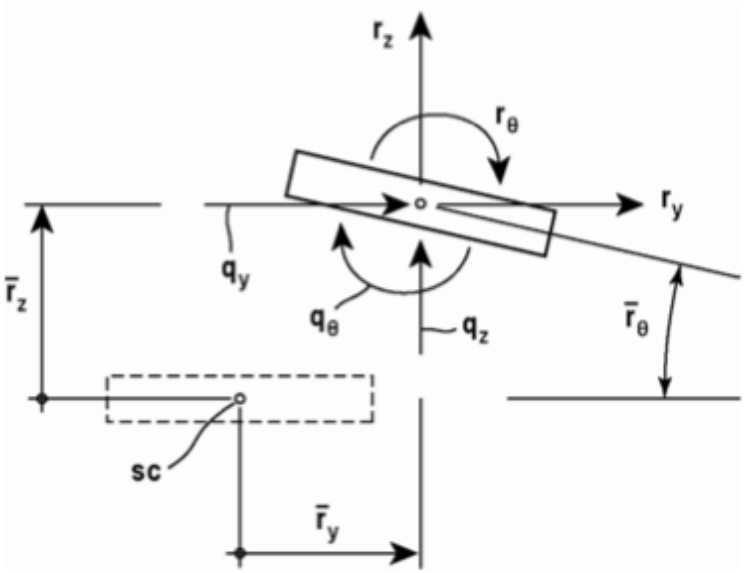

FIGURE 2 MOTION OF A BRIDGE SPAN [5]

The response of the bridge section may be viewed in terms of a quasi-static part and a dynamic part due to the corresponding assumptions of the environmental loading situation [5]. The quasi-static response is considered constant throughout the duration of the analysis. This response is determined through traditional static response analysis by applying the environmental loading that may be regarded as static within the time interval of the analysis. In the above figure the quasi-static response at a point along the bridge span is denoted by the response vector $\bar{\bar{r}} = \left[\bar{r}_y\ \bar{r}_z\ \bar{r}_\theta\right]^{\mathrm{T}}$. The static deflection is considered to represent the position of the bridge span at which the dynamic response takes place. The dynamic response of the bridge section is thus considered to oscillate about the quasi-static position. The dynamic response of the bridge span arises from the time-dependent parts of the environmental loading. In the above figure, the oscillating dynamic response is expressed in terms of the time-dependent load components.

$$r(t) = \left[r_y(t)\ r_z(t)\ r_\theta(t)\right]^{\mathrm{T}}$$

$$q(t) = \left[q_y(t)\ q_z(t)\ q_\theta(t)\right]^{\mathrm{T}}$$

The total response of the bridge span within the time domain of the dynamic analysis is thus expressed by a summation of the quasi-static and the time-dependent responses over the entire span of the bridge.

$$\mathbf{r}_{\mathrm{tot}}(t) = \bar{\mathbf{r}} + \mathbf{r}(t)$$

It is the time-dependent part of the response that is of concern in the dynamic analysis of the structure.

As the bridge structure to be evaluated is a floating bridge, some naval terminologies are adapted to denote the motion of the bridge components. The motivation for this is the extensive research and literature provided within the field of naval engineering, which in turn applies to the description of the fluid-structure interaction encountered when evaluating a floating bridge structure. These terminologies are illustrated below, and are applied throughout the report when describing the different modes of motions of both the pontoons and the bridge superstructure.

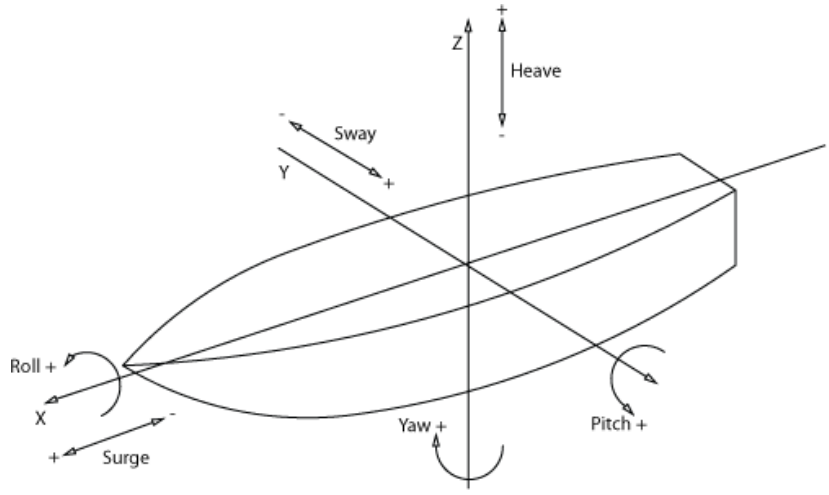

FIGURE 3 MOTION OF A NAVAL STRUCTURE [7]

For a continuous-pontoon floating bridge design, the motion of the bridge may be viewed in terms of a 3DOF response in every point over the bridge span. The considered responses are thus, according to the naval terminology, the heave, sway and roll responses of the bridge section. When considering a pontoon-separated floating bridge design, the motion of the bridge span is considered similarly. However, the underlying pontoons may not be restricted to the three-abovementioned modes of motion. Depending on the orientation of the pontoons relative to the surrounding wave climate, these may, and probably will, be excited in all modes of motion presented on the above figure. The forces and moments transferred to the above lying bridge span are in turn dependent on

the orientation of the pontoons relative to the bridge span at the points of connection, and the rigidity of the connections. The relative pontoon orientations will thus dictate which modes of the bridge span being excited from the modes of motion of the pontoons, which are subjected to wave loading.

6. HYDRODYNAMIC MODEL

The properties of the wave climate at the site of construction form the basis for the external wave loading on the floating body. A true sea state is seen as confused and irregular due to the adding and cancelling of waves of different properties, and is associated with uncertainties normally tackled by statistical means. To obtain a realistic loading situation on a floating bridge, the spatial distribution and local irregularities of the sea state are to be incorporated properly in the modelling.

A floating body is considered greatly affected by its surrounding fluid. The fluid-structure interaction results in a system that needs to be regarded as a whole when evaluating the dynamic behaviour. The floating bridge construction will have different system properties and effectively a different dynamic behaviour when considered separate from the surrounding fluid. Thus, a "dry" response analysis of the purely structural bridge provides limited information of the true behaviour of the fluid-structure system. The effect of the fluid-structure interaction is investigated by comparing the "wet" and "dry" natural frequencies of the floating bridge model. The findings are included in the appendices A.3 and A.4, respectively, and discussed in later sections of the thesis. The hydrodynamic interaction effects are seen to be frequency dependent and will as a result contribute differently to the dynamic properties of the system at different frequencies of motion. The proper determination of the hydrostatic and hydrodynamic restoring forces on the floating bridge is considered vital in order to obtain a realistic behaviour of the dynamic system.

This section proposes descriptions for an irregular sea state as well as outlining methods for determination of the hydrostatic and hydrodynamic forces on a floating body.

6.2. MODELLING OF THE SEA SURFACE

The oncoming wave field is considered to constitute the primary source of dynamic loading on the floating bridge. The spatial distribution of the waves at the site of construction is regarded a function of both time and space and representing a confused and irregular sea state. Resulting in expectations of low correlation of the surface elevation between points in space. A proper simulation of a representative sea state is considered vital to obtain reasonable results in the dynamic analysis of the fluid-structure system.

6.2.1. AN INTRODUCTION TO LINEAR WAVE THEORY

The simplest wave theory applicable to coastal processes is known as linear wave theory, or Airy wave theory. This theory is based on the assumption that the water is incompressible, inviscid, that the flow is irrotational and that there

exists a velocity potential within the water volume. The velocity potential is evaluated as to satisfy the Laplace equation through boundary conditions [8].

$$\nabla^2 \Phi = 0$$

The velocity potential forms the basis for determination of other properties of the waves. Being particle velocities or accelerations at specific depths or the dynamic pressure fluctuations from passing waves. The equations are modified somewhat to apply in shallow, intermediate and deep water, classified by the depth-wavelength ratio. The physical interpretation of the linear wave theory is that the water particles move in elliptical orbits with decreasing orbital dimension when moving down the water column. The net motion of a water particle is assumed to be zero. An illustration of the basic concepts of linear wave theory is presented in figure 4.

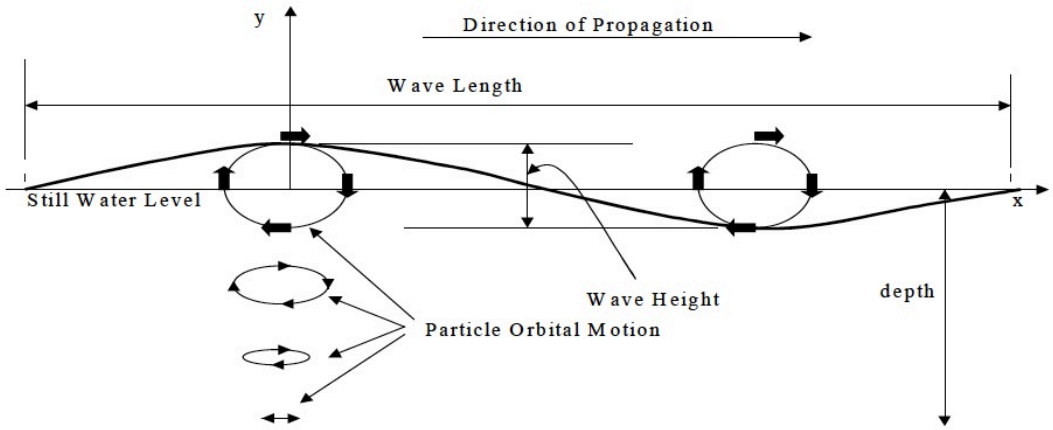

FIGURE 4 ILLUSTRATION OF LINEAR WAVE THEORY [9]

The assumptions of linear wave theory are considered to apply quite well with real behaviour of waves at large water depths. As the waves move into shallower waters there will be a net forward movement as waves break and the water is flushed onshore. Hence, for shallow water, other wave theories, such as Cnoidal wave theory and Solitary wave theory, express the behaviour of the water particles better than do linear wave theory. At intermediate water depths, higher order wave theories may be applied to better describe the configuration of the surface elevation. Thus, expanding the description from the linearized expressions of the linear Airy theory. Figure ? illustrates the applicability of a selection of wave theories according to water depth.

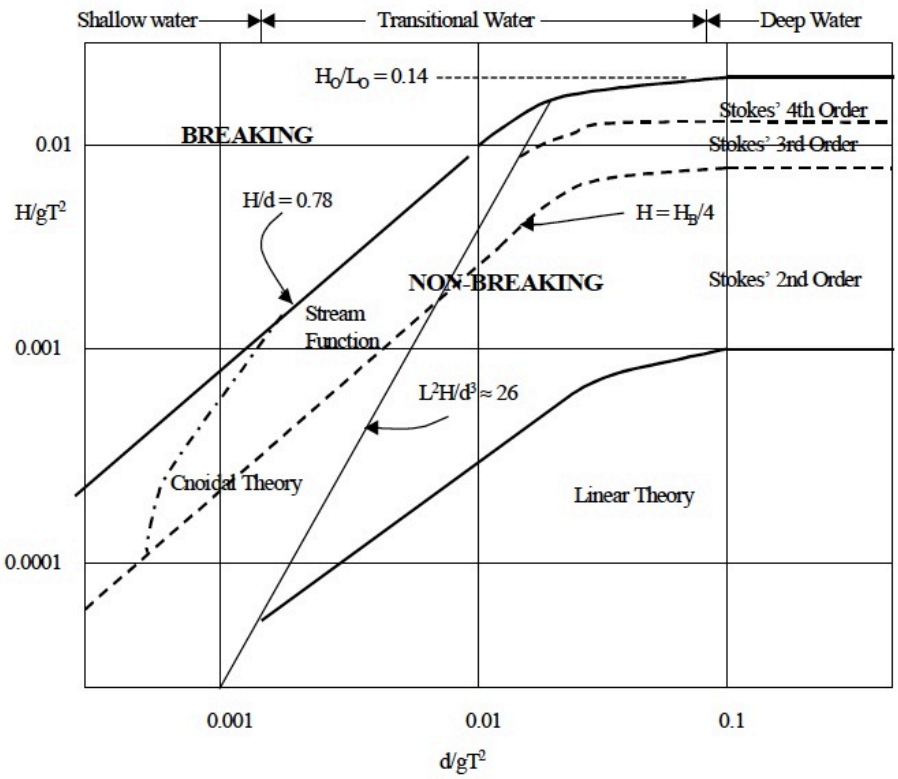

FIGURE 5 APPLICABILITY OF WAVE THEORIES [9]

On the basis of the linear wave theory and the bathymetry of the coastline, wave characteristics such as shoaling, diffraction and refraction may be determined for waves approaching the coastline. These features indicate the wave energy distribution along the coastline as the waves bend perpendicular to the seabed contours. The wave energy in a unit length wave crest transmitted to the coastline is quantified according to linear wave theory as.

$$E = \rho_w g \frac{H^2}{8}$$

A time scale for the impact forces may be introduced by establishing an energy velocity, also called the group velocity of a wave train or set. The wave energy travels with a different velocity than do the waves. This can be seen as waves "disappear" in front of a set and "reappear" at the rear and seem to "move through" the set as it is propagating. The group velocity is given by the expression.

$$C_G = n \cdot C$$

$$n = \frac{1}{2}\left[1 + \frac{(4\pi d/L)}{(sinh\, 4\pi d/L)}\right]$$

$C =$ wave celerity according to linear wave theory.

By combining the above equations, an expression for the wave power transmitted to the coastline per unit width of the wave crest may be established.

$P = E\,C_G$

The three-dimensional surface elevation is expressed as function of space and time for a single long-crested wave with wave angle of approach θ.

$$\eta(x,y,t) = \eta_0\, e^{\{-i(k(x\sin\theta + y\cos\theta) - \omega t)\}}$$

In order to include waves approaching from any direction, incorporating the adding and cancelling effect of surface waves, an integration over the wave-angle-of-approach domain, $\{-\pi/2 \le \theta \le \pi/2\}$, is performed. In addition, a spreading function is included to express the degree of multi-directionality of the sea state. The effect of the spreading function is determined by the value of the spreading index, *s*, which dictates the degree of multi-directionality. The directional spreading function also incorporate a mean wave angle of approach, $\bar{\theta}$, around which the wave spectrum is spread out. The spreading function is further scaled by the N_s-parameter such that the total wave energy within the wave field remains unchanged. A random phase angle, φ, is introduced, which is considered uniformly distributed in the range $0 \le \varphi \le 2\pi$.

$$\eta^{(3D)}(x,y,t) = \int G(\theta)\,\eta_0 e^{-ik\left(x_m \sin(\theta-\bar{\theta}) + y_m cos(\theta-\bar{\theta}) - \omega t + \varphi\right)} d\theta$$

$$G(\theta) = \begin{cases} N_s cos^{2s}(\theta-\bar{\theta}) & -for\ |\theta-\bar{\theta}| \le {}^{\pi}/_{2} \\ 0 & -otherwise \end{cases}$$

$$N_s = \frac{1}{\int cos^{2s}(\theta-\bar{\theta})\, d\theta}$$

The spreading function is seen to approach the Direc-Delta function for high values of the spreading index, *s*, and is considered to model ultra-narrow banded sea states corresponding to long-crested sinusoidal waves as a limiting case.

An illustration of spreading functions for different values of the spreading index, *s*, is presented on the following page.

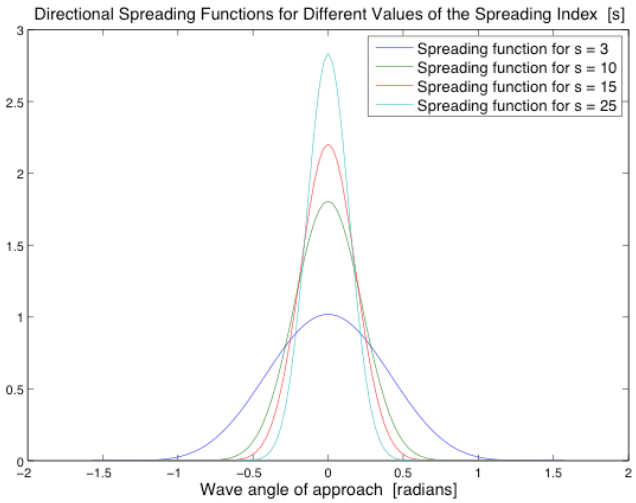

FIGURE 6 DIRECTIONAL SPREADING FUNCTIONS

The mean wave angle of approach, $\bar{\theta}$, and the spreading index, s, are set to represent different sea states. The effect of the mean angle of approach is to produce a skewed wave field for values $\bar{\theta} \neq 0$, as the wave distribution becomes asymmetrically distributed with respect to the global axes of the model. The effect of the spreading index is to scale the contributions of the waves over the wave-angle-of-approach domain. A plot of the surface elevation at an instant in time, $\eta^{(3D)}(x, y)$, is presented on the following page to illustrate the spatial distribution for a sea state at frequency $\omega = 0.9\, rad/s$. For deep-water wave conditions, this corresponds to a wavelength of $\lambda \simeq 76m$. The sea state is modelled for unit amplitude waves, $\eta_0 = 1$, with a low degree of multi-directionality, $s = 15$, and with a mean wave angle of wave approach $\bar{\theta} = \pi/8$.

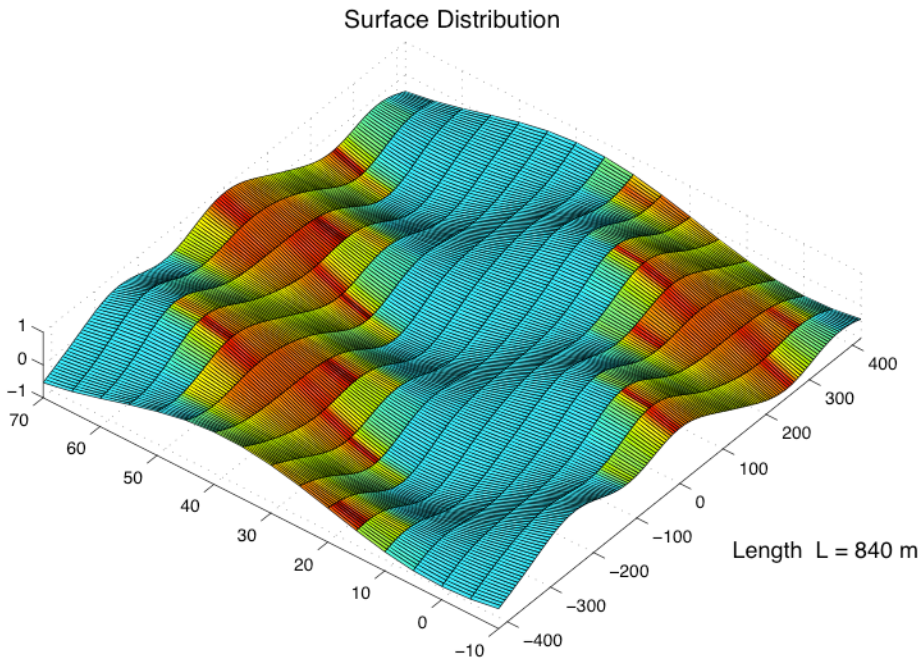

FIGURE 7 ILLUSTRATION OF A SURFACE ELEVATION

The sea state modelled represents a scaled summation of long-crested waves approaching within the wave-angle-of-approach domain. A true sea state is, however, more commonly expressed through spectral densities. Such a wave spectrum represents the statistical properties of the wave field in the frequency domain. To incorporate the spatial distribution of the surface waves, an expression for a directional wave spectrum is developed in the following section.

6.2.2. DIRECTIONAL WAVE SPECTRUM

A directional wave spectrum is sought through the application of a JONSWAP spectrum. The JONSWAP spectrum was originally developed during a joint research project as a one-dimensional wave spectrum for north-sea conditions [8]. It is mathematically expressed as a peak-enhanced Pierson-Moskowitz spectrum. The JONSWAP wave spectrum is considered applicable to simulate the wave conditions at most sites along the Norwegian western coastline.

$$S_{PM}(f) = \frac{5}{16} H_s^2 \frac{f_p^4}{f^5} exp^{-\frac{5}{4}\left(\frac{f_p}{f}\right)^4}$$ - Pierson-Moskowitz wave spectrum.

H_s is the significant wave height, and f_p is the peak frequency of the sea state.

$$S_\eta(f) = S_{PM}(f)\,\gamma^{exp^{-\left(\frac{(f-f_p)^2}{2\sigma^2 f_p^2}\right)}}$$ - JONSWAP wave spectrum.

The γ-term is thus considered the additional peak enhancement factor, where γ assumes values in the range $1 < \gamma < 7$, and σ denotes the relative measure of the width of the peak with recommended values given below.

$$\sigma = \begin{cases} 0.07 & f < f_p\ (low\ frequency\ side) \\ 0.09 & f > f_p\ (high\ frequency\ side) \end{cases}$$

A plot of a Pierson-Moskowitz wave spectrum together with the peak enhanced JONSWAP wave spectrum, as functions of dimensionless frequency, is presented below to illustrate the effect of the peak enhancement factor.

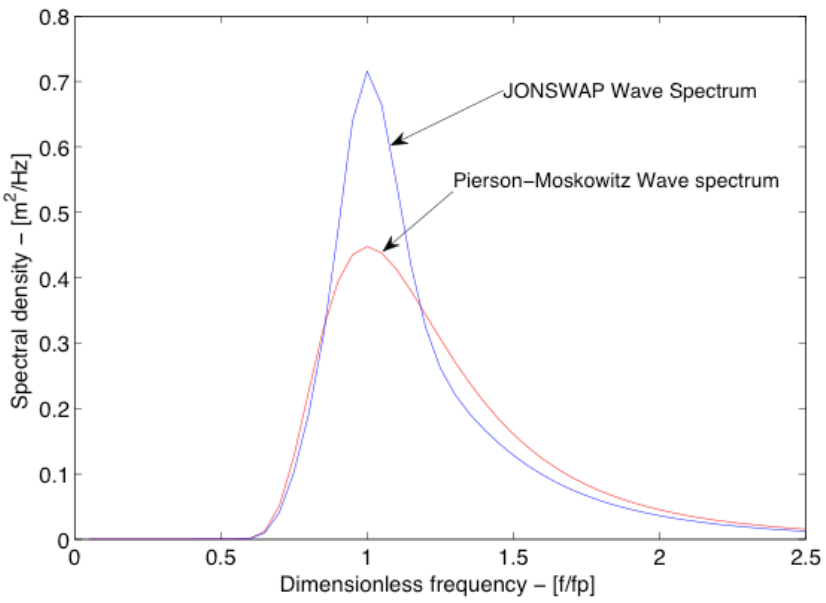

FIGURE 8 PIERSON-MOSKOWITZ AND JONSWAP WAVE SPECTRA

The JONSWAP spectrum describes the spectral density of a single sea state specified by the significant wave height, H_s, and peak period, T_p. Long-crested swell waves generally approach the shoreline with periods in the range $T_{long} = 8 - 12$ seconds, while the local wind generated surface waves are considered to have periods in the range $T_{short} = 3 - 5$ seconds. The JONSWAP spectrums for describing these sea states will consequently have different spectral density distributions. The irregular sea state generated by the local wind field superpose on the swell waves to form the confused state of the sea surface. Realizing that both sea states are present simultaneously, a combined JONSWAP

spectrum is developed, representing the added spectral densities of the two sea states. The wave spectrum parameters applied to form the combined JONSWAP spectrum are peak period values of $T_{p,long} = 10\ sec$ and $T_{p,short} = 3\ sec$, and a significant wave height of $H_s = 1m$ for both sea states.

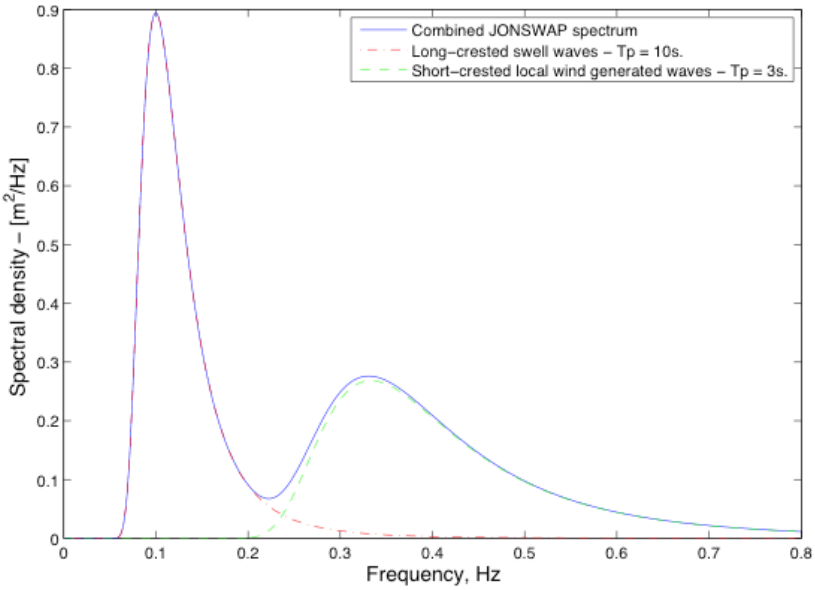

FIGURE 9 JONSWAP SPECTRUM FOR COMBINED SEA STATES

The JONSWAP spectrum representing the long-crested swell waves is seen to have a narrow banded spectral density with its peak corresponding to the peak frequency of the sea state. This represents a rather homogenous sea state and a low degree of multi-directionality is expected for the long-crested swell waves. The spectral density of the short-period waves is seen to be a more wide-banded process, illustrating a larger variety of the wave periods. These low-period waves are assumed to represent a more irregular sea state with a high degree of multi-directionality.

An extension to a two-dimensional wave spectrum is obtained by combining the one-dimensional wave spectrum with the directional spreading function. The spreading index, s, dictates the degree of multi-directionality. The wave spectrum is spread out over the mean wave angle of approach, $\bar{\theta}$, and the scaling parameter, N_s, now ensures the total wave energy within the directional wave spectrum to equal the wave energy within the one-dimensional spectrum.

$$S_\eta(f,\theta) = S_\eta(f)\, G(\theta)$$

The two-dimensional directional wave spectrums are computed for constant values of the spreading index, and are functions of both frequency and direction of the waves. The long-crested swell waves were assumed to have little directional spread, while the short-crested waves were considered to have more random directions of approach. The JONSWAP spectrums representing the

different sea states are consequently applied to spreading functions of different spreading index values, corresponding to the desired degree of multi-directionality of the two. An illustration of one realization for the spectral density of the combined sea states as function of both frequency and wave angle is presented below.

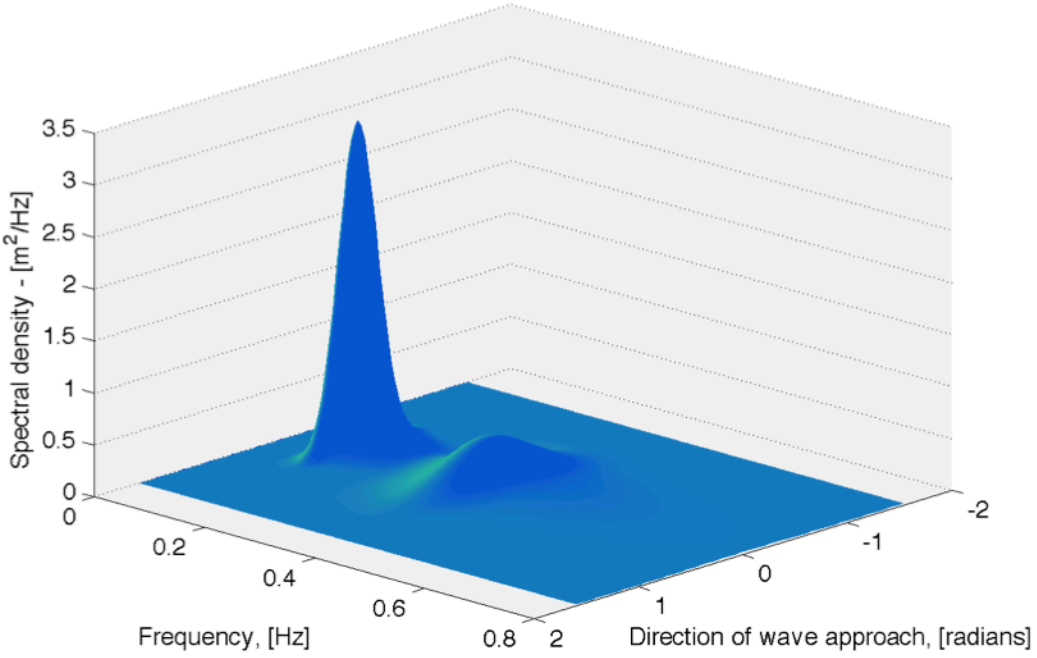

FIGURE 10 DIRECTIONAL WAVE SPECTRUM COMBINED SEA STATES

A spreading function with spreading index $s_{long} = 15$ is applied to the long-crested JONSWAP spectrum, while a spreading index, $s_{short} = 3$, is introduced in the spreading function applied to the short-crested JONSWAP spectrum. Both sea states are modelled with a mean angle of approach $\bar{\theta} = 0$ in the above plot of combined directional sea states. Generally, the approach angles of the swell waves and the short-crested waves may not be considered to coincide for an actual sea state. Different mean wave angles of approach are readily introduced in the expressions for the sea states and the effects of various relative angles between the more unidirectional swell waves and the multi-directional short-crested waves may be assessed.

A wave spectrum has been considered to describe the sea state at a site of interest from wave field characteristics of significant wave height, H_s, and peak period, T_p. For the modelled wave spectrum to be applicable, the sea state parameters employed need to reflect the physical wave field at the site. The statistical determination of some sea state parameters is discussed in the following section.

6.2.3. DETERMINATION OF THE WAVE SPECTRUM PARAMETERS

The expressions for the sea state parameters presented in the following are assumed to apply within the concept of short-term wave statistics. This implies that the sea state is evaluated over a satisfactorily short time-window, of half an hour to a couple of hours so that the sea state may be evaluated as a stochastic stationary process.

Wave recordings are essential to obtain knowledge of the wave properties at a specific site. Such recordings may be done by means of a wave rider buoy. This is a floating instrument that follows the surface elevation under wave action, recording the changes in elevation by an accelerometer. Some of these buoys also have instruments to detect the angle of the propagating waves. A time-domain recording from such a buoy is random, but when evaluating different recordings from a single wave rider buoy, one may see that the results are of the same appearance. We may say that the general properties of the time-series are the same; hence the process is considered stochastic stationary. This implies that certain statistical measures may be applied to the record. However, recordings have to be carried out over a reasonable amount of time, say a year or two, to be able to do any meaningful statistics on the recorded data.

An example of a time-series recording of the surface elevation is presented in figure 11.

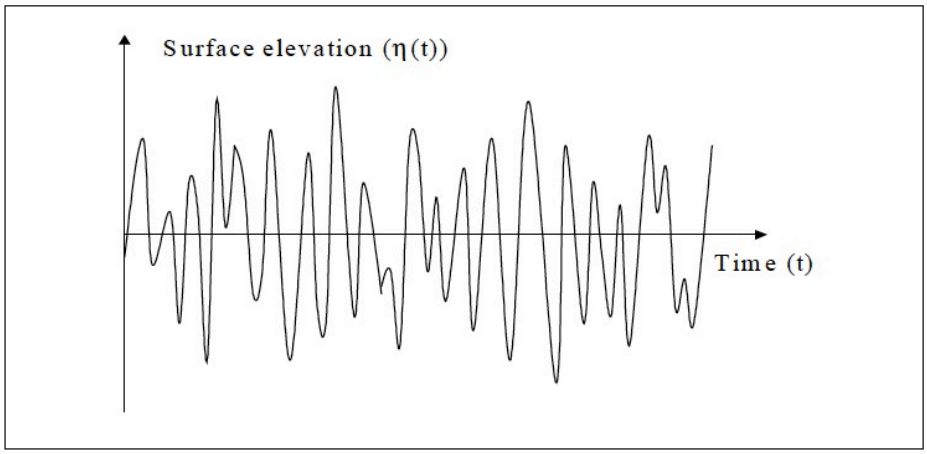

FIGURE 11 SURFACE ELEVATION TIME RECORD [9]

In modelling of a sea surface wave spectrum the most commonly used parameters are the significant wave height, H_s, and the zero crossing wave period, T_z [9]. These wave parameters may be determined by applying statistics on the recorded surface elevation time-series. When considering the time-series record of the surface elevation we determine a time interval, t_i, at which the surface elevation is within a small increment, $d\eta$. Then summing up the total time for which the surface elevation is within this small increment. The probability density function for the surface elevation may then be determined by

evaluating the total time within each surface increment, $d\eta$, over the total time-domain of the wave record.

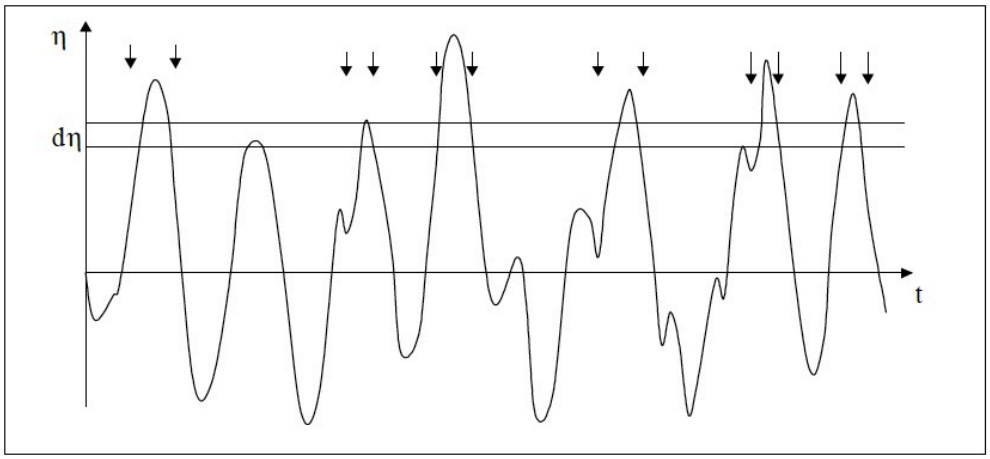

FIGURE 12 PROBABILITY DENSITY FUNCTION DETERMINED FROM A TIME RECORD [9]

$$\left(\eta_j - {}^{d\eta}/_2\right) < \eta \leq \left(\eta_j + {}^{d\eta}/_2\right)$$

$$p(\eta_j) = \lim_{T\to\infty} \frac{\sum_{i=1}^{N} t_i}{T}$$

The surface waves are assumed independent and random for the phase shift, $0 \leq \phi \leq 2\pi$. For variables resulting from a large number of independent causes, the central limit theorem states that the probability density function is normal distributed. Hence, for a simplified modelling of the surface elevation the probability density function of the surface elevation may be approximated as a zero-mean Gaussian distribution.

$$p(\eta) = \frac{1}{\sqrt{2\pi\sigma_\eta}} e^{\left\{\frac{\eta}{2\sigma_\eta^2}\right\}}$$

With σ_η being the standard deviation of the surface elevation time-record.

The assumption of a Gaussian probability density distribution for the surface waves is an approximation to the stochastic process of the wave structure. The approximation is employed with reasonable accuracy for ocean waves, but for the wave conditions in coastal regions, major deviations can be experienced.

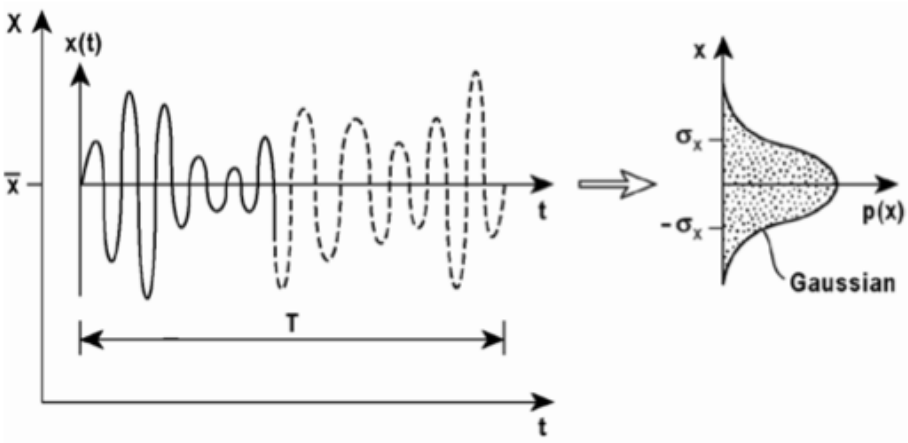

FIGURE 13 GAUSSION IDEALIZATION OF A TIME-DOMAIN PROCESS [5]

Based on the joint probability distribution of the surface elevation, η, and its time derivatives, the probability density function of the wave height may be established. The wave height density is seen to follow a Rayleigh distribution. This is illustrated in figure 14.

$$p(H) = \frac{H}{4\sigma_\eta^2} e^{\left\{-\frac{H^2}{8\sigma_\eta^2}\right\}}$$

$\bar{H} = 2.51\sigma_\eta$ - Mean wave height

$H_{1/3} = 4\sigma_\eta$ - Significant wave height (H_s)

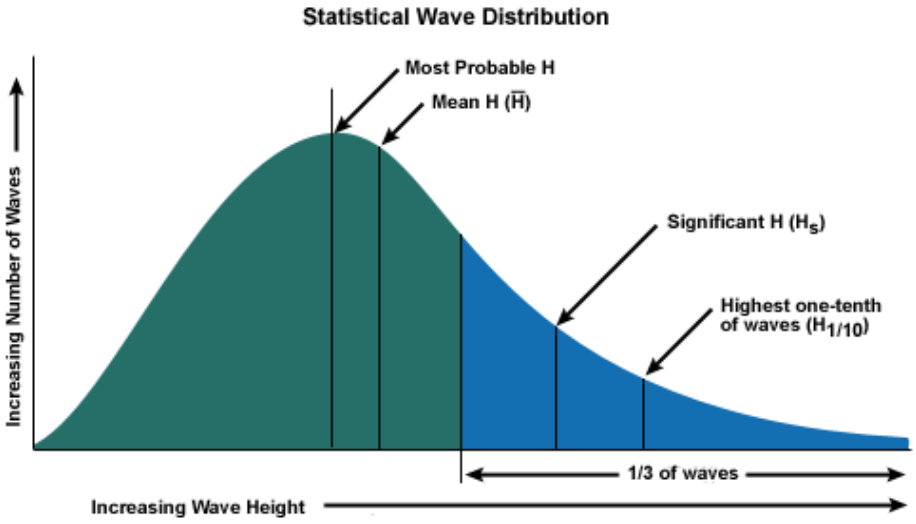

FIGURE 14 RAYLEIGH DISTRIBUTION OF WAVE HEIGHTS [9]

The maximum expected wave height within N waves is further estimated by the following expression [8].

$$E|H_{max}| = H_s\left(\sqrt{\frac{\ln N}{2}} + \frac{0.5772}{\sqrt{8\ln N}}\right)$$

For a sea state of a duration T $[sec]$ the number of waves within the time-window may be estimated by means of the average wave period considered for the wave spectrum.

$$N = \frac{T}{T_{m0}}$$

$$T_{m0} = \left[\frac{\int_{-\infty}^{\infty} S_\eta(f)\, df}{\int_{-\infty}^{\infty} f^2 S_\eta(f)\, df}\right]^{1/2}$$

The wave characteristics of a sea state may conveniently be expressed in terms of angular frequency, ω $[rad/s]$, by employing the relationship.

$$\omega = 2\pi f$$

As the wave recordings often are limited in time and space, an evaluation of the wave record relative to the normally more thoroughly recorded wind field at the site may reveal some information on the validity of the extreme value estimations.

6.3. Fluid-structure interaction and hydrodynamic loads

As a body moves relative to a surrounding fluid, both hydrostatic and hydrodynamic effects are present along the interface of the body and fluid. The motion of the body will interact with the fluid, resulting in the fluid becoming an integral part of the dynamic system. The dynamic forces exerted on the floating body may be evaluated by considering two types of loading situations. The first loading situation arises from the forced oscillatory motion of a body in still water. The second loading situation is evaluated as the external loading on a fixed body from an oscillating wave field. The sum of these loading situations makes up the total hydrodynamic loading on the floating body. This is disregarding viscous effects at the fluid-structure boundary.

$$F_{tot}^{(h)}(t) = F_{\Delta}^{(h)}(t) + F_{wave}^{(h)}(t)$$

The dynamic parts of the loading are thus considered functions of time.

The hydrodynamic effects arise due to oscillating fluid pressure over the wetted surface of the floating body, and are often evaluated as steady-state

hydrodynamic forces and moments exerted on the body due to rigid body motions. These forces and moments are obtained by integrating the fluid pressure over the surface of the body [10].

The hydrodynamic restoring forces and moments are associated with the forces and moments acting on an oscillating body, as to oppose the motion. The most intuitive restoring force on a floating body is the one associated with buoyancy. A relative vertical displacement between the fluid and the body will alter the fluid pressure distribution underneath the body, and ultimately change the buoyancy force. The change in the buoyance force is directly related to the change in the displaced water volume and is only considered in the vertical direction. Thus, generally for the heave, roll and pitch modes of motion. Due to the linear relation between the restoring buoyancy force and the displacements of the above mention modes, the restoring force is often expressed by an additional hydrostatic stiffness contribution. The hydrostatic stiffness for a floating body is expressed below in terms of the associated mode of motion [11].

$k_z^{(h)} = \rho_w g A_{wp}$ - Heave displacement

$k_\theta^{(h)} = \rho_w g \Delta\forall \overline{GM}_T$ - Roll displacement

$k_\phi^{(h)} = \rho_w g I_{wp,yy}$ - Pitch displacement

$k_{z\phi}^{(h)} = -\rho_w g M_{wp,yy}$ - Combined heave-pitch displacement

$k_{z\theta}^{(h)} = \rho_w g M_{wp,zz}$ - Combined heave-roll displacement

$$F_{\Delta,stat,j}^{(h)}(t) = k_j^{(h)} r_j(t)$$

In these expressions A_{wp} is the water plane area, $\Delta\forall$ is the displaced water volume due to roll motion, $\overline{GM}_T$ is the transverse metacentric height, $I_{wp,yy}$ is the moment of inertia of the water plane about the *y*-*y*-axis, and $M_{wp,jj}$ is the area moments of the water plane. The additional expression for the combined heave-roll displacement is normally not included in ship engineering. It is, however, considered necessary to include this term here, due to the nearly rectangular shape of the pontoons, so that both heave and sway motion are regarded as coupled with roll motion.

The remaining restoring forces acting at the boundary of the floating body are termed as dynamic forces. These forces arise due to the relative oscillating motion of the fluid-body and may be assessed in terms of the three-dimensional velocity potential of the fluid according to linear wave theory [8].

$$\Phi = \frac{\eta_0 g}{\omega} \frac{\cosh k(z+h)}{\cosh(kh)} e^{\{-i(k(x\sin\theta + y\cos\theta) - \omega t)\}}$$

The dynamic forces on a floating body may be expressed by establishing a diffraction-radiation problem. The diffraction problem employs the incident and scattered velocity potential and is a representation of the wave field on the stationary body. The radiation problem represents the velocity potential of the refracted waves generated at the boundary of the body oscillating in still water. A boundary value problem is established and solved for the velocity potentials. The wave-exciting force on the stationary structure is determined by evaluating the fluid pressure from the incident and scattered velocity potentials over the wetted surface of the body. The hydrodynamic coefficients in terms of the added mass and hydrodynamic damping are determined by integration of the dynamic pressure from the radiated potential. The added mass, $m^{(h)}$, and hydrodynamic damping, $c^{(h)}(\omega)$, constitute a pair of harmonic conjugates and are thus seen to be functions of the acceleration and velocity of the oscillating body, respectively. These are in turn determined from the real and imaginary parts of the complex radiation potential. The dynamic wave loading may then be expressed in terms of an exciting wave force and the hydrodynamic restoring forces from the incident, scattered and radiated velocity potentials at the boundary of the body [12].

$$p_d(x,y,z,t) = -\rho_w \frac{\partial \Phi}{\partial t} = i\omega\rho_w \Phi$$

$$F^{(h)}_{wave,j}(t) = i\omega\rho_w \int (\Phi_i + \Phi_s)\, n_j \, dS_w = Re\left[q_j(\omega) \int e^{\{-i(k(x\sin\theta + y\cos\theta) - \omega t)\}} d\theta\right]$$

$$F^{(h)}_{\Delta,dyn,j}(t) = i\omega\rho_w \dot{r}_j \int \Phi_r \, n_j \, dS_w = -\left\{m^{(h)}_j(\omega)\, \ddot{r}_j(t)\right\} - \left\{c^{(h)}_j(\omega)\dot{r}_j(t)\right\}$$

$$m^{(h)}_j(\omega) = \rho_w \, Re\left[\int \Phi_r \, n_j \, dS_w\right]$$

$$c^{(h)}_j(\omega) = \rho_w \omega \, Im\left[\int \Phi_r \, n_j \, dS_w\right]$$

The pressure integrations are performed over the wetted surface, S_w, of the floating body with n_j being a unit inward normal on the body surface associated with the *j*'th mode of motion. Φ_i, Φ_s and Φ_r represents the incident, scattered and radiated potentials, respectively. $q_j(\omega)$ is the frequency dependent complex load amplitude associated with the *j*'th mode.

The added mass and hydrodynamic damping coefficients are seen to be dependent on both the frequency and mode of motion of the body. Consequently,

the hydrodynamic coefficients associated with a mode of motion will assume different values corresponding to the frequency of oscillation. The added mass may even assume negative values at certain frequencies. Furthermore, the geometric shape of the floating body plays a significant part in the determination of the hydrodynamic coefficients. The width-draft ratio and the presence of sharp corners on the body affect the hydrodynamic coefficient values greatly [10]. As a result, the hydrodynamic coefficients should be determined specifically for the floating structure at hand.

The complex load amplitudes, $\bar{q}_j(\omega)$, associated with the different modes of motion, show the same dependencies as the hydrodynamic coefficients for added mass and hydrodynamic damping. At low frequencies the wave loading in heave is assumed to correspond to the displaced water volume, resulting in the floating body following the surface elevation of the oncoming wave field. For the sway and roll load transfer, no load is assumed to be transferred to the floating body as $\omega \to 0$. The motivation for these assumptions is the fact that as $\omega \to 0$ the wavelengths of the oncoming waves approach infinity and the wave field is represented by a surface elevation increase in every point in space, associated with water particle motion purely in the vertical direction. The loads transferred to a floating body are seen to generally decrease at higher frequencies. The complex load transfer functions express this frequency dependence and are included to evaluate the proper wave loading as function of the frequency of motion. The frequency dependent loads per unit length are expressed below in terms of the dimensionless hydrodynamic load transfer functions.

$$q_j(\omega) = q_{Wave,j}\, \bar{q}_{0,j}(\omega)$$

$$q_{Wave,y} = \rho_w g B_p d k \eta_0$$

$$q_{Wave,z} = \rho_w g B_p \eta_0$$

$$q_{Wave,\theta} = \rho_w g \frac{B_p}{12} d k \eta_0$$

In the above expressions ρ_w is the mass density of the fluid, g is the gravitational constant, B_p is the width of a rectangular floating cylinder, d is the draft, k is the wavenumber and η_0 is the wave amplitude.

Fluid-structure interaction is dealt with in various manners throughout the literature. The classical strip theory has been a commonly applied strategy in naval architecture to determine the hydrodynamic restoring forces on ships [10]. The underwater part of the floating body is considered in a piecewise fashion, divided into strips of a small finite length in the longitudinal direction. The two-dimensional hydrodynamic coefficients are determined for each of the cross-sections and eventually combined over the full length of the floating body.

Additional end-effects are to be considered as the strip theory implies that the variation of the flow in the cross-sectional plane is much larger than in the longitudinal direction. This will, however, not be the case at the ends of the floating body.

The hydrodynamic coefficients in this report are taken from Langen [13], which in turn has derived these from results given by Vugts [2]. The values of the hydrodynamic coefficients have been computed for a rectangular floating cylinder in two-dimensional flow for a width-draft-ratio $B/d = 4$. The pontoons applied in this report are rectangular with a width-draft-ratio of $B_p/d \simeq 4.48$. The hydrodynamic coefficients are thus considered to have good relevance the model developed in this report. The hydrodynamic coefficients are further expressed per unit length and are regarded constant over the length of the pontoons. The non-dimensional hydrodynamic added mass, hydrodynamic damping and load transfer functions associated with heave, sway and roll modes of motion are presented graphically in the appendix A.1.

The total hydrodynamic loading on a floating body in the *j*'th mode may then be expressed as.

$$F_j^{(h)}(t) = F_{wave,j}^{(h)}(t) + F_{\Delta,dyn,j}^{(h)}(t) + F_{\Delta,stat,j}^{(h)}(t)$$

This expression may be further developed to express the load per unit length on a floating body in the *j*'th mode in terms of the hydrodynamic restoring coefficients.

$$q_j^{(h)}(\omega, t) = q_{wave,j}^{(h)}(t) - m_j^{(h)}(\omega)\ddot{r}_j(t) - c_j^{(h)}(\omega)\dot{r}_j(t) - k_j^{(h)}r_j(t)$$

7. FORMULATION OF THE EQUATIONS OF MOTION AND SOLUTIONS METHODS

7.1. THE EQUATIONS OF MOTION OF A FLUID-STRUCTURE SYSTEM

The dynamic response of a general structural system is evaluated through its equation of motion. This equation states the dynamic equilibrium condition and predicts the time-dependent response, $r(t)$, from an external time-dependent loading, $R(t)$, by incorporation of the mass, damping and stiffness properties of the dynamic system.

$$\mathrm{M}^{(s)}\ddot{r}(t) + C^{(s)}\dot{r}(t) + K^{(s)}r(t) = R(t)$$

The structural properties of the bridge construction are expressed by the structural mass, $\mathrm{M}^{(s)}$, damping, $C^{(s)}$ and stiffness, $K^{(s)}$. These properties reflect the floating bridge construction when the surrounding environment is disregarded. A dynamic analysis using only these properties as input, with no external loading $R(t) = 0$, will render the free response of the construction as if being placed in still air or vacuum.

A fluid-structure system has a more complicated dynamic behaviour due to strong interaction effects. All relevant properties of the system are to be included to obtain an accurate estimation of the physical response. Thus, the structural properties, the fluid-structure interaction effects and the environmental loading, all need to be evaluated in the equation of motion.

$$\mathrm{M}^{(s)}\ddot{r}(t) + C^{(s)}\dot{r}(t) + K^{(s)}r(t) = F^{(h)}_{wave}(t) + F^{(h)}_{motion,dyn}(t) + F^{(h)}_{motion,stat}(t)$$

The hydrodynamic and hydrostatic forces are expressed in terms of added mass, hydrodynamic damping and a hydrostatic stiffness contribution. Recognizing their respective association with the acceleration, velocity and relative displacement of the structure, the hydrodynamic and hydrostatic contributions are effectively included in the system properties. Resulting in a complete representation of the fluid-structure system. A dynamic evaluation of the fluid-structure system properties, disregarding any environmental loading, results in the free response of the bridge construction in its proper environment. Such an analysis may be used to determine the natural frequencies and mode shapes of the fluid-structure system, and to develop general frequency response functions for desired response parameters.

$$\mathrm{M}^{(s)}\ddot{r}(t) + C^{(s)}\dot{r}(t) + K^{(s)}r(t) = -M^{(h)}(\omega)\ddot{r}(t) - C^{(h)}(\omega)\dot{r}(t) - K^{(h)}r(t)$$

$$\left(\mathrm{M}^{(s)} + M^{(h)}(\omega)\right)\ddot{r}(t) + \left(C^{(s)} + C^{(h)}(\omega)\right)\dot{r}(t) + \left(K^{(s)} + K^{(h)}(\omega)\right)r(t) = 0$$

To obtain the true behaviour of the floating bridge structure the proper external environmental loadings are to be determined. The loading is introduced on the right hand side of the above equation of motion, resulting in a forced response of the system.

7.2. SOLUTION METHODS TO THE EQUATIONS OF MOTION

For classically damped systems the dynamic properties are solely determined by the mass and stiffness properties of the system. Such systems may be obtained by use of proportional damping. Then, the equations of motion may be decoupled by a modal analysis. Assumed mode shapes of the system form the basis for the analysis, and the total response of the system is determined by a summation of scaled mode shapes as functions of the frequency of motion. Mode shapes associated with natural frequencies in the vicinity of the response frequency will dominate the total response of the bridge structure. Though, for systems with closely spaced Eigen frequencies, the total response may be difficult to ascribe to specific mode shapes.

For systems with non-classical damping, the damping matrix is not readily diagonalized, and the dynamic properties are dependent of the damping, as well as of the mass and stiffness properties of the system. The solution to such a system involves transformation of the second order differential equations, i.e. the dynamic equilibrium conditions, to first order differential equations. The response of the system is assumed to decay as a function of time, and a complex notation is adopted. The solution to the non-classically damped dynamic system renders complex Eigen values and complex Eigen modes, containing both real and imaginary parts [14].

Due to rapid improvements in computational power over recent decades, numerical solutions to dynamic analyses have become an attractive approach.

7.2.1. SOLUTION METHODS IN TIME DOMAIN

The response of the system may be evaluated as a function of time. This implies that the equations of motion are functions of space and time only. However, the hydrodynamic coefficients of added mass and hydrodynamic damping have been found to be functions of the frequency of motion. These frequency dependent variables, which constitute part of the fluid-structure system properties, may be evaluated at constant-frequency intervals or by use of a convolution integral [15]. Thus, allowing only for time as the field variable at given points in space, with the frequency dependence of the dynamic response being accounted for in the time domain analysis for the latter approach. The external loadings on the system are modelled as functions of time and position in space. Time-series for

modelling of the wave load on the floating bridge may be developed by a an extension of the multi-directional, three-dimensional wave field discretized in terms of summations of the wave loading in every degree of freedom of the system [4]. The time-series representing the wave load is considered a random time-domain stochastic process.

$$Q_W(x,y,t) = \Delta \sum_{i=1}^{n} \sum_{j=1}^{m} \eta_{0,ij} q_{ij} R_{ij} G(\theta) e^{-i\left(k_i \mathrm{x} \sin(\theta_j - \bar{\theta}) + k_i \mathrm{y} \cos(\theta_j - \bar{\theta}) - \omega_i t + \varphi_{ij} + \varepsilon_{ij}\right)}$$

The wave loading in a degree of freedom is allocated from an appropriate segment length, Δ, determined by the discretization of the model. The q_{ij}-term denotes the complex load amplitude associated with the frequency and mode of motion. ε_{ij} expresses the frequency dependent force phase. The R_{ij}-terms is introduced as a force-reduction factor for the oblique wave-angle-of-approach relative to the orientation of the bridge segment, $\bar{\theta}_j$.

$$R_{ij}\left(k_i, \Delta, \bar{\theta}_j\right) = \frac{\sin\left(k_i\Delta / 2\cos(\bar{\theta}_j)\right)}{\left(k_i\Delta / 2\cos(\bar{\theta}_j)\right)}$$

Based on the statistical properties of the environmental loading, one possible load situation is simulated. Time-series of the load process are generated randomly and applied to the system. At an instant in time, the total load situation is evaluated over the structure to obtain an instantaneous response. The possible realizations of the external loading, and the subsequent response situations of the system, are evaluated in time steps to constitute a collection of possible outcomes. This procedure may be accomplished by a Monte Carlo simulation [16], or an appropriate numerical integration technique can be implemented in the evaluation of each time step. Further statistics may be performed on this collection to determine mean and extreme values of response parameters of interest, as well as their corresponding standard deviations.

7.2.2. Solution methods in frequency domain

The response of the system may be sought through an analysis performed in the frequency domain. The dynamic equations of motion are transferred to the frequency-domain by considering both the loading on, and the response of the fluid-structure system as spectral processes associated with the corresponding stochastic time-domain processes. Such a transformation between time-domain and frequency-domain is generally governed by Fourier Transforms. For a zero-mean time variable, a Fourier Transformation expresses the process as a

summation of harmonic components with the Fourier constants a_k and b_k as amplitudes of the harmonicas [5].

$$x(t) = \int_{-\infty}^{\infty} a_x(\omega)\, e^{-i\omega t} d\omega$$

$$a_x(\omega) = \frac{1}{2}(a_k - ib_k)$$

The response quantities obtained in the frequency domain are thus regarded as the complex Fourier amplitudes, $a_x(\omega)$, of the corresponding time-domain representation.

Expressing the time-domain response, $x_r(t)$, and loading, $x_R(t)$, as summation of harmonic components results in the response and load components of the equation of motion being expressed in terms of frequency. The response and loading terms on the right hand side of the expressions, $r(\omega)$ and $R(\omega)$ are thus the complex Fourier amplitudes of the time-domain process.

$$x_r(t) = \int r(\omega)\, e^{i\omega t}\, d\omega$$

$$\dot{x}_r(t) = \int i\omega\, r(\omega)\, e^{i\omega t}\, d\omega$$

$$\ddot{x}_r(t) = \int -\omega^2 r\, e^{i\omega t} d\omega$$

$$x_R(t) = \int R(\omega)\, e^{i\omega t}\, d\omega$$

Inserting for the response and loading in the expression of the fluid-structure system equation of motion in time-domain, and cancelling the harmonic integration terms, renders the equation of motion for the frequency-domain dynamic analysis.

$$\left[-\omega^2\left(\mathrm{M}^{(s)} + M^{(h)}\right) + i\omega\left(C^{(s)} + C^{(h)}\right) + \left(K^{(s)} + K^{(h)}\right)\right] r(\omega) = R(\omega)$$

The frequency domain response, $r(\omega)$, may then be evaluated by the following expression.

$$r(\omega) = H(\omega)\, R(\omega)$$

$$H(\omega) = \left[-\omega^2\left(\mathrm{M}^{(s)} + M^{(h)}\right) + i\omega\left(C^{(s)} + C^{(h)}\right) + \left(K^{(s)} + K^{(h)}\right)\right]^{-1}$$

By the direct application of the system properties, the $H(\omega)$-matrix in frequency-domain, a general frequency response function can be determined to evaluate the response sensitivities of the system. Such a function may be considered a

frequency-domain equivalent to the time-domain free vibration response; providing the dynamic behaviour of the system disregarded any external forcing. This frequency response function may be viewed as an initial response spectrum. Expressing a mapping of the frequency-dependence, or frequency-sensitivity, of the response. Combined with a loading situation, representing the characteristics of the external load, the frequency response function is scaled and corresponding response amplitudes are obtained for the dynamic system. Large responses will thus occur if the evaluated response parameter of the system is sensitive to loading in the frequency range of the external oscillating load.

The frequency domain response solution may also be pursued by probabilistic means by evaluating the spectral densities of the load and response processes. Such an approach provides the population statistics of the dynamic response from the statistical parameters of the loading situation. The response of the system is expressed by a response spectrum, which may be statistically evaluated to determine extreme values and corresponding standard deviations of the responses. If the oscillating part of the external load is approximated as a zero-mean Gaussian process, oscillating over the quasi-static load configuration, the dynamic response of the bridge may be considered correspondingly. And the dynamic response of the floating bridge model is expressed through the spectral density of the response process.

The spectral density of the response contains the frequency domain properties of the response process and may be viewed as the frequency domain counterpart of the concept of variance. The definition of the single sided auto-spectrum of a time-dependent process, $x(t)$, is given by.

$$S_x(\omega) = \lim_{T\to\infty} \frac{1}{\pi T} [a_x(\omega) \cdot a_x^*(\omega)\,] = E[a_x(\omega) \cdot a_x^*(\omega)\,]$$

Where T denotes the time interval of the process and $a_x(\omega)$ represents the complex Fourier amplitude of the time-domain process. The asterix on the Fourier constant, $a_x^*(\omega)$, denotes the complex conjugate.

The response spectrum for the frequency-domain response is established correspondingly.

$$S_r(\omega) = E[r(\omega)\, r^{*\mathrm{T}}(\omega)]$$

$$S_r(\omega) = H(\omega)\, S_R(\omega)\, H^{*\mathrm{T}}(\omega)$$

Here, $S_R(\omega)$ is the load spectrum determined for the external loading process.

The load spectrum may be considered as a transfer function, relating the external loading process to the response process of the dynamic system. Other transfer functions may be developed to suit the purpose of the analysis, and can

represent the transfer from an external loading situation to virtually any response parameter of the system. Consequently, response spectrums may be developed to represent the displacements, velocities and accelerations in nodes, just as much as they may represent internal forces and moments in structural members.

The spectral densities of the response process may further be employed to estimate extreme value response parameters of the dynamic system. The standard deviation of the response process is determined by integration over the response spectrum of the response.

$$\sigma_r = \left(\int_{-\infty}^{\infty} S_r(\omega)\ d\omega\right)^{1/2}$$

The largest expected maximum response within a time interval, T, may be estimated by applying extreme value statistics.

$$E[\boldsymbol{r}_{max}] = \sigma_{\mathbf{r}} \left\{ \sqrt{2ln\left(T/T_Z\right)} + \frac{0.5772}{\sqrt{2ln\left(T/T_Z\right)}} \right\}$$

With the corresponding extreme value standard deviation determined from the expression.

$$\sigma[\boldsymbol{r}_{max}] = \sigma_r \frac{\pi}{\sqrt{6}} \frac{1}{\sqrt{2ln\left(T/T_Z\right)}}$$

The zero crossing period, T_Z, is determined from the spectral moments of the process.

$$T_Z = 2\pi \sqrt{\frac{m_0}{m_2}}$$

With the k'th spectral moment given from the response spectrum by the following expression.

$$m_k = \int_{-\infty}^{\infty} \omega^k\, S_r(\omega)\, d\omega$$

7.3. TIME DOMAIN ANALYSIS VS. FREQUENCY DOMAIN ANALYSIS

A time domain analysis is an intuitive approach to a dynamic response problem. Environmental effects, such as wind and waves, are often recorded as functions of time and the desired response parameters may be expressed likewise. Furthermore, second order terms may be included conveniently in the time step

analysis to account for non-linear effects of the system. A drawback of the time-domain analysis when evaluating a fluid-structure system is, however, the frequency dependent hydrodynamic coefficients. Another, more general, challenge to the time domain dynamic analysis arise due to the random realizations of the environmental load time-series. The time-dependent loading applied to the system at an instant is merely one possible realization based on the statistical properties of the load. The resulting load situation is not necessarily representative for the true load situation on the structure. However, the validity of the response can be evaluated by computing several realizations, based on the same statistical properties, for comparison. Producing the desired amount of data to obtain confident response results may nevertheless prove as a demanding numerical task.

During a frequency domain analysis the frequency content of the external loading forms the basis for the response estimation. The frequency domain approach encompasses the population statistics of the external loadings. A load spectrum will as a result not be one possible realization, moreover a representation of the entire loading situation presented as a function of frequency. The resulting response spectrum is thus a representation of the variance of the process as function of frequency. For a study in the field of hydrodynamics, the frequency domain approach may be considered preferable, due to the frequency dependence of the hydrodynamic coefficients. However, a main drawback of the frequency domain approach is the lack of simultaneous response parameter analysis. This affects the possibility to determine several response parameters for a specific loading situation. Consequently, the effect of simultaneously occurring internal forces and moments in a structural member may not be assessed easily in the frequency domain. Also, second order effects of a non-linear system are generally more troublesome to include in the frequency-domain analysis.

There are strengths and weaknesses to both approaches. One should employ the approach that best suits the purpose of the dynamic analysis. For hydrodynamic systems of assumed small excitations for which the analysis may be regarded linear, a frequency-domain analysis is likely to be favourable. Such an analysis will serve to provide information on the overall response of the system. For instance, revealing the natural frequencies and modes of motion, or expected accelerations and displacements at critical points. Thus, being a desired approach for an estimate of the behaviour of the structure for a typical serviceability limit state.

The time-domain analysis may be employed to determine the dynamic properties of the system for the same purposes as the abovementioned frequency-domain analysis. Though, a time-domain approach will generally be somewhat more computationally demanding for a hydrodynamic system. The

obvious advantage of the time-domain analysis is for an ultimate limit state evaluation of the structure. This becomes evident as non-linearity and the simultaneous occurrence of forces and moments in structural members may be readily assessed.

8. FINITE ELEMENT APPROACH TO DYNAMIC ANALYSIS

8.1. FINITE ELEMENT ANALYSIS OF A FLOATING BRIDGE

The dynamic analysis of the floating bridge model is performed through a finite element approach. The model is discretised by the use of three-dimensional finite beam elements with six degrees of freedom in each node. The mass and damping properties are considered constant over the length of each element in the analysis, but are presented herein to allow for variable properties over an element. The stiffness properties are determined from traditional Euler-Bernoulli beam theory, with shear strain excluded, and St. Venant theory is applied to determine the torsional stiffness of the elements. Loading on the fluid-structure system is evaluated over the exposed elements of the model, and included as nodal forces consistent with the element formulation of the floating bridge model. The area centre and the shear centre of the beam element cross-section are assumed to coincide. Thus, the axial and torsional displacements, as well as the bending degrees of freedom about the horizontal and vertical plane, may be considered uncoupled. This assumption is valid for double-symmetric cross-sections. Thus, the assumption is not completely valid for the adopted generic floating bridge model due to the superstructure cross-section not being perfectly axisymmetric. It is nevertheless considered as a good approximation and the assumption is kept to ease further computations.

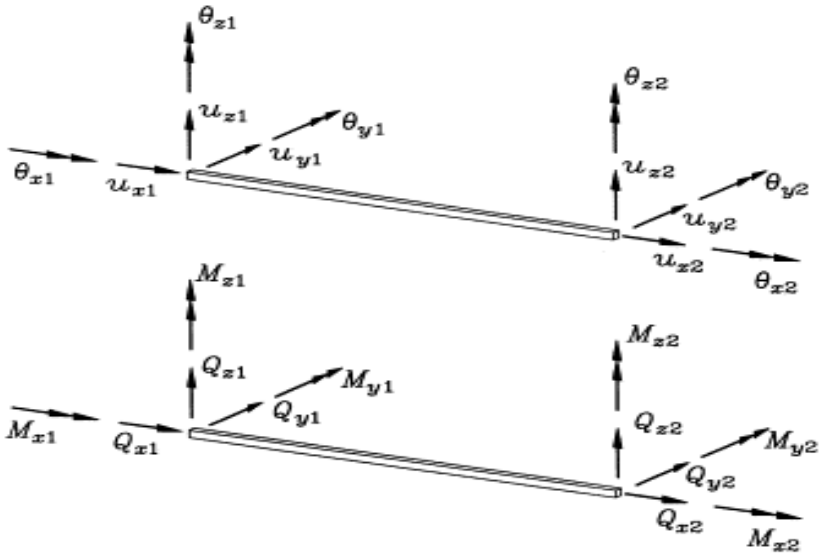

FIGURE 15 12DOF BEAM ELEMENT

As the outer dimensions of the floating bridge model are kept constant, an increase in the number of finite elements in use will lead to a more accurate solution to the dynamic problem. The response solutions obtained by the finite element method are considered to approach the correct values from below.

Meaning that the system will normally render response displacements smaller than the correct values. This is due to the assumed element deformations, which are interpolated by element shape functions. The essence of the finite element method is the piecewise polynomial interpolation over each element. Thus, a finite element can only describe a field variable to the same degree as the interpolation included in its formulation. These are either correct, or the elements are forced to deform different from the physical response, which result in an increased stiffness of the system [17]. For a dynamic system, an increase in stiffness is associated with an increase in the natural frequencies of motion.

A set of interpolation functions is employed as field variables to describe the field response of the beam element in terms of the nodal displacements, velocities and accelerations. The mass, damping and stiffness properties of the element are all described consistent with these interpolation functions. Thus, mass-, damping- and stiffness matrices are initially developed at the element level by integration over the element length. Structural parts with varying cross-sections or varying material properties over the element may be accounted for by introducing these parameters as field variables in the integration. Similarly, the same interpolation functions are utilized to allocate the distributed loading over the element to a corresponding nodal force vector. The property matrices of the element and the load vector are established in compliance with a column vector representing the degrees of freedom of the element.

The following expressions are employed for determination of the structural mass, damping and stiffness properties, and the load vector, for the elements employed in the floating bridge model. In these expressions, the cross-sectional area, $A_{cs}(x)$, the damping per unit length, $c(x)$, stiffness per unit length, $k(x)$, and the external loading per unit length, $q(x)$, may vary over the element.

$\boldsymbol{m}_{el}^{(s)} = \rho g \int \boldsymbol{N}^{\boldsymbol{T}}(x)\, A_{cs}(x)\, \boldsymbol{N}(x)\, dx$ - Element structural mass matrix

$\boldsymbol{c}_{el}^{(s)} = \int \boldsymbol{N}^{\boldsymbol{T}}(x)\, c(x)\, \boldsymbol{N}(x)\, dx$ - Element structural damping matrix

$\boldsymbol{k}_{el}^{(s)} = \int \boldsymbol{N}^{\boldsymbol{T}}(x)\, k(x)\, \boldsymbol{N}(x)\, dx$ - Element structural stiffness matrix

$\boldsymbol{R}_{el} = \int \boldsymbol{N}^{\boldsymbol{T}}(x)\, q(x)\, dx$ - Element consistent load vector.

The interpolation functions employed for the integration over the element, $\boldsymbol{N}(x)$, depend on which of the DOF's of the element the mass, damping and stiffness properties and external loading are associated with. The deformations over the element in the axial and torsional directions are interpolated by linear shape functions, as there are two DOF's in the element formulation describing each of these deformation modes.

$$\boldsymbol{N}_{linear} = \begin{bmatrix} 1 - {}^{x}/_{Le} & {}^{x}/_{Le} \end{bmatrix}$$

Hermitian interpolation functions are employed for the determination of the field displacement over the element associated with transverse deformations in the horizontal and vertical directions. This is a consequence of there being 4 DOF's at the element level governing each of the transverse responses.

$$\boldsymbol{N}^{T}_{Hermittan} = \begin{bmatrix} 1 - {3x^2}/{Le^2} + {2x^3}/{Le^3} \\ x - {2x^2}/{Le} + {x^3}/{Le^2} \\ {3x^2}/{Le^2} - {2x^3}/{Le^3} \\ -{x^2}/{Le} + {x^3}/{Le^2} \end{bmatrix}$$

The finite element model is constructed by connecting the element nodes to form the desired geometry of the physical structure. Elements with different geometry, material properties and loading are introduced to represent different parts of the structure. The degrees of freedom at a node shared by two, or more, elements are linked to ensure compatibility of the final model. Such a compatibility requirement is necessary for the model to represent the propagation of effects from one element to another. A common way to properly link the element DOF's to the DOF's of the finite element model is by the use of connectivity matrices. These matrices are developed for each of the elements included in the model and establish the following connection between the element DOF's and the global DOF's.

$$\boldsymbol{v}^{i}_{el} = \boldsymbol{a}^{i}\, \boldsymbol{v}_{Glob}$$

Where, $\boldsymbol{v}^{\boldsymbol{i}}_{el}$ is a vector representing the DOF's of element *i*, $\boldsymbol{v}_{Glob}$ is a vector containing the global DOF's and $\boldsymbol{a}^{\boldsymbol{i}}$ is the connectivity matrix linking the DOF's of element *i* to the global DOF's. If the element DOF's are oriented according to the global system axes, the connectivity matrices will contain simple one-to-one relations between the DOF's. As the connectivity matrices establish the relation between an elements DOF's and the global system, these may also be employed to obtain the element mass and stiffness properties, and element loading, in terms of the global DOF's. The global property matrices and the global load vector are obtained by summing over all elements, *N*, of the finite element model.

$\boldsymbol{M}^{(s)}_{G} = \sum_{i=1}^{N} \left(\boldsymbol{a}^{i}\right)^{T} \boldsymbol{m}^{(s)}_{el}\, \boldsymbol{a}^{i}$ - Global structural mass matrix

$\boldsymbol{C}^{(s)}_{G} = \sum_{i=1}^{N} \left(\boldsymbol{a}^{i}\right)^{T} \boldsymbol{c}^{(s)}_{el}\, \boldsymbol{a}^{i}$ - Global structural damping matrix

$\boldsymbol{K}^{(s)}_{G} = \sum_{i=1}^{N} \left(\boldsymbol{a}^{i}\right)^{T} \boldsymbol{k}^{(s)}_{el}\, \boldsymbol{a}^{i}$ - Global structural stiffness matrix

$\boldsymbol{R}_{G} = \sum_{i=1}^{N} \left(\boldsymbol{a}^{i}\right)^{T} \boldsymbol{R}_{el}$ - Global loading vector

The global property matrices and the global load vector are consistent with a column vector representing the global degrees of freedom of the finite element model.

The hydrostatic and hydrodynamic contributions to the system stiffness, damping and mass properties are obtained similarly as for the structural properties. The difference being that as every element in the model has structural properties, only the elements used in modelling parts of the structure in contact with the surrounding fluid will contribute with hydrostatic and hydrodynamic properties. The resulting hydrostatic stiffness and hydrodynamic mass and damping global matrices are consequently sparser matrices with more terms equal to zero.

$\boldsymbol{m}_{el}^{(h)}(\omega) = \; m_{hydro}(\omega) \int \boldsymbol{N^T}(x)\, \boldsymbol{N}(x)\, dx$ - Element structural mass matrix

$\boldsymbol{c}_{el}^{(h)}(\omega) = \; c_{\boldsymbol{hydro}}(\omega) \int \boldsymbol{N^T}(x)\, \boldsymbol{N}(x)\, dx$ - Element structural damping matrix

$\boldsymbol{k}_{el}^{(h)} = \; k_{hydro} \int \boldsymbol{N^T}(x)\, \boldsymbol{N}(x)\, dx$ - Element structural stiffness matrix

Here, $m_{hydro}(\omega)$, $c_{\boldsymbol{hydro}}(\omega)$ and k_{hydro} are the two-dimensional frequency dependent hydrodynamic added mass and damping coefficients per unit length and the hydrostatic stiffness per unit length, respectively. The development of the hydro-elastic elements employed in the finite element model is outlined in the subsequent section.

The global hydrodynamic property matrices are added to the structural property matrices to form the matrix formulation of the fluid-structure system in terms of finite element notation. The structural damping is considered to be negligible compared to the hydrodynamic damping contribution.

$$\boldsymbol{M}_G(\omega) = \boldsymbol{M}_G^{(s)} + \boldsymbol{M}_G^{(h)}(\omega)$$

$$\boldsymbol{C}_G(\omega) = \boldsymbol{C}_G^{(s)} + \boldsymbol{C}_G^{(h)}(\omega) \simeq \; \boldsymbol{C}_G^{(h)}(\omega)$$

$$\boldsymbol{K}_G = \boldsymbol{K}_G^{(s)} + \boldsymbol{K}_G^{(h)}$$

The equations of motion are established in a matrix format for evaluation according to the finite element approach. The matrix formulation is a set of coupled differential equations. The number of equations equals the number of DOF's of the discretized finite element model. In the general equation of motion of a fluid-structure system, the mass and damping properties are assumed being frequency dependent due to the addition of hydrodynamic added mass and damping. The external loading on the system, and the resulting response of the system, are considered functions of time at a given node. The load vector on the right hand side may include load effects from several types of loading.

$$\mathbf{M}_G(\omega)\ddot{\boldsymbol{r}}(t) + \boldsymbol{C}_G(\omega)\dot{\boldsymbol{r}}(t) + \boldsymbol{K}_G\boldsymbol{r}(t) = \boldsymbol{R}_G(t)$$

The elements that make up the finite element model will generally not have their local coordinate system oriented according to the global coordinate axes. The loading on the system and the resulting response of the complete model are, however, most favourably described in terms of the global DOF's. Transformation matrices are developed to describe the orientation in space of the local element coordinate system relative to the global axes. These are further employed to express the element properties in terms of global DOF's. The transformation matrices employed for linking the three-dimensional translational and rotational DOF's at a node is expressed as follows [18].

$$\boldsymbol{v}^i_{el,t,\theta} = \boldsymbol{t}_r\, \boldsymbol{v}_{Glob}$$

$$\boldsymbol{t}_r = \begin{bmatrix} \cos(x,\bar{x}) & \cos(x,\bar{y}) & \cos(x,\bar{z}) \\ \cos(y,\bar{x}) & \cos(y,\bar{y}) & \cos(y,\bar{z}) \\ \cos(z,\bar{x}) & \cos(z,\bar{y}) & \cos(z,\bar{z}) \end{bmatrix}$$

In the above transformation matrix, $\boldsymbol{t}_r$, the angles applied to the cosine terms are defined as the angles between the local element axes, $\{x, y, z\}$, and the global axes, $\{\bar{x}, \bar{y}, \bar{z}\}$.

The complete transformation matrix for the 12DOF element is thus expressed as a [4×4]-matrix with the $\boldsymbol{t}_r$-matrices on the diagonal.

$$\boldsymbol{T}_r = diag[\boldsymbol{t}_r]$$

A transformation matrix is developed for each of the elements having their local axes rotated from the global axes. The element property matrices, and the element load vector, are transformed to apply to the global coordinate axes by the following relations for element, *i*.

$$\overline{\boldsymbol{m}^i_{el}} = \left(\boldsymbol{T}_r{}^i\right)^T \boldsymbol{m}^i_{el}\, \boldsymbol{T}^i_r$$

$$\overline{\boldsymbol{c}^i_{el}} = \left(\boldsymbol{T}_r{}^i\right)^T \boldsymbol{c}^i_{el}\, \boldsymbol{T}^i_r$$

$$\overline{\boldsymbol{k}^i_{el}} = \left(\boldsymbol{T}_r{}^i\right)^T \boldsymbol{k}^i_{el}\, \boldsymbol{T}^i_r$$

$$\overline{\boldsymbol{R}^i_{el}} = \left(\boldsymbol{T}^i_r\right)^T \boldsymbol{R}^i_{el}$$

The terms within the transformed element property matrices and the transformed element load vector may then be allocated to properly apply to the global DOF's by the connectivity matrices incorporating the simple one-to-one relation between the element DOF's and the global DOF's.

8.2. DEVELOPMENT OF A HYDRO-ELASTIC BEAM ELEMENT

The hydrostatic and hydrodynamic restoring forces on a floating body are conveniently included as an integral part of the fluid-structure system properties. To include these effects efficiently in the dynamic analyses performed by a finite element approach, it is of interest to express them in a finite element format. As a result, the hydro-effects are introduced in the element formulation as functions of the nodal displacements and the element interpolation functions. From this, hydro-elastic matrices are obtained; containing the effects of the hydrostatic restoring stiffness and the hydrodynamic added mass and damping contributions related to the proper nodal DOF's. The hydro-effects are added properly into the purely structural property matrices of an element to form the complete hydro-elastic element formulation. The hydro-elastic elements are introduced for the parts of the floating bridge in contact with the surrounding fluid. A preliminary analysis of a single, freely floating hydro-elastic element is conducted to verify the hydrostatic stiffness contribution from rigid body displacements in the fluid. The procedure is included in the appendix A.2.

The basis for the development is the three-dimensional beam element with twelve degrees of freedom (3D-12DOF). Hermitian interpolation functions are employed for the transverse horizontal and vertical field displacement interpolation. While linear interpolation functions are in use for interpolation of the axial and torsional displacements over the element.

8.2.1. HYDROSTATIC ADDITIONAL STIFFNESS CONTRIBUTION

The hydrostatic additional stiffness contribution is exerted on a floating body as a function of its vertical displacement in the fluid, and is commonly referred to as the buoyancy. As the buoyancy force is proportional to displacement, it may be regarded as an additional stiffness contribution to the structural stiffness of the element. The hydrostatic stiffness is derived as the change in vertical force, ΔF_v, on a floating body as function of its change of position in the vertical plane, Δw. The hydrostatic stiffness contributions associated with different modes of motion were presented in section 6.3 of the thesis. The general expression for the hydrostatic restoring loading per unit length in mode *j* is reproduced below.

$$q_j^{(h)}(t) = k_j^{(h)} r_j(t)$$

The hydrostatic stiffness coefficients, $k_j^{(h)}$, are assumed in the following to be expressed in terms of stiffness per unit length over the elements.

The heave displacement of a beam element is described in terms of its nodal translational DOF's in the vertical z-direction and by the nodal rotational DOF's

in the x-z-plane. The vertical displacement at an arbitrary point on the element is determined by the nodal displacements in the vertical direction, $\boldsymbol{v}_z$, of the element and the proper interpolation functions, $\boldsymbol{N}_z(x)$, as field variables.

$$w(x) = \boldsymbol{N}_z(x)\, \boldsymbol{v}_z$$

The hydrostatic load on a beam element in the vertical z-direction may be derived by integration of the buoyancy force per unit length over the length of the element.

$$\boldsymbol{R}_z^{(h)} = \int_0^{Le} \boldsymbol{N}_z^T(x)\, q_z^{(h)}(x)\, dx$$

The buoyancy force per unit length over the element is a function of the displacement of the element, and may be expressed by the hydrostatic stiffness and the field displacement along the element.

$$q_z^{(h)}(x) = k_z^{(h)}\, w(x)$$

Inserting the above equations in the expression for the restoring force on a beam element results in the vertical hydrostatic stiffness contribution, $\boldsymbol{k}_{el,z}^{(h)}$, consistent with the finite element formulation of the floating bridge model.

$$\boldsymbol{R}_z^{(h)} = k_z^{(h)} \int_0^{Le} \boldsymbol{N}_z^T(x)\, \boldsymbol{N}_z(x)\, dx\ \ \boldsymbol{v}_z$$

$$\boldsymbol{k}_{el,z}^{(h)} = k_z^{(h)} \int_0^{Le} \boldsymbol{N}_z^T(x)\, \boldsymbol{N}_z(x)\, dx$$

The interpolation functions in use for the vertical field variable, $\boldsymbol{N}_z(x)$**,** are identical to the Hermitian interpolation functions in use for a two-dimensional, four degrees of freedom beam element with only vertical and rotational degrees of freedom at the nodes. The vertical hydrostatic stiffness contribution is thus stored in a [4x4]-matrix corresponding to the four vertical DOF's of an element. The additional stiffness contribution for pitch displacement of a pontoon is considered to be included in the formulation of the hydrostatic stiffness contribution in heave. The motivation for this assumption is the ability of the elements that model the pontoons to display vertical displacements over their length corresponding to pitch displacement.

For a structural part in the fluid with its length being of much greater size than its width, the developed vertical hydrostatic stiffness contribution may be considered sufficient to describe the hydrostatic restoring force on an element. The proposed model for the pontoon-separated floating bridge does however include pontoons that are close to quadratic in the water plane. As a result, it is considered necessary to also include the restoring moments arising from roll motion of the pontoons.

The roll displacement of an element is expressed by the rotational DOF's about the local element x-axis. As a pontoon is rotationally displaced about the longitudinal axis, vertical displacement over the width of the pontoon is determined as a function of the distance from the axis of rotation. Hydrostatic restoring moments will thus arise from a purely rotational displacement. The hydrostatic restoring moments on a hydro-elastic pontoon element is developed similarly as for the vertical restoring force.

$$\boldsymbol{R}_{\theta}^{(h)} = k_{\theta}^{(h)} \int_{0}^{Le} \boldsymbol{N}_{\theta}^{T}(x)\, \boldsymbol{N}_{\theta}(x)\ dx\ \boldsymbol{v}_{\theta}$$

$$\boldsymbol{k}_{el,\theta}^{(h)} = k_{\theta}^{(h)} \int_{0}^{Le} \boldsymbol{N}_{\theta}^{T}(x)\, \boldsymbol{N}_{\theta}(x)\, dx$$

As there are two DOF's of an element expressing the rotational displacement, the rotations over the element is interpolated linearly. The hydrostatic stiffness contribution from roll displacement is consequently stored in a [2x2]-matrix corresponding to the rotational DOF's at each node, $\boldsymbol{v}_{\theta}$.

The hydrostatic stiffness contributions are allocated properly in a [12×12]-element stiffness matrix to apply to the vertical and rotational nodal DOF's. Terms in the hydrostatic element stiffness matrix corresponding to other DOF's than the vertical and torsional remain zero. The hydrostatic stiffness contributions are added into the structural stiffness matrix of the element to form the complete hydro-elastic element stiffness matrix.

$$\boldsymbol{k}_{el}^{(h)} = \boldsymbol{k}_{el,z}^{(h)} + \boldsymbol{k}_{el,\theta}^{(h)}$$

$$\boldsymbol{k}_{el} = \boldsymbol{k}_{el}^{(s)} + \boldsymbol{k}_{el}^{(h)}$$

8.2.2. HYDRODYNAMIC ADDED MASS

The hydrodynamic added mass is considered proportional to the acceleration of motion of the floating body. The added mass depends strongly on the geometry of the body and will generally differ for the different modes of motion. The hydrodynamic added mass is therefore evaluated separately for the different directions of motion. The DOF's representing the vertical, horizontal and rotational motions are extracted to obtain systems describing single modes of motion for an element. The hydrodynamic loading on the element is evaluated by integrating the distributed loading over the element interpolation functions corresponding to each of the separate modes of motion.

$$\boldsymbol{F}_{mass,j}^{(h)} = \int \boldsymbol{N}_{j}^{T}(x)\, q_{mass,j}^{(h)}(x)\ dx$$

$$q_{mass,j}^{(h)}(x) = m_{jj}^{(h)}\,\ddot{r}_j(x) = m_{jj}^{(h)}\,\boldsymbol{N}_j(x)\,\ddot{\boldsymbol{v}}_j$$

The load per unit length on the element is determined by applying the two-dimensional added mass per unit length associated with motion in the *j*'th mode, $m_{jj}^{(h)}$, multiplied with the acceleration at an arbitrary point on the beam element, $\ddot{r}_j(x)$. The field acceleration is expressed by the nodal accelerations according to the finite element discretization. The hydrodynamic added mass matrix for the *j*'th mode of motion is extracted from the rewritten expression for the hydrodynamic loading associated with the acceleration of the body.

$$\boldsymbol{F}_{mass,j}^{(h)} = m_{jj}^{(h)} \int \boldsymbol{N}_j^T(x)\;\boldsymbol{N}_j(x)\,dx\,\ddot{\boldsymbol{v}}_j$$

$$\boldsymbol{m}_{el,j}^{(h)} = m_{jj}^{(h)} \int \boldsymbol{N}_j^T(x)\;\boldsymbol{N}_j(x)\,dx$$

The interpolation functions employed, $\boldsymbol{N}_j(x)$, are consistent with the element formulation of the *j*'th mode of motion and $\ddot{\boldsymbol{v}}_j$ is the nodal accelerations in the DOF's describing the *j*'th mode.

The common terms of the translational displacement in the y-direction and the torsional displacement of the element establish the coupled sway-roll motion for inclusion of the corresponding hydrodynamic added mass.

$$\boldsymbol{m}_{el,y\theta}^{(h)} = m_{y\theta}^{(h)} \int \boldsymbol{N}_y^T(x)\;\boldsymbol{N}_\theta(x)\,dx$$

The resulting added mass matrix contains off-diagonal terms in the positions linking the horizontal transverse displacement and the torsional displacement of the element. In addition, the heave motion due to rotation of the pontoon about the longitudinal axis is evaluated. This is done as a result of the nearly quadratic shape of the pontoons. Heave acceleration terms are developed as functions of the roll accelerations and the distance, *y*, from the rotational axis. The hydrodynamic moment due to roll is integrated over the width of the pontoons to represent a hydrodynamic loading in the heave direction as function of the roll acceleration.

$\ddot{\boldsymbol{v}}_z(y) = y\,\ddot{\boldsymbol{v}}_\theta$ - Heave acceleration as function of roll acceleration

$$\boldsymbol{F}_{mass,\theta}^{(h)} = m_{zz}^{(h)} \iint \boldsymbol{N}_z^T(x)\,\boldsymbol{N}_z(x)\,y\,\ddot{\boldsymbol{v}}_\theta\,dydx$$

$$\boldsymbol{F}_{mass,z\theta}^{(h)} = \frac{B_p m_{zz}^{(h)}}{4} \int_0^{Le} \boldsymbol{N}_z^T(x)\,\boldsymbol{N}_z(x)\,dx\;\ddot{\boldsymbol{v}}_\theta$$

Where B_p is the width of the pontoon. The added mass terms are added into the added mass matrix developed for heave motion at positions associated with roll motion.

The added mass contribution from the N considered modes of motion are allocated properly into [12x12]-matrices associated with each mode of motion, $\boldsymbol{m}_{el,j}^{(h)}$. The complete hydrodynamic added mass matrix for a 3D-12DOF element is obtained by summation of all the contributions.

$$\boldsymbol{m}_{el}^{(h)} = \sum_{j=1}^{N} \boldsymbol{m}_{el,j}^{(h)}$$

The mass matrix of a hydro-elastic element is finalized by adding the hydrodynamic added mass contributions to the structural mass matrix of the 3D-12DOF element. The hydro-elastic mass matrices are allocated properly in the global mass matrix by use of the connectivity matrices developed for the elements in contact with the surrounding fluid.

$$\boldsymbol{m}_{el}^{hydro} = \boldsymbol{m}_{el}^{(s)} + \boldsymbol{m}_{el}^{(h)}$$

$$\boldsymbol{M}_{G}^{(h)} = \sum_{i=1}^{m} \left(\boldsymbol{a}^{i}\right)^{T} \boldsymbol{m}_{el}^{hydro} \boldsymbol{a}^{i}$$

8.2.3. HYDRODYNAMIC DAMPING

The dissipation of energy associated with the radiation potential of a forced harmonic motion of a body in still water is proportional to the velocity of motion, and is as a result regarded as the hydrodynamic damping of the motion. This effect is included in a finite element format by considering the velocity at an arbitrary point along a beam element. The hydrodynamic damping coefficients are also strongly dependent on the geometry of the body, and generally differ for the different modes of motion. By employing the interpolation functions of the beam element for the different modes of motion, the field velocity is predicted through the velocity of the nodal degrees of freedom. As a result, a damping matrix for a beam element associated with the *j*'th mode is obtained by integrating the hydrodynamic loading associated with the velocity of the beam element over the interpolation functions in a similar fashion as was done for the added mass matrix.

$$\boldsymbol{F}_{damp,j}^{(h)} = c_{jj}^{(h)} \int \boldsymbol{N}_j^T(x)\ \boldsymbol{N}_j(x)\, dx\, \dot{\boldsymbol{v}}_j$$

$$\boldsymbol{c}_{el,j}^{(h)} = c_{jj}^{(h)} \int \boldsymbol{N}_j^T(x)\ \boldsymbol{N}_j(x)\, dx$$

The coupled effects of sway and roll motion, as well as the additional heave motion arising from roll motion, are included similarly as for the hydrodynamic added mass. The complete hydro-elastic damping properties are obtained by summing the damping matrices corresponding to all the N modes of motion associated with hydrodynamic damping and the proper connectivity matrices are employed to allocate the damping terms in the global damping matrix of the finite element model.

$$\boldsymbol{c}_{el}^{(h)} = \sum_{j=1}^{N} \boldsymbol{c}_{el,j}^{(h)}$$

$$\boldsymbol{c}_{el}^{hydro} = \boldsymbol{c}_{el}^{(s)} + \boldsymbol{c}_{el}^{(h)} \simeq \boldsymbol{c}_{el}^{(h)}$$

$$\boldsymbol{C}_{G}^{(h)} = \sum_{i=1}^{m} \left(\boldsymbol{a}^{i}\right)^{T} \boldsymbol{c}_{el}^{hydro} \boldsymbol{a}^{i}$$

For the modelling of the pontoons, additional hydrodynamic effects are included to incorporate the longitudinal surge motion of the pontoons. The longitudinal effects are considered necessary to include due to the nearly quadratic shape of the pontoons. The pontoons are modelled with four beam elements, but for the longitudinal direction the pontoons are considered as one element. Letting the axial degree of freedom of the first node of the first element, and the axial degree of freedom of the second node of the fourth element, represent the nodal displacements regarding the horizontal longitudinal motion. The hydrodynamic added mass and damping terms for surge motion is added into the mass and damping matrices of the pontoon sub-system at positions common to the two above-mentioned axial displacements. The added mass and hydrodynamic damping associated with pitch motion of the pontoons are regarded as included by the heave mode as the finite element formulation allows for pitch-type motion over the length of the pontoons.

The property matrices of the hydro-elastic elements are modified somewhat to represent the pontoon shape introduced to the finite element model of this report. The motivation for these alterations is, as previously stated, the nearly quadratic shape of the pontoons. Thus, modelling the pontoons by the original beam element formulation is considered as an overly rough estimate of their hydrodynamic behaviour. Disregarding the modifications, the hydro-elastic element formulation is however considered general, and may be employed to represent any floating structure.

8.3. Assembly of the global finite element model

The structural and hydro-elastic elements for the modelling of the floating bridge have been developed and transformed properly to apply to the global coordinate

system. Pure structural beam elements are introduced in the model for the parts that are not in contact with the surrounding fluid. These elements apply to the modelling of the entire superstructure bridge span as well as to the connector rod elements. The hydro-elastic elements incorporate the hydrostatic and hydrodynamic effects associated with the relative fluid-structure motion and are developed specifically for the modelling of the pontoons. All element property matrices have dimensions of [12 x 12] due to the twelve DOF's of each element.

The three-dimensional floating bridge model is initially divided into separate sub-systems. The bridge superstructure is considered as one sub-system and modelled as an arched beam in the x-y-plane. A pontoon-connector sub-system is developed to represent a floating pontoon with a stiff rod to represent the connection to the bridge superstructure. Pontoon-connector sub-systems are introduced to the superstructure sub-system at the positions of the pontoons to complete the model. The individual pontoon-connector sub-systems are oriented normal to the bridge span at the location of assembly.

The bridge superstructure sub-system is assembled by use of 24 purely structural beam elements. The DOF's of each element making up the bridge superstructure are related to the global coordinate system by the individual element transformation matrices. The transformed element property matrices are further assembled to form the property matrices of the superstructure sub-system by means of sub-system connectivity matrices, developed to link the element DOF's to DOF's of the sub-system. The element property matrices are referred to the global axes prior to the assembly of the superstructure sub-system. The coordinate system of the superstructure sub-system is chosen consistent with the global coordinate system of the model, resulting in the property matrices of the sub-system automatically being referred to the global axes. The total number of DOF's of the superstructure sub-system adds up to 150 due to 25 nodes along the bridge span.

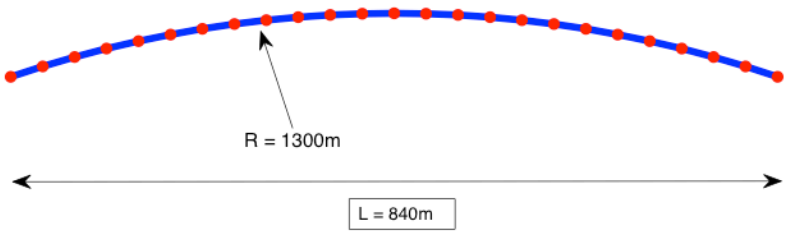

FIGURE 16 ARCH SHAPED FINITE ELEMENT MODEL OF BRIDGE SUPERSTRUCTURE

The pontoon-connector sub-system is developed by first assembling the elements of the sub-system in a local coordinate system. The assembly is performed by use of connectivity matrices developed to link the DOF's of the elements to the DOF's of the pontoon-connector sub-system. Four hydro-elastic elements are used for the pontoon-part of the sub-system, while a single, purely structural element is employed for the connector rod. Resultantly, the pontoon-connector sub-system property matrices include the hydrostatic and hydrodynamic effects expressed through the hydro-elastic elements. The property matrices of the pontoon-connector sub-system are of dimension [36×36] as there are a total of 36 DOF's describing the motion of the sub-system. The pontoon-connector sub-system is to be introduced multiple times along the bridge superstructure in the final model, each time with different orientation in space. Consequently, it is regarded favourable to develop the sub-system in the local element coordinate system at first. Then, transforming the property matrices of each sub-system to the global coordinate system according to the individual sub-system orientations. The transformation of each pontoon-connector sub-system is carried out similarly as was done for the transformation of the individual superstructure elements. A transformation matrix is developed for each of the pontoon-connector sub-systems, corresponding to the orientation of the local sub-system axes relative to the global coordinate axes. Throughout the model, the orientation of the pontoons is taken as the mean of the above superstructure elements that are connected in the common node as the pontoon-connector sub-system is introduced to.

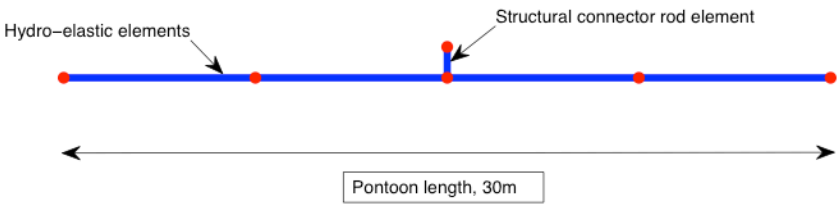

FIGURE 17 FINITE ELEMENT MODEL OF PONTOON-CONNECTOR SUB-SYSTEM

The final three-dimensional floating bridge model is achieved through assembly of the superstructure sub-system and the desired number of pontoon-connector sub-systems. This assembly is carried out by means of connectivity matrices. Individual connectivity matrices are developed for each of the sub-systems introduced in the final model and a single one for the superstructure sub-system, linking the DOF's of the sub-systems to the global DOF's. The property matrices of the sub-systems are transformed to apply to the global coordinate system in previous steps, resulting in a one-to-one relation between the sub-system DOF's and the DOF's of the floating bridge model. The global property matrices are of

dimensions [360×360] due to a total of 360 DOF's in the global model. The global property matrices are developed consistent with the numbering of the global DOF's.

A configuration that is considered to describe the physical landside-connections satisfactorily is introduced. The bridge span is assumed as a pinned simply supported beam with respect to the vertical plane. The translational and rotational DOF's associated with horizontal displacement in the global y-direction are set as fixed. Fixed connections are also introduced to restrain the torsional displacement at the landside points. No additional boundary conditions are introduced to the bridge span. The boundary conditions for the fluid-structure interaction at the pontoons are assumed described by the element formulation of the hydro-elastic elements.

9. METHODS OF ANALYSIS

A frequency-domain solution is applied for the response analysis of the floating bridge model. The dynamic equations of motion are transferred to the frequency-domain by considering both the loading on, and the response of the fluid-structure system as spectral processes of the time-domain processes. The dynamic analyses are assumed carried out over a sufficiently short time period for which the statistical properties of the sea state remain constant. Thus, the wave loading process may be regarded stochastic stationary. For all analyses carried out in this section the three-dimensional finite element floating bridge model has formed the basis for the structural properties. The structural damping is regarded negligible compared to the hydrodynamic damping contribution and is disregarded throughout the analyses. The boundary conditions are as described in the previous section. Where applicable, the dynamic analyses have been performed for different sea states.

The methods for the dynamic analyses are presented and discussed herein, while the findings are discussed in later sections and presented as appendices.

9.1. EIGENVALUE PROBLEM - UN-DAMPED MOTION

The initial study of the floating bridge model is performed as an Eigenvalue problem of the un-damped dynamic system. The damping is neglected and the natural frequencies and the corresponding natural modes of motion are determined from constant values of the mass and stiffness properties of the system. An Eigenvalue analysis is performed for the fluid-structure system, including the hydrostatic stiffness contribution and constant values of the hydrodynamic added mass. A second analysis is performed for the purely structural properties of the bridge model, excluding hydrostatic and hydrodynamic effects. The latter analysis may be termed as a “dry” analysis of the fluid-structure system, as the surrounding fluid is disregarded. The natural frequencies and corresponding mode shapes determined from the Eigenvalue analyses of the floating bridge model are presented in the appendices A.3 and A.4.

The equations of motion of the un-damped fluid-structure system are expressed time-domain as.

$$\boldsymbol{M}\ddot{\boldsymbol{x}}_r(t) + \boldsymbol{K}\boldsymbol{x}_r(t) = \boldsymbol{x}_R(t)$$

Assuming harmonic response and loading of the system.

$$x_r(t) = \int r(\omega)\, e^{i\omega t}\, d\omega$$

$$\ddot{x}_r(t) = \int -\omega^2 r\, e^{i\omega t} d\omega$$

$$x_R(t) = \int R(\omega)\, e^{i\omega t}\, d\omega$$

Where r and R on the right hand side represents the frequency-domain complex response amplitudes and load amplitudes of the harmonic time-domain response and loading, respectively. For the free response of the dynamic system, that is for no external loading ($\boldsymbol{R} = \boldsymbol{0}$), the un-damped equations of motion may be rewritten and expressed as.

$$[\boldsymbol{K} - \omega^2 \boldsymbol{M}(\omega_n)]\boldsymbol{r} = \boldsymbol{0}$$

Which has the non-trivial solution that forms the Eigen-value problem. The Eigen-value problem is in turn solved to obtain the natural frequencies, ω_n, and the corresponding mode shape vectors, $\boldsymbol{\Phi}(n)$, of the un-damped dynamic system.

$$[\boldsymbol{K} - \omega^2 \boldsymbol{M}(\omega_n)] = \boldsymbol{0}$$

The frequency dependence of the hydrodynamic added mass is illustrated in the above formulation, as an added mass value corresponding to the frequency ω_n is included.

The Eigenvalue analysis of the fluid-structure system will generally not include the frequency dependence of the hydrodynamic added mass. To allow for this frequency dependence, the proper hydrodynamic added mass is determined by iteration at each natural frequency. The hydrostatic buoyancy stiffness contribution from the surrounding fluid is included in the element formulation of the hydro-elastic elements. The stiffness contribution is regarded independent of the frequency of motion.

The number of natural frequencies and corresponding mode shapes that may be obtained through an Eigen-value analysis equals the number of DOF's of the dynamic system. As not all of these natural frequencies are considered of relevance to the dynamic response of the floating bridge, the natural frequencies are evaluated over a frequency range of $0 \leq \omega \leq 5\ [rad/s]$ for the fluid-structure Eigenvalue analysis.

The second Eigenvalue analysis is evaluated by the non-trivial solution of the free response of the purely structural system. Thus, the stiffness contribution and mass of the system remains constant throughout the analysis.

$$\left[\boldsymbol{K}^{(s)} - \omega^2 \boldsymbol{M}^{(s)}\right] = \boldsymbol{0}$$

The same number of natural frequencies and corresponding mode shapes are evaluated from the "dry" Eigenvalue analysis as was found within the prescribed

frequency range of the “wet” Eigenvalue analysis. This is motivated by the “dry” natural frequencies and mode shapes being considered merely of trivial significance to the true response of the fluid-structure system, and developed mainly for comparison to the “wet” response of the fluid-structure system. The comparison is nevertheless considered interesting as the effects of the hydrostatic stiffness contribution and hydrodynamic added mass may be assessed.

9.2. Frequency Response Functions (FRF’s)

The next solution method employed to estimate the dynamic response of the floating bridge model is by development of frequency response functions (FRF’s). The properties of the fluid-structure system are frequency dependent in both that the frequency of motion is included in the formulation and in that the hydrodynamic coefficients are frequency dependent. The frequency response function approach solves the response in each degree of freedom (DOF) from the fluid-structure properties at individual frequency steps. This allows for proper inclusion of the frequency dependent properties of the system. The results obtained from the frequency response function analyses are presented in the appendices A.5, A.6 and A.7.

The basis for the frequency response function approach is the damped equations of motion of the system, presented here in time-domain.

$$\mathbf{M}(\omega)\ddot{\boldsymbol{x}}_r(t) + \boldsymbol{C}(\omega)\dot{\boldsymbol{x}}_r(t) + \boldsymbol{K}\boldsymbol{x}_r(t) = \boldsymbol{x}_R(t)$$

The fluid-structure mass and damping matrices are regarded frequency dependent due to the inclusion of the hydrodynamic added mass and damping contribution. The response and loading of the fluid-structure system are considered harmonic, and the equations of motion may be expressed in frequency-domain as.

$$[\boldsymbol{K} - \omega^2\boldsymbol{M}(\omega) + i\omega\boldsymbol{C}(\omega)]\boldsymbol{r}(\omega) = \boldsymbol{R}(\omega)$$

This leads to the direct frequency response solution method by solving for the invers matrix of the fluid-structure properties.

$$\boldsymbol{r}(\omega) = \boldsymbol{H}(\omega)\,\boldsymbol{R}(\omega)$$

Where, $\boldsymbol{H}(\omega) = [\boldsymbol{K} - \omega^2\boldsymbol{M}(\omega) + i\omega\boldsymbol{C}(\omega)]^{-1}$

The $\boldsymbol{H}(\omega)$-matrix represents the frequency dependent properties of the fluid-structure system. These are stored in a matrix array of length equal to the number of frequency steps of the analysis. At each frequency step, the response values at DOF’s of interest may be extracted. As this is continued at each

frequency step, the responses as functions of frequency are obtained and evaluated over the frequency domain. The response of DOF *j*, for the *k*'th frequency step, $\boldsymbol{r}_{j,k}$, is thus obtained as the summation over the *j*'th row vector of the $\boldsymbol{H}\big(\omega(k)\big)$-matrix developed at frequency step $\omega(k)$**.**

$$\boldsymbol{r}_{j,k} = \boldsymbol{H}(j,1,k)\boldsymbol{R}(1) + \boldsymbol{H}(j,2,k)\boldsymbol{R}(2) + \boldsymbol{H}(j,3,k)\boldsymbol{R}(3) + \cdots + \boldsymbol{H}(j,N,k)\boldsymbol{R}(N)$$

Where *j* is the number of the DOF that the response is to be determined for, *k* represents the number of the frequency step, and N is the total number of DOF's of the system.

9.2.1. General FRF analysis

By introducing the load vector, $\boldsymbol{R}_{unit}$, as a frequency independent unit vector, each of the DOF's of the fluid-structure system is scaled with unit loading. That is, at every DOF throughout the system a unit force or moment is applied, depending on the DOF being translational or rotational. The frequency response functions (FRF's) developed may be regarded as general as they include all the response contributions scaled equally. Representing the system response sensitivity in every DOF regardless of the load situation. Though, a general FRF includes no information of the external loading situation and will consequently not depict the true response of the floating bridge exposed to an environmental loading. A general FRF will nevertheless reveal interesting characteristics of the fluid-structure system. A plot over the frequency domain of the response in a DOF will contain distinct peaks at the natural frequencies of motion associated with that DOF. Plotting the FRF's of the damped fluid-structure system together with the FRF's of the un-damped system will give an idea of the influence of the system damping on the response related to frequency and mode of motion. This damping may further be quantified at each frequency step to evaluate the frequency dependence of the hydrodynamic damping contribution.

9.2.2. Load-scaled FRF analysis

In the development of the general FRF's of the system, a constant unit load vector was employed to illustrate the dynamic properties of the fluid-structure system. Such a loading situation will hardly be an alternative to consider as the environmental loading on a floating bridge. The wave force transferred to a floating object is seen to generally be dependent on the frequency of motion. A frequency dependent load vector may thus be included in the equations of motion of the dynamic fluid-structure system to incorporate this effect. The response in every DOF of the system is calculated at individual frequency steps as discussed above, but now also including a frequency dependent load vector

which is to be determined at every frequency step. The total response of the dynamic system may then be expressed by the following expression.

$$\boldsymbol{r}(\omega) = \boldsymbol{H}(\omega)\, \boldsymbol{R}(\omega)$$

The frequency dependent load vector is built up by terms corresponding to the wave loading on the floating bridge. The wave loading on a floating object may be expressed by the surface elevation of a wave profile according to linear wave theory, combined with a frequency dependent complex load amplitude transfer function.

$$\boldsymbol{q}(\omega, t) = \overline{\boldsymbol{q}}(\omega)\, \eta_{unit}(\omega, t)$$

With $\eta_{unit}(\omega, t)$ being the expression for the spatial distribution of unit amplitude surface waves, and $\overline{\boldsymbol{q}}(\omega)$ being a vector of frequency dependent complex load amplitude transfer functions, corresponding to the modes of motion.

The approaching waves are assumed harmonic within the theory of linear waves. The harmonic term of the wave loading is thus cancelled towards the harmonic term of the response in the development of the response equations of the dynamic system in frequency-domain. As a result, the frequency dependent load amplitudes, $\overline{\boldsymbol{q}}(\omega)$, remain as the external loading of the system. The load amplitudes express load and moment per unit length of the exposed parts of the floating bridge for translational and rotational modes of motion, respectively. The frequency dependent wave loading is further expressed as a fraction of the maximum wave loading per unit length of a pontoon element by introducing the dimensionless load amplitude transfer functions.

$$\overline{\boldsymbol{q}}(\omega) = \boldsymbol{q}_{Wave}\, \overline{\boldsymbol{q}}_0(\omega)$$

$$\boldsymbol{q}_{Wave} = diag\left[q_{Wave,x}\ \ q_{Wave,y}\ \ q_{Wave,z}\ \ q_{Wave,\theta}\right]$$

$$\overline{\boldsymbol{q}}_0(\omega) = \left[\bar{q}_{0,x}\ \ \bar{q}_{0,y}\ \ \bar{q}_{0,z}\ \ \bar{q}_{0,\theta}\right]^{\mathrm{T}}$$

The $\boldsymbol{q}_{Wave}$-matrix contains the maximum wave loading per unit length for the different modes of motion on the diagonal and the $\overline{\boldsymbol{q}}_0(\omega)$-vector represents the corresponding dimensionless load transfer functions. Due to the nearly rectangular shape of the pontoons in the water plane, the wave load in surge motion is assumed expressed analogously to the wave loading in sway.

Only some of the DOF's of the floating bridge model will be exposed to loading from the oncoming wave field. These are the DOF's of the hydro-elastic elements utilized to model the pontoons of the floating bridge. The wave loading in the DOF's of the pontoon elements is determined by integrating the load amplitudes per unit length over the shape functions of the hydro-elastic pontoon elements.

Employing the Hermitian cubic interpolation functions for the heave and sway nodal loading, and linear interpolation functions for the surge and roll loading. The load vector of a 3D-12DOF hydro-elastic beam element, *m*, may then be developed consistent with the element formulation of the floating bridge model.

$$\boldsymbol{R}_m^{el}(\omega) = \int_{\mathbf{0}}^{Le} \boldsymbol{N}^{\mathrm{T}}\, \overline{\boldsymbol{q}}(\omega)\, dx$$

with $\boldsymbol{N^T}$ representing the interpolation functions of the element.

The element load vector terms are further allocated into the global load vector by use of the corresponding element connectivity matrices.

$$\boldsymbol{R}^G(\omega) = \sum_{N_{el}} \boldsymbol{a}_m^{\mathrm{T}}\, \boldsymbol{R}_m^{el}(\omega)$$

Resultantly, the load vector is modified to only contain terms at positions associated with the DOF's of surge, sway, heave and roll excitation of the pontoons. The response calculated in a DOF at frequency step, $\omega(k)$, is thus the response due to a single long-crested wave of unit amplitude at frequency $\omega(k)$. The oncoming waves are further assumed to excite every point of contact on the floating bridge equally at the same instant. This type of long-crested response analysis models the behaviour of the fluid-structure system with complete load correlation between the points of excitation.

9.2.3. Spatially scaled FRF analysis

The idealized long-crested response analysis is seen to generally overestimate the response of floating objects. This is easily understood by considering the real state of a wave field. Waves may approach from different angles, with different frequencies, and the wave crests are generally not seen to correlate well along the span of a floating bridge. Especially for larger floating structures, such as a floating bridge, the sea surface elevation is considered to show little degree of correlation between various points on the structure. This is due to the continuous process of adding and cancelling of wave components, which in turn make up the true sea state.

A procedure is proposed to distinguish the sea surface elevation at the positions of the pontoon elements for various angles of wave approach. From the arch shape of the floating bridge model, it becomes evident that a long-crested wave will not excite every point along the bridge span equally. As the wave crest passes the location of one pontoon, other pontoons may experience being in a trough, or more likely, in a position in between the crest and trough of the wave profile. Realizing that the local wave climate at each pontoon is likely to differ,

this needs to be taken into consideration in the response evaluation. Furthermore, as the frequency associated with the sea state increases, the wavelengths, λ, of the oncoming waves decrease. For angular frequencies in the vicinity of $\omega \simeq 1.5\ rad/s$ the wavelengths are of the same magnitude as the pontoon dimensions. Consequently, it is in addition considered necessary to evaluate the wave load distribution over each pontoon, as the wave loading on a single pontoon may only be considered uniform for a small part of the lower frequency interval.

To incorporate the spatial variation of the sea surface elevation along a linear wave, the three-dimensional spatial distribution term is included in the expression for the wave loading. The surface elevations at the hydro-elastic elements are determined as functions of their positions along the wave profile of the oncoming wave. Thus, the expression for the surface elevation is dependent on both the frequency and angle of approach of the long-crested wave. The load per unit length on a hydro-elastic element, m, may then be expressed as.

$$\boldsymbol{q}_m(\omega, \theta) = \overline{\boldsymbol{q}}_m(\omega)\, e^{-ik(x_m sin(\theta) + y_m cos(\theta))}$$

Where $k = \omega^2/g$ is the deep water wave number determined at each frequency step, x_m and y_m denotes the position of the centre of buoyancy of the hydro-elastic element, m, in the x-y-plane, and θ is the angle of approach of the long-crested wave. Thus, the wave loading at the centre of buoyancy of each hydro-elastic element constitutes the average wave loading over the element.

To include the possibility of long-crested waves approaching from any direction within the wave-angle-of-approach domain, $\{-\pi/2 \leq \theta \leq \pi/2\}$, an integration over the wave angle domain is performed. Thus, allowing for the adding and cancelling effect of the interfering waves. The spreading function is introduced to properly scale the interference effect according to the degree of multi-directionality of the sea state. The wave loading per unit length over an element, m, is then expressed as the maximum potential loading over the element, scaled by the frequency dependent dimensionless load transfer function and a spatial amplification coefficient, $q_{amp,m}$.

$$\boldsymbol{q}_m(\omega) = \boldsymbol{q}_{Wave,m}\, \overline{\boldsymbol{q}}_0(\omega)\, q_{amp,m}$$

$$q_{amp,m} = \int N_s cos^{2s}(\theta - \bar{\theta})\ e^{-ik(x_m sin(\theta - \overline{\theta}) + y_m cos(\theta - \overline{\theta}))} d\theta$$

The spatial amplification coefficient at element m, $q_{amp,m}$, is consistent with the expression for the three-dimensional surface distribution.

The forces and moments applied to the DOF's of the hydro-elastic elements that models the pontoons are resultantly determined individually at each element. These are incorporated consistent with the finite element formulation by the

interpolation functions of the element, and allocated properly into the frequency dependent global load vector by application of the corresponding connectivity matrices.

The response analysis is carried out similarly as for the previous load scaled frequency response analysis, but now with the spatial distribution coefficient included correspondingly to the element positions in space. The mean wave angle of approach is included to evaluate the response sensitivity to the direction of wave approach.

9.3. PROBABILISTIC RESPONSE ANALYSIS

A method of analysis for inclusion of the statistical properties of the actual sea state is proposed in this section. The oscillating part of the external load has been idealized as a zero-mean Gaussian process, oscillating over the quasi-static load configuration. Consequently, the dynamic response of the bridge may be considered correspondingly, and the dynamic response of the floating bridge model is expressed through the spectral density of the response process. The variances and standard deviations for response parameters of interest may be derived from the corresponding response spectrums. These are in turn employed to estimate the largest expected maximum responses and the associated extreme value standard deviations by employing extreme value statistics. The assumptions and procedures employed in the spectral dynamic response analysis are presented in the following. The results of the analysis are collected in the appendix A.8.

The complex Fourier amplitudes of the time-dependent response process are expressed by the wave loading process and the $\boldsymbol{H}(\omega)$-matrix, containing the fluid-structure properties, as presented earlier.

$$\boldsymbol{r}(\omega) = \boldsymbol{H}(\omega)\, \boldsymbol{R}(\omega)$$

The response spectrum of the fluid-structure system is expressed as.

$$\boldsymbol{S}_r(\omega) = E[\boldsymbol{r}(\omega)\, \boldsymbol{r}^{*\mathrm{T}}(\omega)]$$

$$\boldsymbol{S}_r(\omega) = \boldsymbol{H}(\omega)\, \boldsymbol{S}_R(\omega)\, \boldsymbol{H}^{*\mathrm{T}}(\omega)$$

Here, $\boldsymbol{S}_R(\omega)$ is the load spectrum determined for the wave loading process.

To assess and clarify the loading on the floating bridge from the complicated behaviour of a sea state, the load spectrum is developed at intermediate steps. The cross-spectral density of the three-dimensional sea state is initially described as an extension of the two-dimensional wave spectrum in frequency

domain. This modelling is considered applicable within the relatively short time-window of the dynamic analysis [13].

$$S_{\eta_i\eta_j}(\omega) = S_\eta(\omega) \int G(\theta)\, e^{-ik\left((x_i-x_j)\sin(\theta-\overline{\theta})+(y_i-y_j)cos(\theta-\overline{\theta})\right)} d\theta$$

The extension is introduced by the letting the cross-spectral density describe the sea surface related to any point within the spatial domain. Thus, η_i and η_j is the wave amplitudes at the positions (x_i, y_i) and (x_j, y_j) in space, respectively.

The wave load distribution over the pontoons is included consistent with the element formulation by inclusion of the spatial variation of the sea surface in the integration over the elements in a continuous format. The one-dimensional wave spectrum is kept out of the formulation. General element load vectors are consequently developed as functions of the element positions and their spatial extension in space.

$$\overline{\boldsymbol{R}}_m^{el} = \int \boldsymbol{N}_m^{\mathrm{T}}(s)\boldsymbol{q}_m(\omega) \int G(\theta)\, e^{-ik\left((x_m-s\sin\phi_m)\sin(\theta-\overline{\theta})+(y_m+s\cos\phi_m)cos(\theta-\overline{\theta})\right)} d\theta ds$$

In the above formulation (x_m, y_m) is the position in space of the first node of the element and ϕ_m is the element orientation relative to the global y-axis, measured positive counter clockwise. $\boldsymbol{q}_m(\omega)$ is the frequency dependent dimensional load transfer function and $G(\theta)$ is the spreading function modelling the multi-directionality of the sea state. Integrations are performed both over the wave-angle-of-approach domain and over the spatial extension of the elements, defined by the parameter *s*.

The motivation for excluding the one-dimensional wave spectrum, $S_\eta(\omega)$, from the above expression is the attempt to model a general loading situation on the fluid-structure system. The three-dimensional spatial structure of the waves is evaluated over the geometry of the floating bridge for unit amplitude waves of all frequencies and directions. The general loading situation may be modified within the spectrum analysis by application of relevant wave spectrums. A wave spectrum contains the spectral density of a sea state over the frequency content, and will scale the general load spectrum accordingly.

A spectrum representation of the general load configuration on the floating bridge is developed and regarded as a hydrodynamic transfer function. The hydrodynamic transfer function incorporates the load spectral densities at the points of load transfer as functions of frequency.

$$\boldsymbol{F}^{(h)}(\omega) = E\left[\overline{\boldsymbol{R}}_m^{el}(\omega)\, \overline{\boldsymbol{R}}_m^{el^{*\mathrm{T}}}(\omega)\right]$$

The hydrodynamic transfer function expresses the spatial sea surface distribution and kinematics as well as the frequency dependent load amplitudes

and the spatial orientation of the loaded parts of the fluid-structure system. Combination of the hydrodynamic transfer function with the dynamic properties of the fluid-structure system results in a transfer function for the response of the fluid-structure system.

$$\boldsymbol{\mathcal{F}}^{(h,s)}(\omega) = \boldsymbol{H}(\omega)\, \boldsymbol{F}^{(h)}(\omega)\, \boldsymbol{H}^{*\mathrm{T}}(\omega)$$

The fluid-structure transfer function establishes a relation between the response spectral density of the fluid-structure system and the spectral density of the spatial wave field distribution. The fluid-structure transfer function may be regarded as the spectrum analysis equivalent of the general frequency response functions. Auto-transfer functions for the unit amplitude sea state responses at desired degrees of freedom of the model may be extracted from the fluid-structure transfer function. Thus, revealing the general dynamic response sensitivity of the fluid-structure system. The spectrum representation of a loading situation representative for an actual sea state is achieved by introducing the corresponding one-dimensional wave spectrum.

$$\boldsymbol{S}_R(\omega) = \boldsymbol{\mathcal{F}}^{(h,s)}(\omega)\, S_\eta(\omega)$$

The complete response spectrum for the dynamic response of the floating bridge is consequently expressed by the following.

$$\boldsymbol{S}_r(\omega) = \boldsymbol{H}(\omega)\, \boldsymbol{\mathcal{F}}^{(h,s)}(\omega)\, \boldsymbol{H}^{*\mathrm{T}}(\omega)\, S_\eta(\omega)$$

For the practical dynamic analysis in terms of the finite element method, a response spectrum for the response in a DOF of interest is extracted from the complete response spectrum. The standard deviation and expected maximum value is then computed for the response in that DOF, by employing extreme value statistics.

The spatial correlation of the wave loading over the floating bridge is considered to be crucial in dictating the final response of the system. A quantification of the degree of correlation may prove as a valuable asset in evaluating the expected accuracy of the response computations. A coherence spectrum is as a result established to evaluate the relative magnitude of the wave loading at different points on the structure. The coherence spectrum is established from the hydrodynamic transfer function, as the spatial variation of the sea surface at the interface between the fluid and structure is expressed herein.

$$Coh_{\boldsymbol{F}_i^{(h)}\boldsymbol{F}_j^{(h)}}(\omega) = \frac{\left|\boldsymbol{F}_{ij}^{(h)}(\omega)\right|^2}{\boldsymbol{F}_{ii}^{(h)}(\omega)\boldsymbol{F}_{jj}^{(h)}(\omega)}$$

If the coherence spectrum values are seen to drop rapidly as function of distance in space, the wave loading process may be considered to show a low degree of

correlation over the structure. As a result, the computation of the hydrodynamic transfer function, $\boldsymbol{F}^{(h)}(\omega)$, may be performed more efficiently as only a narrow band around the diagonal needs consideration in the analysis. On the other hand, if the wave loading process exhibits a high degree of correlation, which is seen from the coherence spectrum if a large part of the values are close to unity, the full $\boldsymbol{F}^{(h)}(\omega)$-matrix is to be employed in determining the wave loading on the floating bridge.

In addition to quantifying the correlation of the wave loading process over the excited points on the floating bridge, a correlation of the response of the bridge is of great interest. A second coherence spectrum is developed for this purpose. Thus, applying the fluid-structure transfer function that relates the response spectral density to the wave loading spectral density. The coherence spectrum is developed for the heave response in the nodes along the bridge span, as function of both space and frequency.

$$Coh_{r_i r_j}(\omega) = \frac{\left|\boldsymbol{\mathcal{F}}_{ij}^{(h,s)}(\omega)\right|^2}{\boldsymbol{\mathcal{F}}_{ij}^{(h,s)}(\omega)\boldsymbol{\mathcal{F}}_{ij}^{(h,s)}(\omega)}$$

The coherence spectrum of the response is conveniently accompanied by a phase spectrum for the response over the bridge span. The phase spectrum is also expressed as function of distance in space and the frequency of motion, and is given by the following expression.

$$\Theta_{r_i r_j}(\omega) = \tan^{-1}\left(\frac{-Im\left[\boldsymbol{\mathcal{F}}_{ij}^{(h,s)}(\omega)\right]}{Re\left[\boldsymbol{\mathcal{F}}_{ij}^{(h,s)}(\omega)\right]}\right)$$

9.4. NUMERICAL ANALYSIS IN MATLAB

The numerical analyses performed throughout the report are computed by use of Matlab, with additional hand-calculations for verification of the computed results. Matlab is a numerical computing environment, written in the programming languages C and Java, and allows for convenient development of algorithms and performance of numerical analyses. The Matlab configuration facilitates the matrix-computations of the dynamic numerical model nicely. The properties of the fluid-structure system are introduced by their respective matrix-formulations and stored as functions in Matlab. The transformation and connectivity matrices employed for the assembly of the finite element model are introduced to the program and stored similarly. Spline interpolation functions are developed for the hydrodynamic coefficients to allow for extraction of values at intermediate frequency steps. The dynamic analyses are performed by

evaluation of the system properties at frequency increments. The structure of the analyses is constructed by storing sub-computations as independent functions and calling these when needed. The motivation for breaking the numerical analyses into sub-scripts is to obtain an orderly layout of the computation procedure and to ease troubleshooting. An additional advantage of the sub-script structure is the possibility of reuse, as a sub-script may serve several main-scripts. Thus, avoiding rewriting of identical scripts for different analyses.

Some of the numerical computations prove expensive with regard to computer time. This is especially experienced when computing the hydrodynamic transfer function, $\boldsymbol{F}^{(h)}(\omega)$. However, due to the Hermitian form of the hydrodynamic transfer function matrix, only the top right triangular of the matrix is computed initially. The matrix is completed by transferring the upper triangle across the diagonal. Letting the remaining terms assume values equal to the cross diagonal terms. This reduces the computational time, but the assembly of the hydrodynamic transfer function is still regarded a time-consuming process.

The scripts developed for the numerical dynamic analysis of the floating bridge model are included electronically as an appendix.

10. NUMERICAL RESULTS AND DISCUSSION

The results presented herein are considered to reflect the dynamic properties of the floating bridge structure within the assumptions of the theories applied in the development of each of the analyse methods. The results obtained from the dynamic analyses differ and their validity must be evaluated in light of the hydrodynamic model that forms the basis for each of the analyses. In the evaluation of the responses, the structural properties of the finite element model will be considered correct within the finite element approach and the hydrodynamic coefficients are assumed as applicable representations the pontoon-water interaction. Any shortcomings of the structural model, or from the hydrodynamic interaction effects in modelling the true behaviour of the system will be introduced similarly in all the analyses, and is thus considered as a minor source to the deviation in the responses. The exception being in the evaluation of the "dry" dynamic properties, where the hydro-effects is excluded. Consequently, the deviation in the response quantities obtained throughout the course of analyses may to a great extent be assigned to the modelling of the external load situation on the system. Hence, the validity of the analyses is in large part considered in line with the assumed validity of the modelled sea state.

10.1. EIGENVALUE ANALYSIS

The first evaluation of the dynamic properties of the floating bridge model was conducted by means of Eigenvalue analyses. The "wet" Eigenvalue analysis includes the hydrostatic stiffness contribution and hydrodynamic added mass, iterated at each natural frequency. The results are considered to reflect the correct dynamic properties of the fluid-structure system in terms of the natural frequencies and dictate the corresponding mode shapes of the bridge structure. This assumption is assumed valid within the restraints of the theory applied in development of the finite element model and the validity of the hydrodynamic added mass contribution. The "dry" Eigenvalue analysis reflects the purely structural dynamic properties of the system, and is expected to resemble the correct dynamic properties of the fluid-structure system. The deviation of the "dry" natural frequencies from those obtained by including the hydro-effects, reflects the contribution from the hydrostatic stiffness and hydrodynamic added mass on the dynamic system. The natural frequencies and corresponding mode shapes obtained from the "wet" and "dry" Eigenvalue analyses are presented in the appendices A.3 and A.4. The natural frequencies and the governing modes of response are reproduced in the table 4. The H, S, and R denote the mode of motion being in heave, sway or roll, respectively.

Natural Frequencies From Eigenvalue Analyses $[rad/s]$												
	ω_1	ω_2	ω_3	ω_4	ω_5	ω_6	ω_7	ω_8	ω_9	ω_{10}	ω_{11}	ω_{12}
"Wet"	0.335	0.905	1.338	1.413	1.712	1.827	2.340	2.934	3.209	3.642	4.198	4.358
Mode	S	S	H	H	H	S	H	S	H	S/H/R	S/H/R	S/H/R
"Dry"	0.143	0.339	0.581	0.913	1.306	1.827	2.320	2.934	3.583	3.930	4.359	5.108
Mode	H	S	H	S	H	S	H	S	H	S/H/R	S/H/R	S/H/R

TABLE 4 NATURAL FREQUENCIES FROM EIGENVALUE ANALYSIS

The "dry" Eigenvalue evaluation reveals two low frequency heave responses, which is not present among the fluid-structure natural frequencies. The hydrodynamic added mass is considered significant at low frequencies, which will result in an increase of the system mass and a softer dynamic behaviour. However, the non-dimensional added mass coefficient in heave drops steeply towards a value of 2 for $\omega \simeq 0.5\ rad/s$, and remains close to this value for the remainder of the frequency domain. Resulting in very high added-mass values only being apparent for very low frequencies of motion. Nevertheless, the hydrostatic stiffness contribution is considered to exceed the added mass contribution as the system shows a behaviour that reflects an increased stiffness, with an increase in the first natural frequencies in heave. This trend is seen for the first three natural frequencies for heave motion, which all is found as lower for the "dry" Eigenvalue analysis than what is obtained from the "wet" analysis. At the fourth natural frequency associated with heave, that is ω_7 of the system evaluation, the values for the two nearly coincides. Reflecting a fluid-structure system where the additional hydrostatic stiffness contribution is balanced by the hydrodynamic added mass. The high natural frequencies of the "dry" analysis are seen to increase more rapidly as compared to the values obtained from the "wet" analysis.

The increase in the natural frequencies is a result of an increased structural stiffness contribution associated with the assumed mode shapes. As the bridge span is "forced" to adopt mode shapes of increasing sinusoids over its length, the structural stiffness increases as the physical length of each buckle decreases. Though, for the "dry" system, the structural mass remains unchanged and the systems shows an increasingly stiffer behaviour. The development of the natural frequencies within the "wet" Eigenvalue analysis is analogous as the mode shapes are assumed as higher degrees of sinusoids as one move through the frequency domain. With mode shapes consisting of several sinusoids, some of the pontoons may be located in points of little or no displacement. Pontoons being located at a maximum displacement point is in addition displaced less than what would be the case at lower frequencies, as the relative amplitude of each buckle decreases with the increasing number of buckles. The hydrostatic

stiffness contribution is directly related to the relative vertical displacement of the bridge structure at the positions of the pontoons. Resulting in a reduced hydrostatic stiffness contribution to the system at high frequency natural modes. The higher value natural frequencies of the "wet" analysis are thus considered mainly governed by the structural stiffness. Though, the non-dimensional hydrodynamic added mass assumes a constant value of approximately 2 for the high frequency domain. Thus, the fluid-structure system behaviour at high frequencies shows a softer response as the added mass remains present with a constant value, while the hydrostatic stiffness contribution becomes negligible compared to the structural stiffness. The natural frequencies for heave motion resulting from the fluid-structure system properties are as a result seen as more closely spaced over the frequency domain. This is an expected characteristic for a floating bridge due to the interaction effects.

The natural frequencies associated with sway motion is seen to be affected little by the introduction of the hydro-effects. This is understandable from considering that there is no hydrostatic stiffness contribution in the horizontal direction, as a relative horizontal displacement of a pontoon in the water will not result in an altered pressure distribution over the wetted surface. In addition, the added mass in sway motion is generally considered low compared to what may be experienced for heave motion. Consequently, the natural frequencies in sway mode from the "dry" and "wet" analyses nearly coincides.

At higher frequencies, combined modes of heave, sway and roll motion are seen to prevail.

The effect of the fluid-structure interaction is considered of greatest significance for heave motion at low frequencies. In this frequency range, the dynamic behaviour of the system is mostly affected by the additional hydrostatic stiffness contribution. For heave motion at higher frequencies, and for sway motion, the hydro-effects are regarded to be of less importance. Generally, hydrodynamic effects are expected to decrease at higher frequencies as less energy is transferred at the fluid-structure interface. Also, the high frequency response properties are considered of less interest in a dynamic analysis of a large floating bridge structure excited by the wave climate, as the low frequency response properties are assumed to govern the response of the structure.

The effect of the hydrostatic stiffness contribution and hydrodynamic added mass is considered to be less for a pontoon-separated floating bridge than what would be the case for a similar continuous-pontoon design. This is due to the hydrostatic stiffness and added mass being linearly related to the water plane area of the floating body, which is notably less for the separated pontoons than for a continuous pontoon.

The natural frequencies obtained from the "wet" Eigenvalue analysis are considered valid for the floating bridge structure and serve as a mapping of the response sensitivity of the system. The actual response of the floating bridge needs evaluation in accordance with a loading situation, which is not included within the Eigenvalue analysis. Nevertheless, the system properties found are considered a good initial procedure, and will serve as a control for the subsequent analyses.

10.2 Frequency Response Function analysis

The next solution method employed for estimation of the dynamic properties of the fluid-structure system is in terms of frequency response functions. This procedure allows for proper inclusion of the frequency dependent hydrodynamic effects of added mass and hydrodynamic damping. Frequency response functions are developed within the finite element method to reflect the dynamic response in degrees of freedom of interest. As a FRF represents the response sensitivity in a single node on the structure, several FRF's should be developed to evaluate the response over the bridge span. The motivation for the development of several FRF's is that some nodes may be in points of little or no motion for a standing-wave sinusoidal mode shape, and may not reflect the overall bridge response. The emphasis of the analysis is on the heave response of the floating bridge.

The first approach was to develop general FRF's to map the response sensitivity at nodes of interest. Such an approach is expected to provide similar results as was found for the "wet" Eigenvalue analysis. The general FRF's developed for the response of the floating bridge finite element model is taken as heave motion at mid-point, L/4-point and L/8-point. The responses at these nodes are assumed sufficient to reflect the system response sensitivity for the frequency range of interest. Plots of the general FRF's for heave motion show distinctive peaks at three frequencies. The first is seen to be in the vicinity of both ω_3 and ω_4 from the Eigenvalue analysis, and reports the largest relative heave displacement sensitivity at mid-node. The second peak is seen to correspond to ω_5, and the last peak with ω_9. Plots of the general FRF's for heave motion at mid-point, and in the L/4- and L/8-points are presented in figure 18 for illustrative purposes. Figure number 19 illustrates the effect of the hydrodynamic damping as the un-damped responses at the natural frequencies exceed the responses of the damped system.

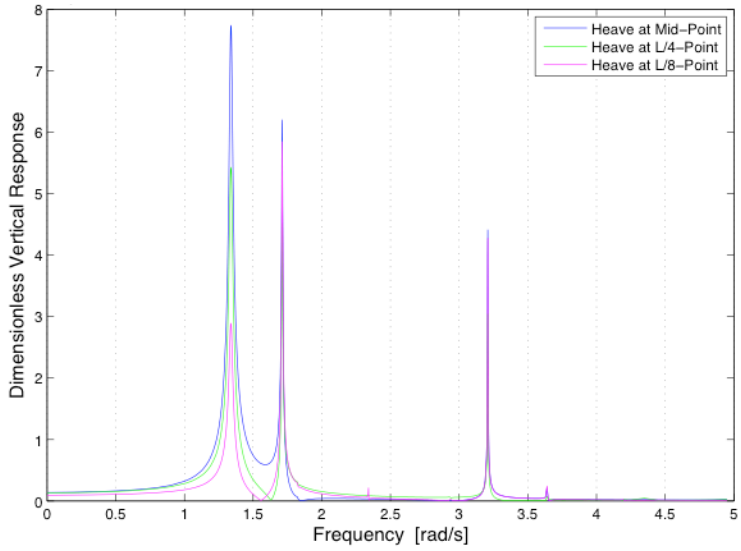

FIGURE 18 GENERAL FRF'S FOR MID-, L/4- AND L/8-POINT

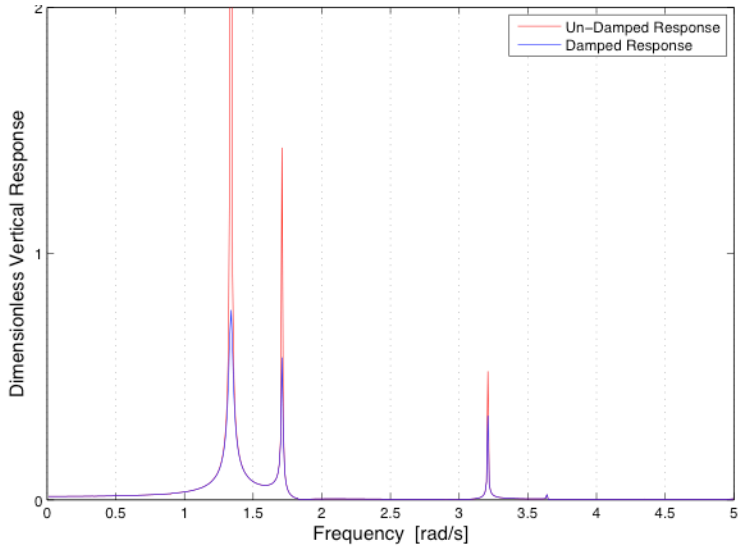

FIGURE 19 GENERAL FRF FOR UN-DAMPED AND DAMPED RESPONSE AT MID-NODE

The FRF's developed correspond well to the Eigenvalue results, with the exception of natural frequency $\omega_7 = 2.34\ rad/s$, which is barely present.

The next step of the FRF analysis was performed by the introduction of a frequency dependent load vector to modify the FRF's as to better reflect the wave loading process. The wave load transferred to the pontoons is assumed proportional to the displaced water volume times the wave amplitude of an oncoming wave as $\omega \to 0$. This represents an infinite wave and a rise in the surface elevation in every point equal to the wave amplitude. Thus, for a unit amplitude wave, the response of the bridge is expected to be in the range of

unity. As the energy transferred at the fluid-structure interface decrease with higher frequency, the wave loading on the floating bridge is expected to decrease as function of increasing frequency. The complex load transfer function was introduced to incorporate this effect into the load vector. The load-scaled frequency response functions are presented below. These are included to illustrate the effect of the frequency dependent load vector on the response peaks. Figure 20 illustrates the damped heave response in the mid-, L/4- and L/8-point, while figure 21 displays the effect of the hydrodynamic damping on the response peaks at mid-point.

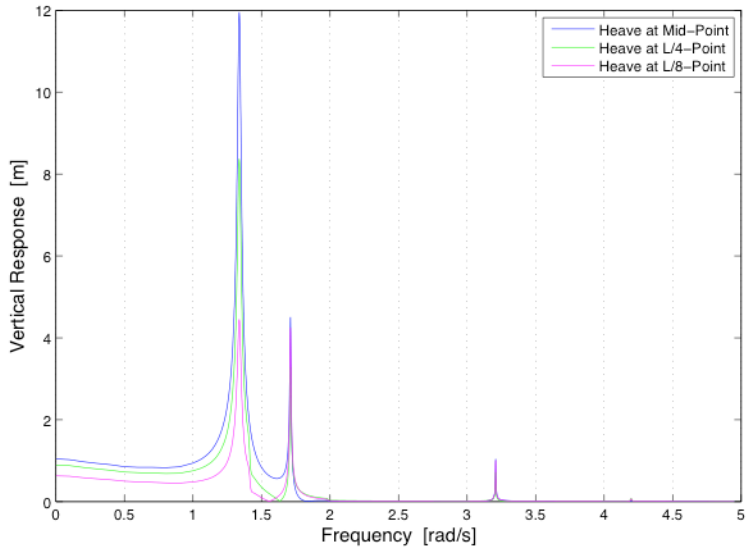

FIGURE 20 LOAD SCALED FRF'S FOR MID-, L/4- AND L/8-POINT

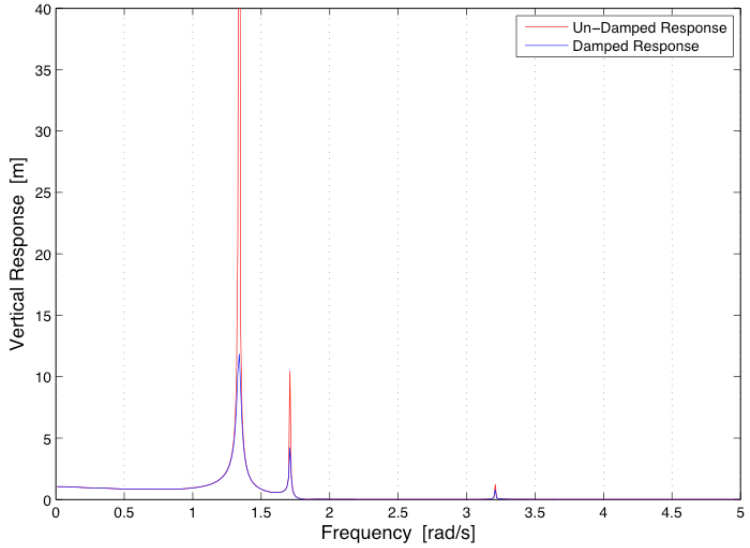

FIGURE 21 LOAD SCALED FRF FOR DAMPED AND UN-DAMPED RESPONSE AT MID-NODE

The load scaled FRF's display the same characteristics as the general FRF's. Peaks are present at the same frequencies, but are scaled according to the load transfer function. Thus, being greatly reduced at higher frequencies of motion.

The mid-point response is seen to equal unity for $\omega = 0$, which reflects the abovementioned expected heave response. The responses at the L/4-point and L/8-point are seen to be somewhat lower, decrease towards the end-supports. This seems reasonable as the restrained vertical displacements at the end-supports affects nodes that are closer more significantly.

The reported resonance response quantities are however not so reasonable. A vertical displacement of approximately 12 meters is seen as the heave maximum response for the mid node. Maximum responses of approximately 8 meters and 4 meters are registered for the L/4-point and L/8-point respectively. The large response quantities are considered to be of little relevance to the actual responses at the points of evaluation. The lack of validity of the responses from the load-scaled frequency response analysis is ascribed to the limited applicability of the modelled wave situation to the physical sea state. The loading situation is modified by its frequency dependence, but no description of the spatial variation of the sea surface is included. The model will as a result provide resonance responses for infinitely long-crested waves exciting every point on the structure equally. Such a wave field is not considered to depict the wave-loading situation on a floating bridge accurately.

Hence, the FRF's are further modified to include the spatial extent of the floating bridge relative to the wave profiles of the long-crested waves. The additional spatial modification of the load vector incorporates the positions of the wave-excited elements, used in the modelling of the pontoons, in the determination of the wave loading over each element. The wave loading over an element is taken as the extension of the value determined at the centre of buoyancy of each element. Thus, the wave loading on the floating bridge structure does not express the spatial surface variation over the length of an element, $L_{el} = 7.5$ meters, but includes a discretized variation over the pontoons by evaluating the surface elevation in four points over the pontoon length, $L_p = 30$ meters. Such a discretization of the surface elevation is considered to be of reasonable accuracy for the low part of the frequency domain, $\omega \leq 2.5\, rad/s$, corresponding to waves of wavelengths longer than the element length. For higher frequencies, the model is regarded unable to include the surface variation over the pontoons, and consequently the resulting total wave load over each pontoon.

The adding and cancelling effect of waves approaching from different angles is included by integration over the wave-angle-of-approach domain, $[\pi/2 \leq \theta \leq \pi/2]$. In the integration, the contribution from the oncoming waves is scaled by a spreading function, which describes the wave distribution around the mean wave angle of approach. The modelled sea surface is regarded as a good approximation of a wave field within the limits of linear wave theory, and the computed results are expected to provide more realistic response quantities. Plots and values of the response parameters reported for different combinations

of spreading index values and mean wave angles of approach are presented in the appendix A.7. The following figures, 22 and 23, are reproduced herein to illustrate the frequency response function responses obtained for spreading index values of $s = 3$ and $s = 15$, respectively, and a mean wave angle of approach $\bar{\theta} = 0$.

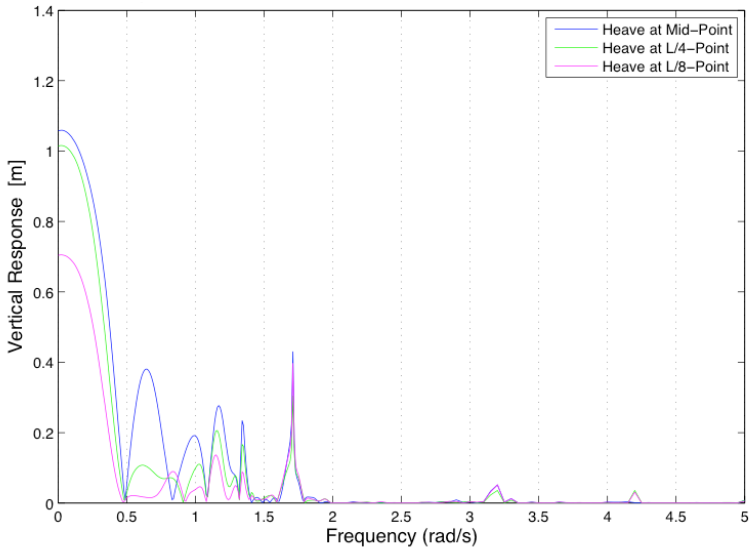

FIGURE 22 SPATIALLY SCALED FRF'S FOR MID-, L/4- AND L/8-POINT – S=3

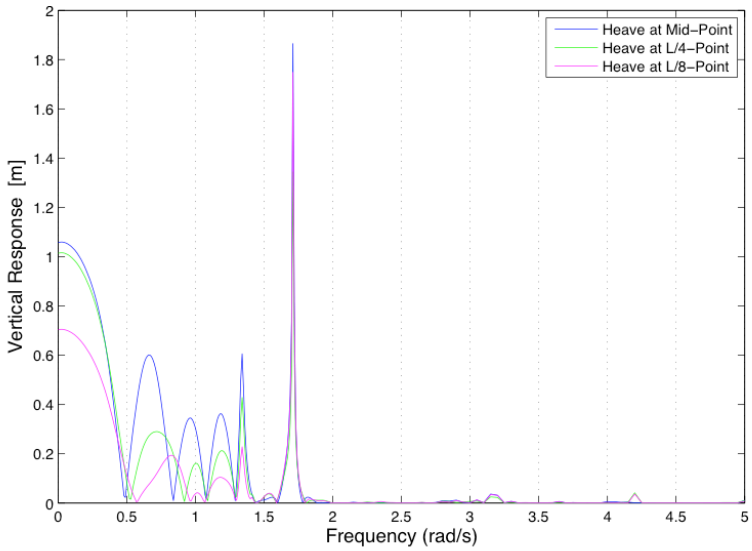

FIGURE 23 SPATIALLY SCALED FRF'S FOR MID-, L/4-, AND L/8-POINT - S=15

The FRF plots for the heave response at the mid-, L/4- and L/8-point of the floating bridge reveal the same distinctive peaks at the heave natural frequencies as seen for the previous analyses. The response peaks in the high frequency range are filtered down to negligible sizes as seen for the load scaled response

analysis. In addition, the FRF's contain disturbances between the peaks. These disturbances can be ascribed to the spatial distribution of the pontoons relative to the waves, which now excite points along the structure differently at a given instant. Thus, the excitation of the submerged parts of the floating bridge model is out of phase and shows a lower degree of correlation. This is as would be expected for a realistic sea state. The in-phase excitation at certain points along the structure is assigned to the random spatial structure of the oncoming waves. Defined by the frequency of the waves, the corresponding wavelengths may be in the range so that different points over the structure is in fact excited in phase.

The reported resonance response quantities are reduced significantly as compared to the foregoing FRF analysis. For $\omega = 0$ the responses are seen to remain close to unity, as would be expected. However, the degree of multi-directionality of the sea state, as dictated by the spreading index, is seen to affect the responses significantly. The frequency response functions computed for a spreading index value of $s = 3$, have a maximum displacement at $\omega = 0$, which is not exceeded at any point throughout the frequency range. Whereas, the frequency response functions computed for a spreading index value of $s = 15$, show a significant resonance response in the vicinity of natural frequency $\omega_5 = 1.7112\ rad/s$. A spreading index value of $s = 15$ corresponds to a sea state similar to that of long-crested waves approaching within a narrow-banded approach-angle domain. Hence, the wave excitation is affected to a little extent by the spreading function as the waves approaching from oblique angles are effectively filtered out, and the wave-loading situation will be governed mainly by the spatial extent of the pontoons in the mean wave angle of approach direction. A spreading index value of $s = 3$, includes waves within a much larger part of the wave angle of approach domain. Allowing for a higher degree of interference between waves of different properties. The largest mid-point resonance response amplitudes obtained from the numerical analysis is $r_{mid} = 0.430$ meters and $r_{mid} = 1.865$ meters for the spreading index values of $s = 3$ and $s = 15$, respectively, and a mean wave angle of approach $\bar{\theta} = 0$.

The effect of an oblique mean wave angle of approach is studied and the results presented in the appendix A.7. The responses found for the multi-directional sea state are seen to increase with an increase in the mean wave angle of approach, whereas the opposite is experienced for the more unidirectional sea state. The results are regarded in line with the linear wave theory applied in the development of the sea state. As the multi-directional sea state shows less symmetry, the interference of equal and opposite wave does not occur to the same extent as is the case for the symmetric sea state around a mean wave angle of approach of $\bar{\theta} = 0$. For the unidirectional sea state, the interference phenomenon is regarded insignificant and an oblique mean wave angle of approach models long-crested waves propagating partly along the structure.

Reduced response amplitudes seems reasonable due to the resulting decrease in the wave load correlation along the bridge span.

It becomes evident that the considered degree of multi-directionality of the actual sea state affects the resulting response quantities to a great extent. If the sea state may be considered to have a high level of multi-directional waves, the interference process is considered to provide a sea state that excites the structure with a low degree of correlation, and resultantly smaller response amplitudes are expected. The effect of the wave angle of approach is harder to quantify as the geometry and spatial extent of the floating bridge will affect the loading situation.

The response analyses carried out by the frequency response function approach have all been concerned with the application and extension of linear wave theory for determination of the wave loading on the floating bridge model. This is an intuitive and rather simple approach for estimating the response parameters of the dynamic fluid-structure system. The response of the system was eventually evaluated for a loading situation developed from a summation of unit amplitude long-crested waves of various approach angles over a prescribed frequency domain. The sea state applied is, however, a questionable description of an actual sea state. Further development of the wave field to better describe a physical sea state may be done by introducing long-crested waves of different amplitudes and frequencies corresponding to the wave spectral density at the site of construction. Though, such a modelling may prove as a tedious task to endeavour. A more attractive approach to include the statistical properties of a sea state is through the probabilistic response analysis, which is considered in the final part of the response analysis.

10.3. PROBABILISTIC RESPONSE ANALYSIS

A probabilistic method of analysis is considered as an accurate procedure for including the statistical properties of the actual sea state. Wave spectrums for measured sea states are readily applied in the response analysis, allowing for analyses of the fluid-structure system subjected to multiple sea states. Two different sea states are initially employed in the response computations. These are chosen to represent a sea state considered close to unidirectional and a sea state associated with a high degree of multi-directional waves.

Sea State Parameters						
Sea State No.	s	$T_p\ [sec]$	$H_s\ [m]$	$T\ [sec]$	$E\lvert H_{max}\rvert\ [m]$	$T_{m0}\ [sec]$
1	15	10	1	7200	1.9343	7.2999
2	3	3	1	7200	2.0557	2.7666

TABLE 5 SEA STATE PARAMETERS APPLIED FOR SEA STATES 1 AND 2

The spatial structure of the wave field is expressed in every point by the cross-spectral density of the three-dimensional sea state, which is included in the determination of the hydrodynamic transfer function. The wave load correlation may be studied as function of both space and frequency by evaluating the coherence spectrum of the wave loading process. In the following, plots of the coherence function with respect to loading in the centre pontoon of the floating bridge model are presented. The plots are presented as functions of the spatial distribution along the bridge span, and the frequency of the waves. The coherence functions are developed for different values of the spreading index, s, to evaluate the effect of multi-directionality. The coherence plots are assembled for values extracted at the element nodes of the hydro-elastic elements modelling the pontoons. Each narrow band of peaks displayed from the pontoon position axis represents the frequency dependent coherence values obtained at the corresponding pontoon nodes, with the mid-pontoon located at position 1. The hydrodynamic transfer function, $\boldsymbol{F}^{(h)}(\omega)$, does not include any information about the sea state between the pontoons, as it is assembled to model the load transfer at the points of the floating bridge being in contact with the fluid. Consequently, the coherence values between the narrow bands representing the pontoons at positions 1-4 may not be given any physical consideration as to represent the sea state between the pontoons.

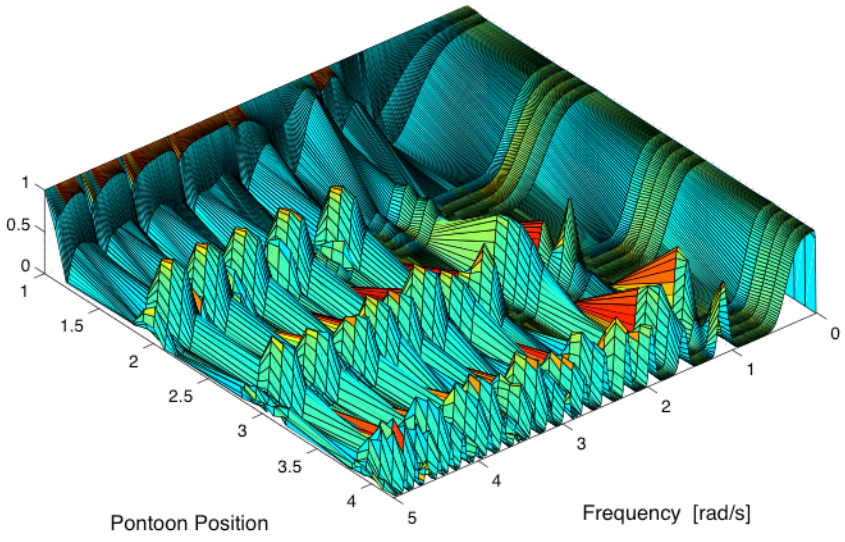

FIGURE 24 COHERENCE SPECTRUM FOR WAVE LOADING WITH RESPECT TO THE CENTRE PONTOON - S=15

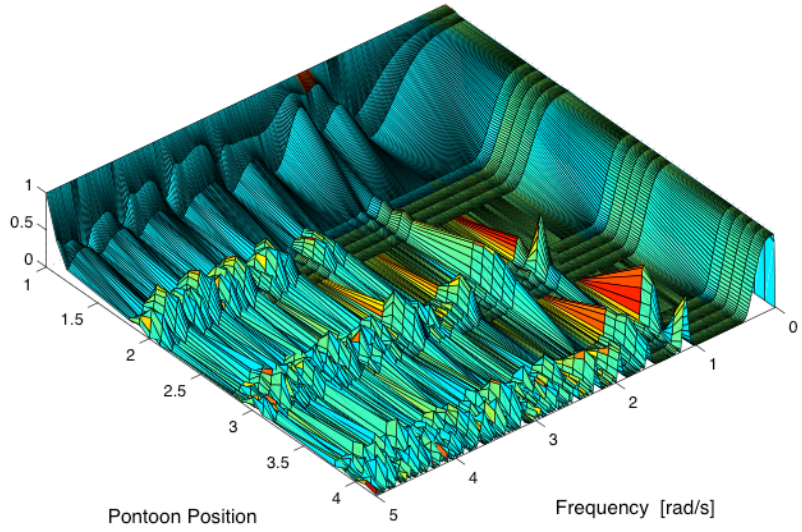

FIGURE 25 COHERENCE PLOT FOR WAVE LOADING WITH RESPECT TO THE CENTRE PONTOON - S=3

The coherence of the wave loading process is seen to generally drop with distance in space and for increased frequencies, as is expected. The high degree of spatial coherence for low frequencies of wave encounter, $\omega \to 0$, is an expected result as the wavelengths approach infinity and every point on the floating bridge structure is excited equally. As the frequency of wave encounter increase beyond $\omega \simeq 0.5\ [rad/s]$ the coherence is seen to generally be low and show a more random character of peaks appearing at certain frequencies. The peaks observed in the coherence spectrum illustrate an increased coherence at the nodes of the pontoons at the given frequencies. As the wave frequency dictates the wavelengths of the oncoming waves, it is seen that the wave loading on the pontoons shows a larger correlation at certain wavelengths. Which is regarded reasonable, as the wave field will have simultaneous surface elevation at certain points in space.

The coherence spectrum for the sea state considered with a low degree of multi-directionality, $s = 15$, generally displays higher values at the positions of the pontoons than what is seen from the sea state considered with a high degree of multi-directionality, $s = 3$. This is expected as a sea state associated with a low degree of multi-directionality is assumed to express a more homogeneous wave field. Thus, the coherence plots supports the theory employed in the development of the wave field and emphasizes the effect of an irregular, short-crested sea state as the wave loading over the structure is considered to show a low degree of correlation for the multi-directional sea state. If the wave loading from an actual sea state at a site of construction shows similar low values in the coherence plot for a short separation in space, the loading processes at each pontoon may be regarded uncorrelated with sufficient accuracy an simplify the dynamic analysis. The physical interpretation of this assumption is that the wave

loading on a pontoon contributes little to the total wave loading on other pontoons of the structure.

The results from the probabilistic analysis are presented in the appendix A.8 accompanied by plots of auto-transfer functions of the heave response at certain nodes and plots of the auto-spectral densities of selected responses. Large deviations are seen for the response quantities obtained from the two evaluated sea states, with the response from the unidirectional sea state completely governing the combined response analysis. The response characteristics of the bridge span subjected to the different sea states are evaluated by employing the coherence spectrums for the heave response. A coherence spectrum for the response describes the relative correlation between the responses in different points on the structure as functions of the frequency of motion. The coherence spectrums presented on the following pages are developed with respect to the response at the mid-point of the bridge span. The mid-point response is evaluated against the response characteristics at the nodes of the finite element model over half the bridge span towards a landside. The coherence spectrums for the response are followed by plots of the corresponding phase spectrums, displaying the phase of the motion at the nodes along the bridge span relative to the phase of motion in the mid-point. The coherence spectrums are developed from the fluid-structure transfer function and incorporate the spectral density of the waves and the fluid-structure properties. The spectrums are developed for different values of the spreading index and does not incorporate the one-dimensional wave spectrum associated with a given sea state. Consequently, the coherence spectrums are viewed in terms of the response sensitivities of the floating bridge subjected to a general wave field with a predetermined degree of multi-directionality.

Coherence and phase spectrums for sea state 1

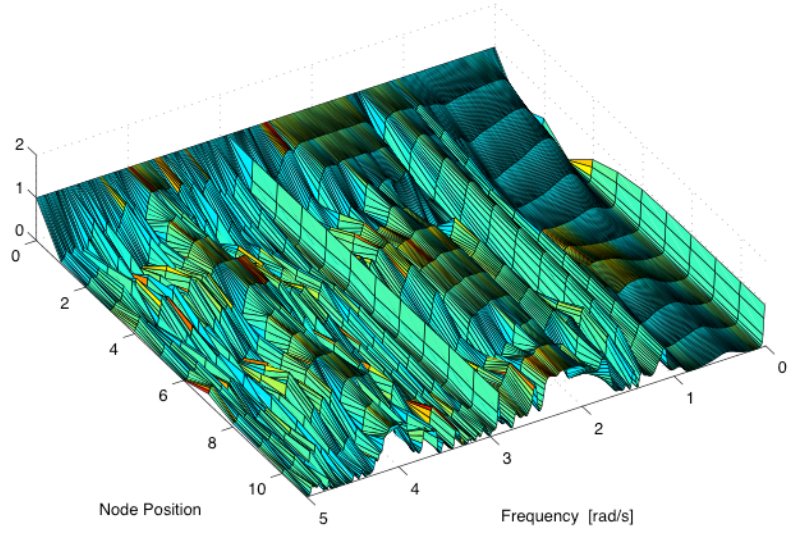

FIGURE 26 COHERENCE SPECTRUM FOR HEAVE RESPONSE WITH RESPECT TO THE MID-POINT - S=15

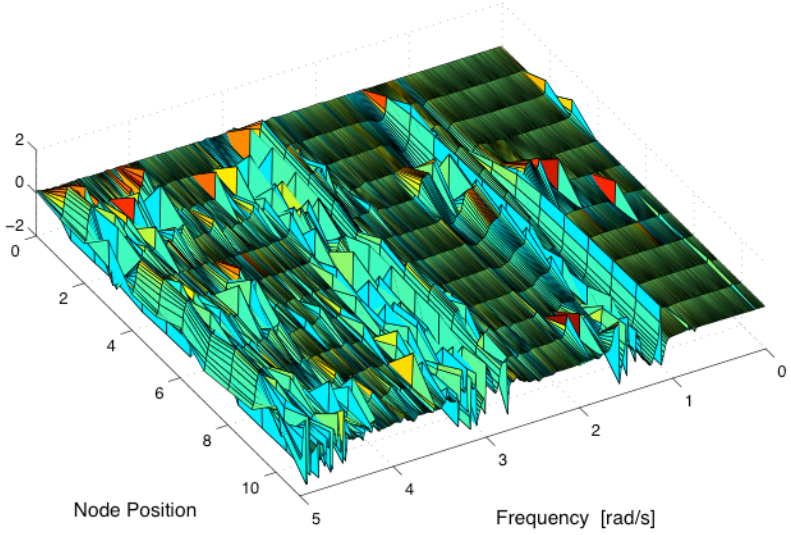

FIGURE 27 PHASE SPECTRUM FOR HEAVE RESPONSE WITH RESPECT TO THE MID-POINT - S=15

Coherence and phase spectrum for sea state 2

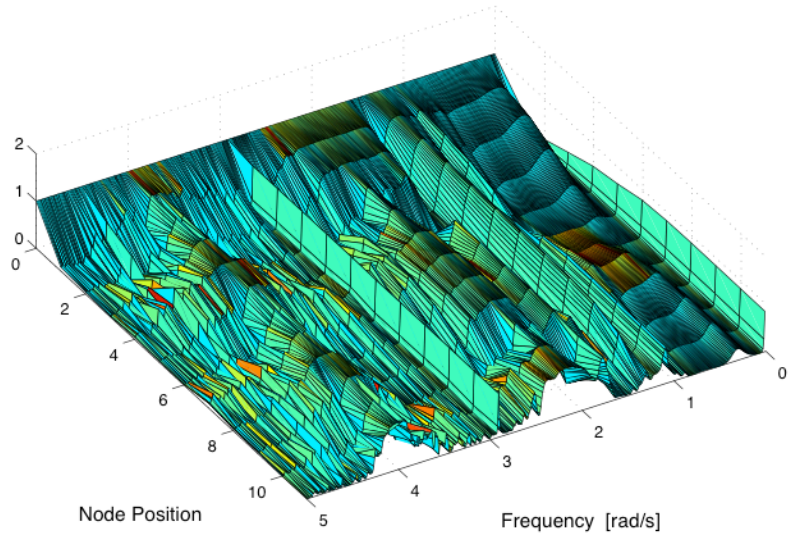

FIGURE 28 COHERENCE SPECTRUM FOR HEAVE RESPONSE WITH RESPECT TO THE MID-POINT - S=3

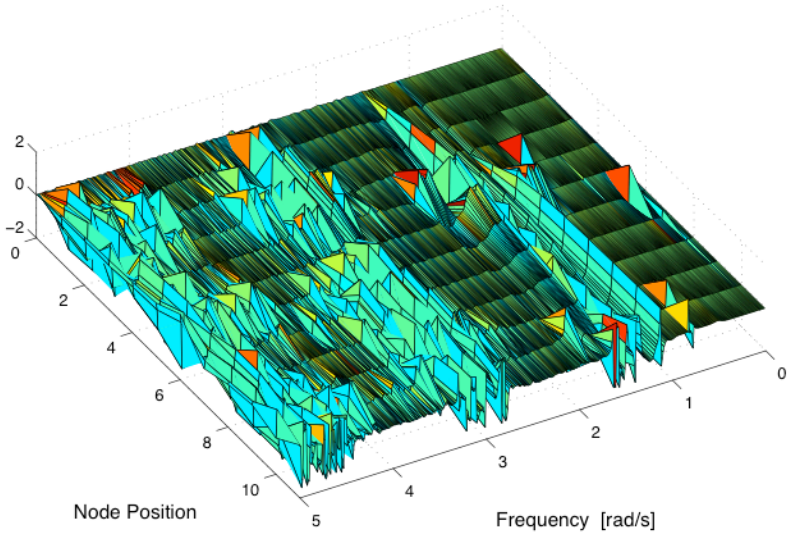

FIGURE 29 PHASE SPECTRUM FOR HEAVE RESPONSE WITH RESPECT TO THE MID-POINT - S=3

The coherence spectrums for the heave response over the bridge span are seen to show a significant response correlation at zero-frequency and frequencies associated with the natural modes of motion. This supports the validity of the numerical model and the physical assumption of resonance response. The phase spectrums reveal significant out-of-phase motion over the bridge span for the same frequencies. By evaluating the phase spectrums at frequencies associated with natural modes of motion of interest, the shape of the mode shape can be determined. At zero-frequency, the coherence spectrums display a correlated response over the bridge span, while the phase-spectrums show no out of phase motion. Thus, the correlated heave displacement of the entire bridge associated with a wave of infinite wavelength is considered represented accurately.

Due to the domination of the first sea state in evaluation of the response for the combined sea state, a second set of sea state parameters is introduced. The new sea states are modified somewhat from the extremes of the previous sea states. These are nevertheless still considered to model one close to unidirectional sea state associated with swell waves, and one multi-directional sea state representing a more confused and irregular state. The computed results for the new set of sea states evaluated separately and combined are included in appendix A.8, followed by plots of their respective response spectral densities.

Sea State Parameters						
Sea State No.	s	$T_p\ [sec]$	$H_s\ [m]$	$T\ [sec]$	$E\lvert H_{max}\rvert\ [m]$	$T_{m0}\ [sec]$
3	12	8	1	7200	1.9610	5.9279
4	5	4	1	7200	2.0333	3.3254

TABLE 6 SEA STATE PARAMETERS APPLIED FOR SEA STATES 3 AND 4

The response calculations performed for the second set of sea states results in lower responses for the close to unidirectional sea state, and an increase in the responses from the multi-directional sea state, as would be expected. However, sea state 3 is still seen to govern the total the response of the floating bridge, though not as completely as was seen for the previous set of sea states. Clearly, the peak period of the sea state affect the total response of the floating bridge. The shape of the auto-transfer functions supports this assumption, as high function values are displayed at low frequencies. At frequencies exceeding $\omega \simeq 1.5\, rad/s$ the auto-transfer function values become negligible.

11. CONCLUSIONS AND FURTHER RECOMMENDATIONS

11.1. CONCLUSIONS

The effects of the fluid-structure interaction are found to dictate the low frequency natural modes of the floating bridge. As the response characteristics of large floating structures are regarded governed by corresponding low frequencies of motion, the development of a proper hydrodynamic model for the fluid-structure system is considered a primary task for the dynamic evaluation of a floating bridge. The hydrodynamic model forms the basis for the subsequent response analysis and a lack of accuracy herein is assumed to greatly affect the validity of the computed responses.

Secondly, the procedure for describing the hydrodynamic wave load situation is found to be of great significance to the responses of the floating bridge. The structural properties of the generic bridge model are readily assessed and are constant and equal for the hydrodynamic response analyses performed. The hydrodynamic restoring forces are included in the formulation of the hydrodynamic model, and is consequently introduced consistent for the analyses. The methods of analysis employed for investigating the dynamic behaviour is nevertheless seen to greatly dictate the computed results. Hence, the large deviations in the computed responses are assigned to the assumptions and discretization employed in the modelling of the wave fields.

The initial attempt to model the wave field in terms of long-crested, unidirectional waves provided unrealistic, but expected, large response amplitudes. As the wave field was modified in terms of the load transfer coefficients, the spatial distribution of the pontoons relative to the wave field, and the inclusion of multi-directional waves, the computed resonance responses ware seen to decrease significantly. If the wave field is modelled with a low degree of multi-directionality, it approaches the unidirectional long-crested sea state as the spreading function approaches the Direc-Delta function, and it is considered of little relevance to a realistic sea state. However, the proposed wave field considered for the spatially scaled frequency response analysis is regarded as a fairly good approximate for short-crested sea states when modelled with a high degrees of multi-directionality. The major drawback of the wave field would be the lack of inclusion of relevant sea state parameters. The wave field is constructed from superposition of scaled unit-amplitude waves of all frequencies, not including the probability density representing an actual sea state variation.

The wave spectrums for an actual sea states is conveniently included in the probabilistic response analysis. Resulting in this method being regarded as the most accurate of the proposed analyses. The cross-spectral density of the surface

waves are expressed with the basis in the superposition of scaled unit-amplitude waves similar as for the final frequency response analysis. Thus, the general procedure for describing the spatial structure of the wave field is not considered to deviate significantly for the two. The major difference is introduced by the inclusion of the wave spectrum for the latter procedure.

Throughout the course of analyses, it has become evident that a proper hydrodynamic model and the introduction of a realistic short-crested sea state is vital in order to obtain reliable dynamic responses of a floating bridge structure. This is supported by the consistent decrease in resonance response amplitudes for increasingly refined wave field models. Thus, allowing for a more economical design of the floating bridge, as the resulting loading on the structure is determined more accurately. A proper dynamic analysis is in turn considered crucial when considering a floating bridge alternative to provide justice to the feasibility of the design.

11.2 Further recommendations

The evaluation of the dynamic behaviour and feasibility of a floating bridge design incorporates a high level of interdisciplinary tasks. Knowledge within the fields of structural engineering, structural dynamics and naval engineering is necessary to assess the properties of the fluid-structure system. In addition, accurate real life recordings of the environmental effects and the corresponding determination of critical parameters for design are important in order to describe a representative sea state at the site of construction. As a result, the list of aspects to consider more thoroughly for a floating bridge design may be close to endless. However, the recommendations for further study herein are limited to highlight two aspects, which are considered of relevance to the work and discussions performed in throughout this thesis.

Firstly, the hydrodynamic effects between the fluid and the submerged parts of the structure are considered to be strongly dependent on the geometry of the floating bodies and the potential influence from nearby objects. To accurately describe the fluid-structure interaction for a floating bridge design, a three-dimensional potential flow model should be applied to the relevant geometries of the pontoons, including their relative separations in space for assessing interactional effects. A properly scaled model test of the bridge design may further be employed to verify the computations.

Secondly, the description of the wave field that is considered to form the main loading situation on a floating bridge is regarded a challenging task. The wave field is continuously changing in time and space, and the mathematical models for describing the propagation of surface waves are merely approximates. Deep-

water waves are considered fairly accurately described within linear wave theory, though large deviations must be considered to occur in costal regions. From this, a study of interest is the application of higher order wave theories in the development of the sea state. The motivation for this is an attempt to model the surface waves more in line with the characteristics seen for real waves. With narrower, sharper crests and longer, shallower troughs, than what is modelled by applying first order linear wave theory.

LIST OF REFERENCES

[1] Wikipedia. [10.02.2012] http://en.wikipedia.org/wiki/Pontoon_bridge

[2] Vugts, J.H. The Hydrodynamic Coefficients for Swaying, Heaving and Rolling Cylinders in a Free Surface. International Ship-builder Programme. 1968;15.

[3] Zhang et.al. Analytical models of floating bridges subjected by moving loads for different water depths. ScienceDirect. 2008;20(5)

[4] Morris. E. et.al. Frequency Domaint Dynamic Analysis of a Floating Bridge. Coastal Structures. 2003.

[5] Strømmen E.N. Theory of Bridge Aerodynamics. New York. Springer; 2010.

[6] Statens Vegvesen. Bergsøysund Bro - detailed structural drawings. 1991.

[7] Ship motion. [14.04.2012] http://www.shipmotion.se/

[8] Krogstad H. and Arntsen Ø. Linear Wave Description and Theory. Trondheim: NTNU; 2003.

[9] Holmes P. Coastal Processes: Waves. Professional Development Programme: Coastal infrastructure design, construction and maintenance. 2001;July

[10] Faltinsen O.M. Sea Loads on Ships and Offshore Structures. Cambridge University Press;1990.

[11] Salvesen et.al. Ship Motions and Sea Loads. The Society of Naval Architects and Marine Engineers. 1970.

[12] Sannasiraj S. A. et.al. Diffraction-radiation of multiple floating structures in directional waves. Ocean Engineering. 2000;28.

[13] Langen I. Frequency domain analysis of a floating bridge exposed to irregular short-crested waves. Trondheim: Sintef; 1980.

[14] Gavin H. Damping estimates from experimental non-linear time-series. Journal of Sound and Vibration. 2001;246(5).

[15] Seif M. S. and Inoue Y. Dynamic analysis of floating bridges. Marine Structures. 1998;11

[16] Langen I. and Sigbjörnsson R. On stochastic dynamics of floating bridges. Eng. Struct. 1980;2.

[17] Cook et.al. Concepts and Applications of Finite Element Analysis. University of Wisconsin: Wiley; 2002.

[18] Bell K. Beregningsmetoder for Fagverk og Rammer. Trondheim: NTNU; 2009.

APPENDECIES

A.1 Hydrodynamic coefficients

A.2 Behaviour of a hydro-elastic beam element

A.3 Eigenvalue analysis of the dynamic properties

A.4 “Dry” Eigenvalue analysis

A.5 General FRF analysis

A.6 Load scaled FRF analysis

A.7 Spatially scaled FRF analysis

A.8 Probabilistic response analysis

A.1 HYDRODYNAMIC COEFFICIENTS

The hydrodynamic coefficients applied in the report are taken from Langen (Frequency domain analysis of a floating bridge exposed to irregular short-crested waves). These were originally derived from results given by Vugts(The Hydrodynamic Coefficients for Swaying, Heaving and Rolling Cylinders in a Free Surface. International Ship-builder Program. 1968;15.). Graphical presentations of the non-dimensional hydrodynamic coefficients are presented herein to illustrate their frequency dependence. All values are determined per unit length of a rectangular floating cylinder with width-draft ratio equal to four, $B_p/d = 4$, and the frequency of motion made non-dimensional by the following expression.

$$\omega_0 = \omega\sqrt{B_p/2g}$$

Where B_p is the width of the rectangular floating cylinder and g is the gravitational acceleration constant.

HYDRODYNAMIC ADDED MASS COEFFICIENTS

The non-dimensional hydrodynamic added mass coefficients in heave, sway and roll motion is presented as functions of dimensionless frequency. The hydrodynamic added mass coefficients have been made dimensionless by the following expressions.

$$m_{z,0}^{(h)} = \frac{m_z^{(h)}}{\rho_w A_{sub}}$$

$$m_{y,0}^{(h)} = \frac{m_y^{(h)}}{\rho_w A_{sub}}$$

$$m_{\theta,0}^{(h)} = \frac{m_\theta^{(h)}}{\rho_w A_{sub} B_p^2}$$

In these expressions ρ_w is the fluid density, B_p is the width of the rectangular cylinder and A_{sub} is the submerged cross-sectional area.

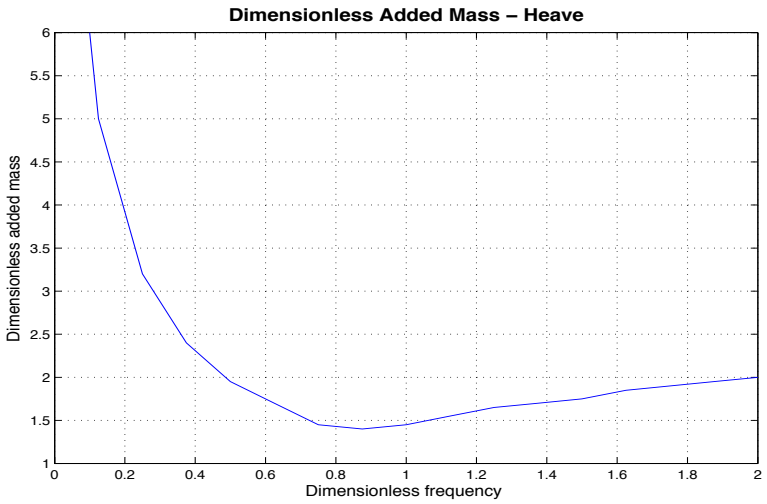
Dimensionless Added Mass – Heave
Dimensionless added mass
Dimensionless frequency
6
5.5
5
4.5
4
3.5
3
2.5
2
1.5
1
0
0.2
0.4
0.6
0.8
1
1.2
1.4
1.6
1.8
2

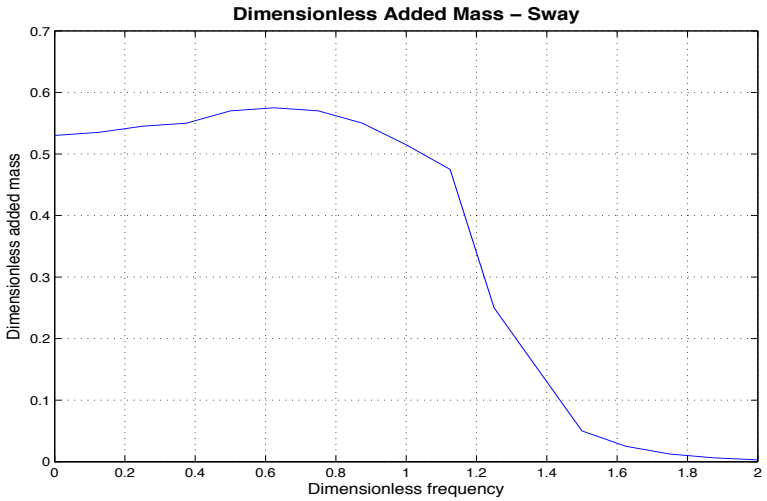
Dimensionless Added Mass – Sway
Dimensionless added mass
Dimensionless frequency
0.7
0.6
0.5
0.4
0.3
0.2
0.1
0
0
0.2
0.4
0.6
0.8
1
1.2
1.4
1.6
1.8
2

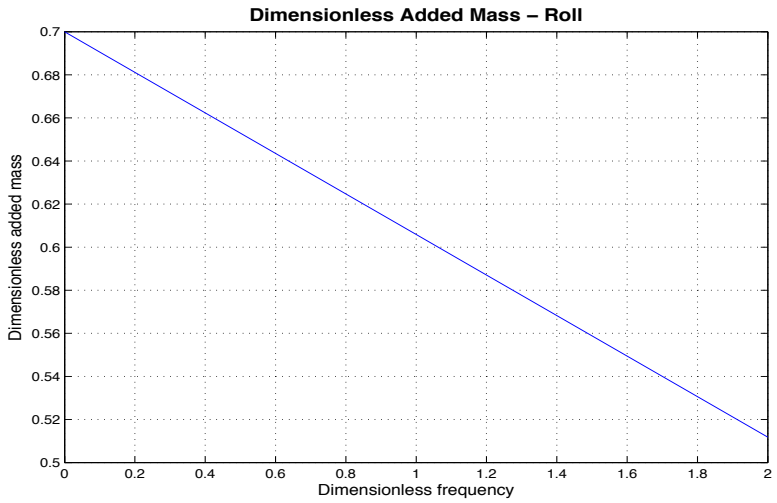
Dimensionless Added Mass – Roll
Dimensionless added mass
Dimensionless frequency
0.7
0.68
0.66
0.64
0.62
0.6
0.58
0.56
0.54
0.52
0.5
0
0.2
0.4
0.6
0.8
1
1.2
1.4
1.6
1.8
2

HYDRODYNAMIC DAMPING COEFFICIENTS

The non-dimensional hydrodynamic damping coefficients for heave, sway and roll motion is presented as functions of dimensionless frequency. The hydrodynamic damping coefficients have been made dimensionless by the following expressions.

$$c_{z,0}^{(h)} = \frac{c_z^{(h)}}{\rho_w A_{sub}} \sqrt{\frac{B_p}{2g}}$$

$$c_{y,0}^{(h)} = \frac{c_y^{(h)}}{\rho_w A_{sub}} \sqrt{\frac{B_p}{2g}}$$

$$c_{\theta,0}^{(h)} = \frac{c_\theta^{(h)}}{\rho_w A_{sub} B_p^2} \sqrt{\frac{B_p}{2g}}$$

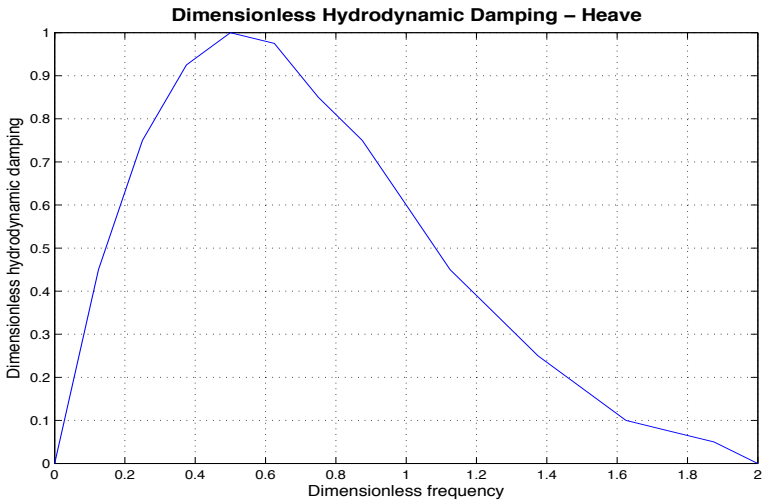
Dimensionless Hydrodynamic Damping – Heave
Dimensionless hydrodynamic damping
Dimensionless frequency
0
0.1
0.2
0.3
0.4
0.5
0.6
0.7
0.8
0.9
1
0.2
0.4
0.6
0.8
1.2
1.4
1.6
1.8
2

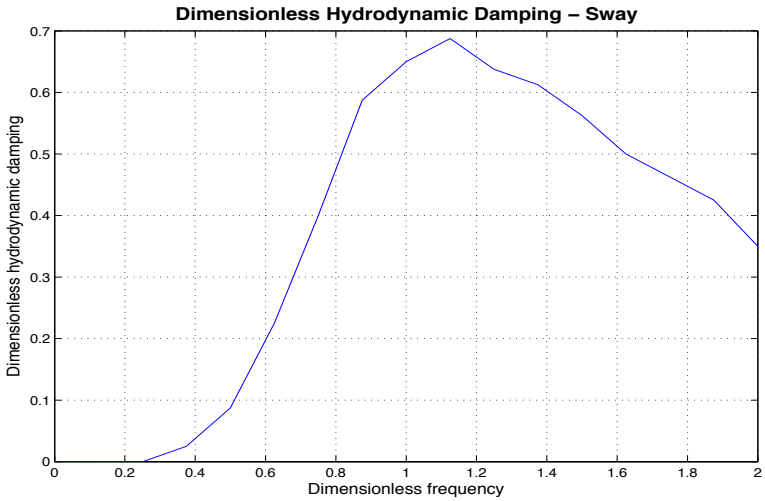
Dimensionless Hydrodynamic Damping – Sway
Dimensionless hydrodynamic damping
Dimensionless frequency
0
0.1
0.2
0.3
0.4
0.5
0.6
0.7
0.2
0.4
0.6
0.8
1
1.2
1.4
1.6
1.8
2

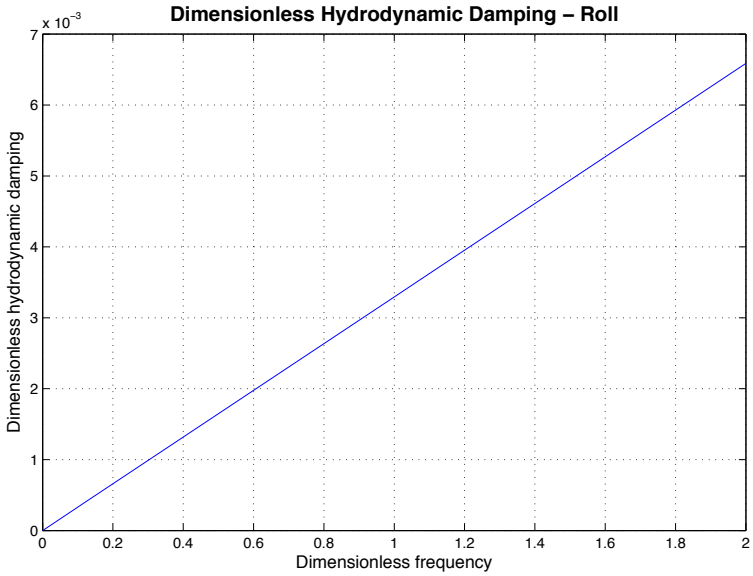
Dimensionless Hydrodynamic Damping – Roll
x 10^-3
Dimensionless hydrodynamic damping
Dimensionless frequency
0
1
2
3
4
5
6
7
0.2
0.4
0.6
0.8
1
1.2
1.4
1.6
1.8
2

HYDRODYNAMIC LOAD TRANSFER FUNCTIONS

The non-dimensional hydrodynamic load transfer functions for heave, sway and roll motion is presented as functions of dimensionless frequency. The hydrodynamic load transfer functions have been made dimensionless by the following expressions.

$$q_{z,0}^{(h)} = \frac{q_z^{(h)}}{\rho_w g B_p \eta_0}$$

$$q_{y,0}^{(h)} = \frac{q_y^{(h)}}{\rho_w g B_p dk \eta_0}$$

$$q_{\theta,0}^{(h)} = \frac{q_\theta^{(h)}}{\rho_w g \frac{B_p}{12} dk \eta_0}$$

The additional terms introduced in these expressions are the wavenumber, k, and the wave amplitude, η_0.

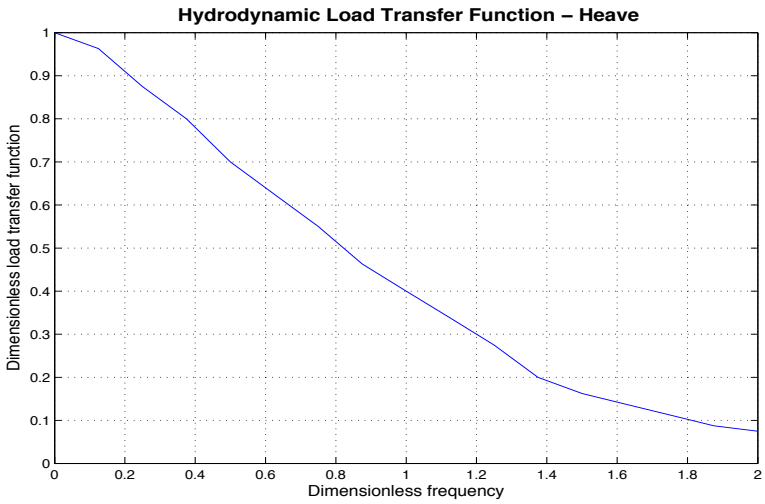
Hydrodynamic Load Transfer Function – Heave
Dimensionless load transfer function
Dimensionless frequency
0
0.1
0.2
0.3
0.4
0.5
0.6
0.7
0.8
0.9
1
0.2
0.4
0.6
0.8
1.2
1.4
1.6
1.8
2

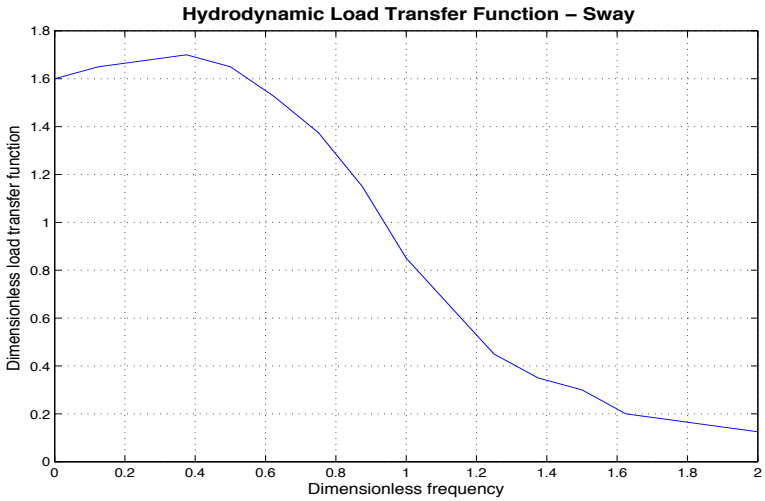
Hydrodynamic Load Transfer Function – Sway
Dimensionless load transfer function
Dimensionless frequency
0
0.2
0.4
0.6
0.8
1
1.2
1.4
1.6
1.8
2

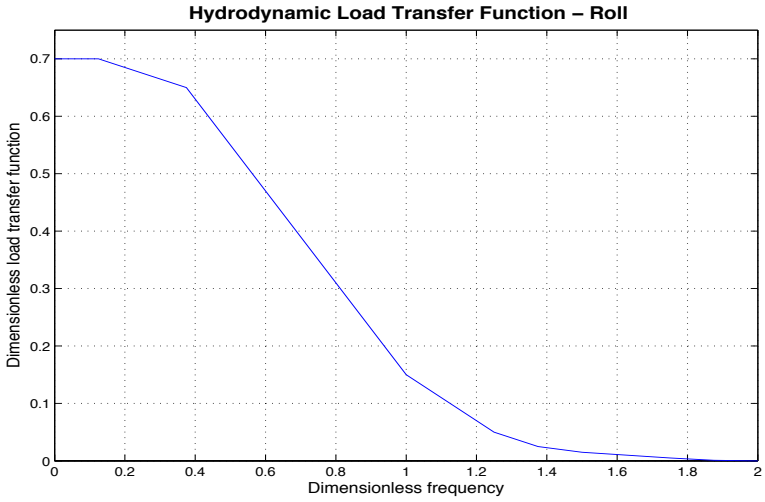
Hydrodynamic Load Transfer Function – Roll
Dimensionless load transfer function
Dimensionless frequency
0
0.1
0.2
0.3
0.4
0.5
0.6
0.7
0.2
0.4
0.6
0.8
1
1.2
1.4
1.6
1.8
2

A.2 BEHAVIOUR OF A HYDRO ELASTIC BEAM ELEMENT

A single hydro-elastic beam element is evaluated to investigate the hydrostatic stiffness introduced in the element formulation. The element is modelled as a square hollow concrete pontoon floating freely. The element evaluation is performed by matrix formulations in Matlab with additional hand calculations to verify the results.

Hydro–elastic Element

The material elasticity modulus is set very high to obtain high structural stiffness relative to the hydrostatic stiffness contribution. The aim of the high structural stiffness is to ensure rigid body motion over the element. The properties of the element, considered necessary for the evaluation of the performance of the hydrostatic behaviour, are tabulated below.

Properties of a single hydro-elastic pontoon element	
Length, L_{el}	2.00 [m]
Width, B_{el}	2.00 [m]
Wall thickness, t_w	0.04 [m]
Cross-section area, A_{cs}	0.2336 [m^2]
Water-plane area, A_{wp}	4.00 [m^2]
Density, ρ	2500 [kg/m^3]
Draft of element, d_{el}	0.285 [m]
Transverse metacentric height, $\overline{GM}_T$	1.118 [m]

Various vertical load configurations are introduced to the element, which is initially restricted to vertical rigid body displacement. The additional displaced water volume due to the external loads is evaluated from the vertical displacements at the nodes of the element. Linear interpolation of the additional displaced water volume is employed as the element is forced into rigid displacement.

$$\Delta\forall_z = \frac{(u_{z,1} + u_{z,2})}{2} B_{el} L_{el} = \frac{(u_{z,1} + u_{z,2})}{2} A_{wp}$$

The hydrostatic restoring force in the vertical direction is expressed as a function of the additional displaced water volume, and the hydrostatic vertical stiffness per unit length is extracted from this expression.

$$\Delta F_{B,z} = \rho_w g \Delta\forall_z$$

$$k_z^{(h)} = \rho_w g B_{el}$$

Hydro–elastic Element – Rigid Body Motion

The element behaves as expected for the vertical loading situations introduced to the element. As the element is forces to displace solely in the vertical plane, the change in the vertical hydrostatic restoring force equals the external vertical loading on the element.

The element is further evaluated for rigid body roll displacement. Various moment loadings are introduced in the torsional DOF's of each node while all other DOF's are considered unloaded. The hydrostatic restoring rotational stiffness for roll motion of a rigid body, as presented by Faltinsen (Sea Loads), is introduced to the stiffness formulation of the hydro-elastic element.

$$k_\theta^{(h)} = \rho_w g \forall \overline{GM}_T$$

$$\forall = B_{el} d_{el}$$

In this expression, the displaced water volume, $\forall$, denotes the volume displaced by the floating body at an equilibrium condition, and is thus taken as the width of the element times the draft for displaced volume per unit length. The transverse metacentric height, $\overline{GM}_T$, is determined as the distance between the centre of gravity, G, of the floating pontoon element and the metacentre, M. The metacentre defines the point around which the roll motion of a floating body acts as a pendulum swing.

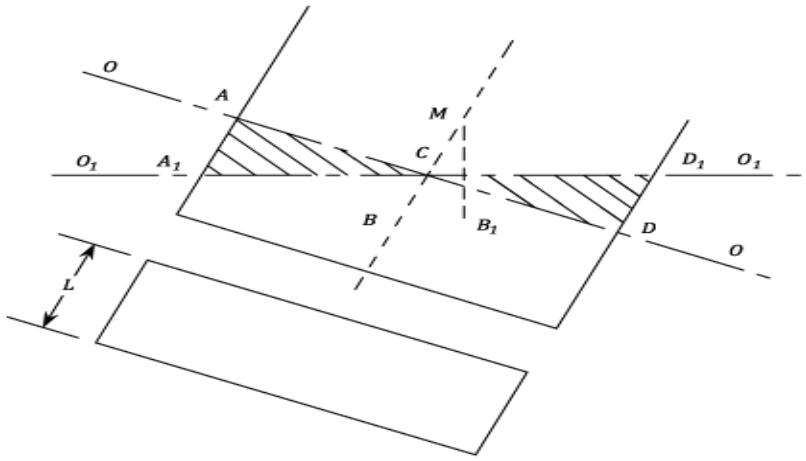

Illustration of the metacentric height

The hydrostatic roll stiffness is in addition evaluated from an expression established exclusively from the geometric properties of the pontoon element. The additionally displaced water volume due to the roll motion of the element is linearly interpolated between the resulting rotations each node, assuming small rotations, θ_x.

$$\Delta\forall_\theta = \frac{\left(\theta_{x,1} + \theta_{x,2}\right)}{4} B_{el}^2 L_{el}$$

The hydrostatic roll stiffness is evaluated from the expression for the restoring roll moment as function of the roll displacement of the element.

$$\Delta M_{B,\theta} = \rho_w g \Delta\forall_\theta \left(\frac{2B_{el}}{3}\right)$$

The initial expression for the roll stiffness, including the draft and metacentric height of the pontoon, is seen to provide a reduced stiffness contribution as compared to the latter expression for the pontoon element. For pontoon dimensions equal to the pontoons of the floating bridge modelled in this report, the hydrostatic roll stiffness per unit length found from the two expressions are given as.

$$k_{\theta,1}^{(h)} = \rho_w g \forall_p \overline{GM}_{T,p} \simeq 5.56 \cdot 10^6 \left[{Nm}/{m}\right]$$

$$k_{\theta,2}^{(h)} = \frac{\rho_w g B_p^3}{6} \simeq 13.40 \cdot 10^6 \left[{Nm}/{m}\right]$$

The effect of the draft and metacentric height of a floating body is noted to be of greater significance as the dimensions of the floating body increase. The inclusion of the draft and metacentric height of a floating structure is regarded necessary for the proper description of its hydrostatic behaviour. The hydrostatic roll stiffness employed in the modelling of the pontoons of the floating bridge in this report will thus be consistent with the initial expression. Including the effects of metacentric height and draft of the pontoons. The validity of this assumption may be further pursued by a study of the roll behaviour of the pontoons. The concept of metacentric height is developed within the context of naval engineering to describe the stability of ships. A ship with insufficient roll stability may be subject to overturning as the roll support of a freely floating body is provided solely from the surrounding fluid. This is however not considered the case for the pontoons as these are attached to above superstructure, and may be expected to behave differently.

A.3 EIGENVALUE ANALYSIS OF THE DYNAMIC PROPERTIES

An Eigenvalue analysis is employed to evaluate the un-damped dynamic properties of the floating bridge model. The Eigenvalue problem is established from the non-trivial solution of the un-damped dynamic equilibrium equation for free response of the system, assuming harmonic response.

$\boldsymbol{M\ddot{r} + Kr = R}$ - Un-damped equation of motion

$\boldsymbol{r} = \bar{\boldsymbol{r}}\, e^{i\omega t}$ - Assumed harmonic response of the system

$[\boldsymbol{K} - \omega^2 \boldsymbol{M}(\omega)]\bar{\boldsymbol{r}} = \boldsymbol{0}$ - Free response of the system

$[\boldsymbol{K} - \omega^2 \boldsymbol{M}(\omega)] = \boldsymbol{0}$ - Eigenvalue problem

The Eigenvalue analysis provides the natural frequencies and the corresponding mode shapes of the system. The number of natural frequencies obtained from the Eigenvalue analysis equals the number of DOF's of the discretised dynamic model. However, considering the environmental loading on the floating bridge structure, only natural frequencies within a certain frequency range are of interest. Frequencies of motion higher than $\omega_{max} = 5\ rad/s$, which corresponds to a period of approximately $T_{min} \simeq 1.25\ sec$, are considered to be of less significance to the dynamic behaviour of the floating bridge. Waves of periods in the vicinity of T_{min} will generally be associated with a confused and irregular sea state that has little ability to excite the large floating structure. As a result, the first twelve natural frequencies, and corresponding mode shapes, are reported herein. These are all found to be in the frequency range $0 \leq \omega \leq 5\ [rad/s]$.

The boundary conditions are assumed simply supported with respect to the vertical direction. Translational displacement in the horizontal plane, torsional displacement and the rotation about the vertical axis are assumed restrained at both supports.

The natural frequencies are obtained by iteration of the hydrodynamic added mass at each frequency. The natural frequencies reported are thus associated with an added mass value corresponding to their frequency of motion. The table below summarizes the natural frequencies and corresponding modes of motion. The associated hydrodynamic added masses for the observed modes of motion are also included. These are assumed to approach constant values with increased frequency. In the high frequency range of the analysis, combined modes of motion are observed. This phenomenon becomes more prevailing as one moves out of the predetermined frequency range and study modes at higher natural frequencies.

The natural frequencies, natural periods and hydrodynamic added mass for the twelve first modes of motion are tabulated below.

No.	Natural frequency $[rad/s]$	Period $[sec]$	Mode of Motion	Added Mass $[kg]$
1	$\omega_1 = 0.3346$	$T_1 = 18.79$	Sway	$M_{yy}^{(h)} = 5.012 \text{ x } 10^4$
2	$\omega_2 = 0.9050$	$T_2 = 6.94$	Sway	$M_{yy}^{(h)} = 4.920 \text{ x } 10^4$
3	$\omega_3 = 1.3381$	$T_3 = 4.70$	Heave	$M_{zz}^{(h)} = 15.505 \text{ x } 10^4$
4	$\omega_4 = 1.4128$	$T_4 = 4.45$	Heave	$M_{zz}^{(h)} = 15.708 \text{ x } 10^4$
5	$\omega_5 = 1.7118$	$T_5 = 3.67$	Heave	$M_{zz}^{(h)} = 17.338 \text{ x } 10^4$
6	$\omega_6 = 1.8269$	$T_6 = 3.44$	Sway	$M_{yy}^{(h)} = 0.065 \text{ x } 10^4$
7	$\omega_7 = 2.3403$	$T_7 = 2.69$	Heave	$M_{zz}^{(h)} = 18.317 \text{ x } 10^4$
8	$\omega_8 = 2.9342$	$T_8 = 2.14$	Sway	$M_{yy}^{(h)} = 0.0092 \text{ x } 10^4$
9	$\omega_9 = 3.2087$	$T_9 = 1.96$	Sway Heave Roll	$M_{yy}^{(h)} = 0.0092 \text{ x } 10^4$ $M_{zz}^{(h)} = 18.317 \text{ x } 10^4$ $M_{xx}^{(h)} = 0$
10	$\omega_{10} = 3.6420$	$T_{10} = 1.73$	Sway Heave Roll	$M_{yy}^{(h)} = 0.0092 \text{ x } 10^4$ $M_{zz}^{(h)} = 18.317 \text{ x } 10^4$ $M_{xx}^{(h)} = 0$
11	$\omega_{11} = 4.1975$	$T_{11} = 1.50$	Sway Heave Roll	$M_{yy}^{(h)} = 0.0092 \text{ x } 10^4$ $M_{zz}^{(h)} = 18.317 \text{ x } 10^4$ $M_{xx}^{(h)} = 0$
12	$\omega_{12} = 4.3565$	$T_{12} = 1.44$	Sway Heave Roll	$M_{yy}^{(h)} = 0.0092 \text{ x } 10^4$ $M_{zz}^{(h)} = 18.317 \text{ x } 10^4$ $M_{xx}^{(h)} = 0$

Plots of the modes of motion associated with the twelve first natural frequencies are presented on the following pages. The prevailing modes of motion stand out for each natural frequency, and the relative contributions from the combined modes are illustrated. Small contributions are seen to occur from the non-dominant modes already at the fifth natural frequency. These contributions are generally seen to increase with the increase of the frequency of motion. At natural frequency number ten it is seen that the contributions from the three modes are of the same magnitude. These are of about 6-7% of the magnitude reported for the modes constituted by a single mode of motion. For natural frequencies eleven and twelve the largest non-dominant mode of motion is about 5% of the dominant, with the heave and sway modes dominating the response, respectively.

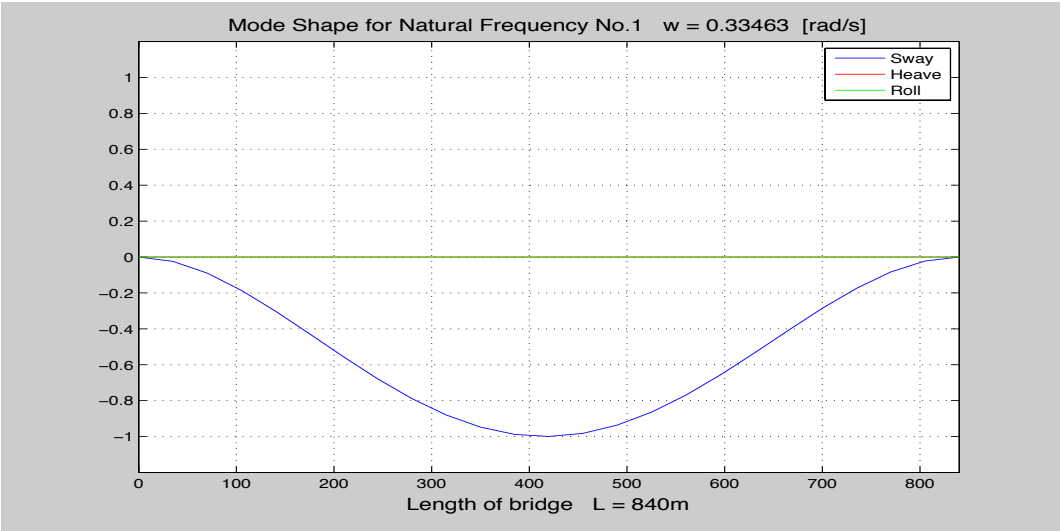
Mode Shape for Natural Frequency No.1 w = 0.33463 [rad/s]
Sway
Heave
Roll
1
0.8
0.6
0.4
0.2
0
−0.2
−0.4
−0.6
−0.8
−1
0
100
200
300
400
500
600
700
800
Length of bridge L = 840m

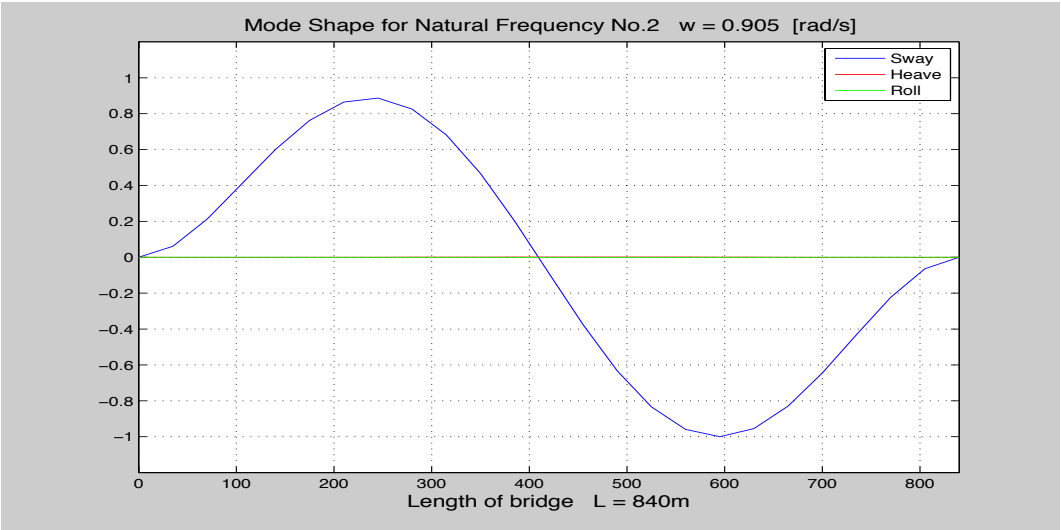
Mode Shape for Natural Frequency No.2 w = 0.905 [rad/s]
Sway
Heave
Roll
1
0.8
0.6
0.4
0.2
0
−0.2
−0.4
−0.6
−0.8
−1
0
100
200
300
400
500
600
700
800
Length of bridge L = 840m

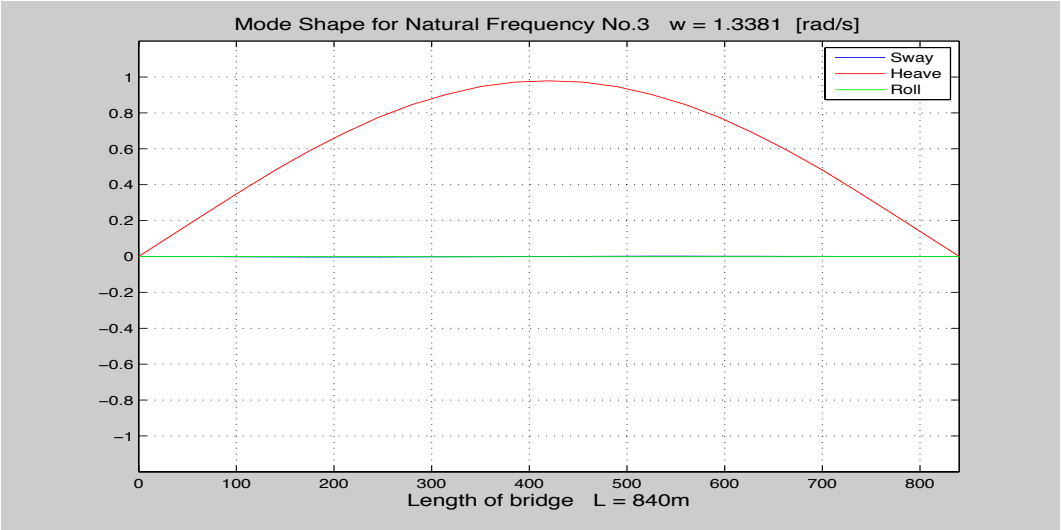
Mode Shape for Natural Frequency No.3 w = 1.3381 [rad/s]
Sway
Heave
Roll
1
0.8
0.6
0.4
0.2
0
−0.2
−0.4
−0.6
−0.8
−1
0
100
200
300
400
500
600
700
800
Length of bridge L = 840m

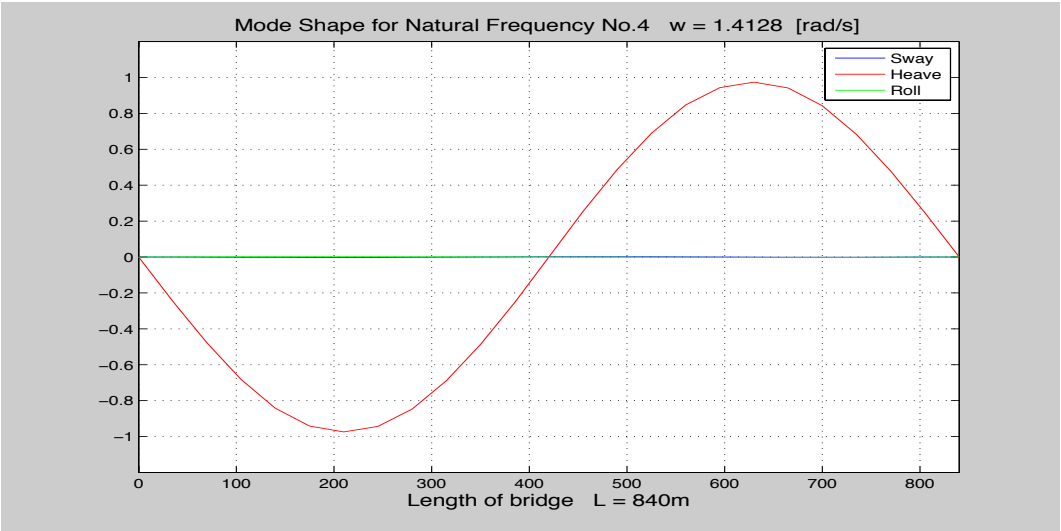
Mode Shape for Natural Frequency No.4 w = 1.4128 [rad/s]
Sway
Heave
Roll
1
0.8
0.6
0.4
0.2
0
−0.2
−0.4
−0.6
−0.8
−1
0
100
200
300
400
500
600
700
800
Length of bridge L = 840m

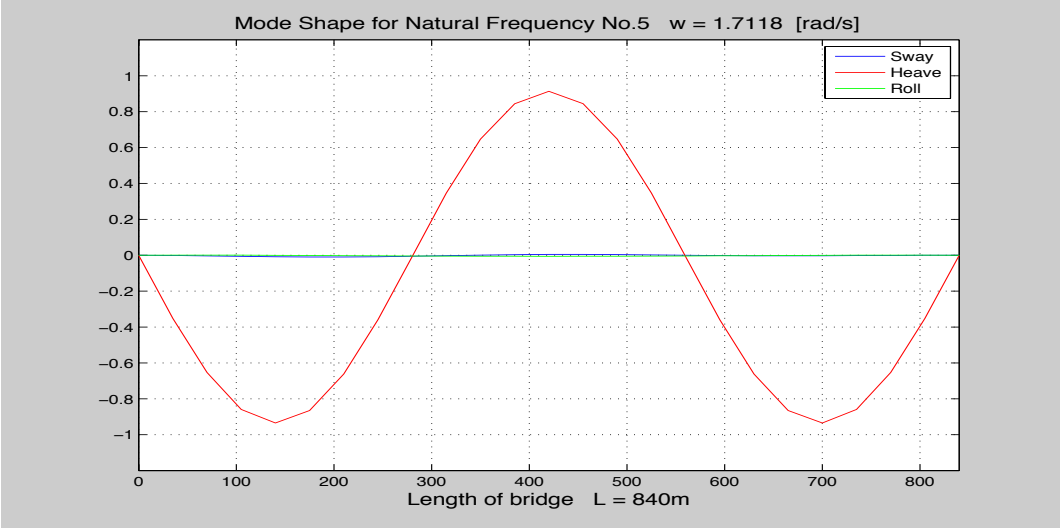
Mode Shape for Natural Frequency No.5 w = 1.7118 [rad/s]
Sway
Heave
Roll
1
0.8
0.6
0.4
0.2
0
−0.2
−0.4
−0.6
−0.8
−1
0
100
200
300
400
500
600
700
800
Length of bridge L = 840m

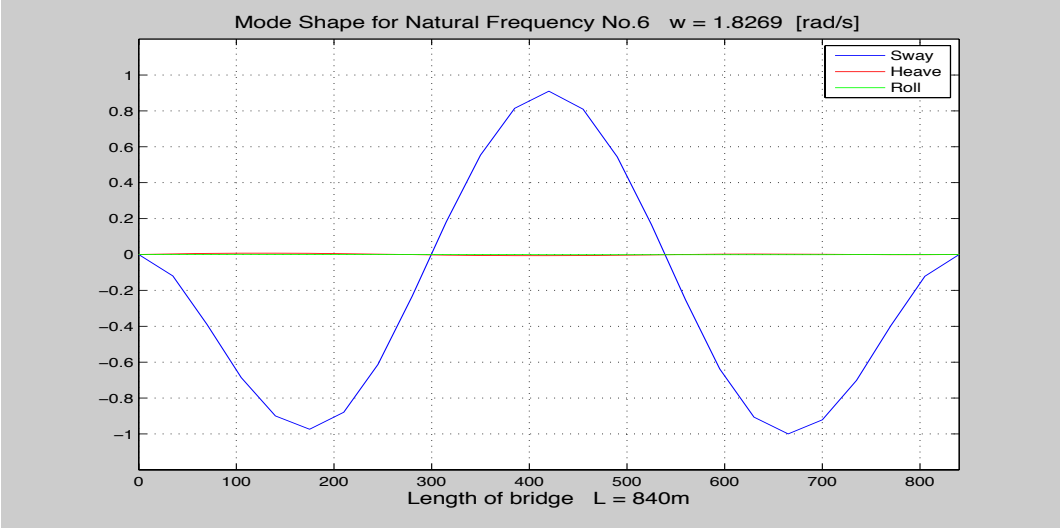
Mode Shape for Natural Frequency No.6 w = 1.8269 [rad/s]
Sway
Heave
Roll
1
0.8
0.6
0.4
0.2
0
−0.2
−0.4
−0.6
−0.8
−1
0
100
200
300
400
500
600
700
800
Length of bridge L = 840m

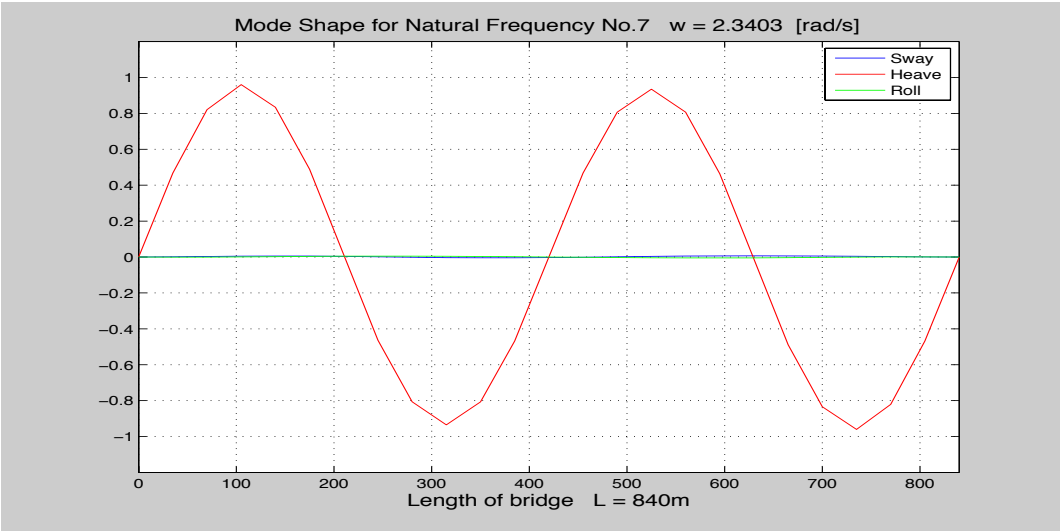
Mode Shape for Natural Frequency No.7 w = 2.3403 [rad/s]
Sway
Heave
Roll
1
0.8
0.6
0.4
0.2
0
−0.2
−0.4
−0.6
−0.8
−1
0
100
200
300
400
500
600
700
800
Length of bridge L = 840m

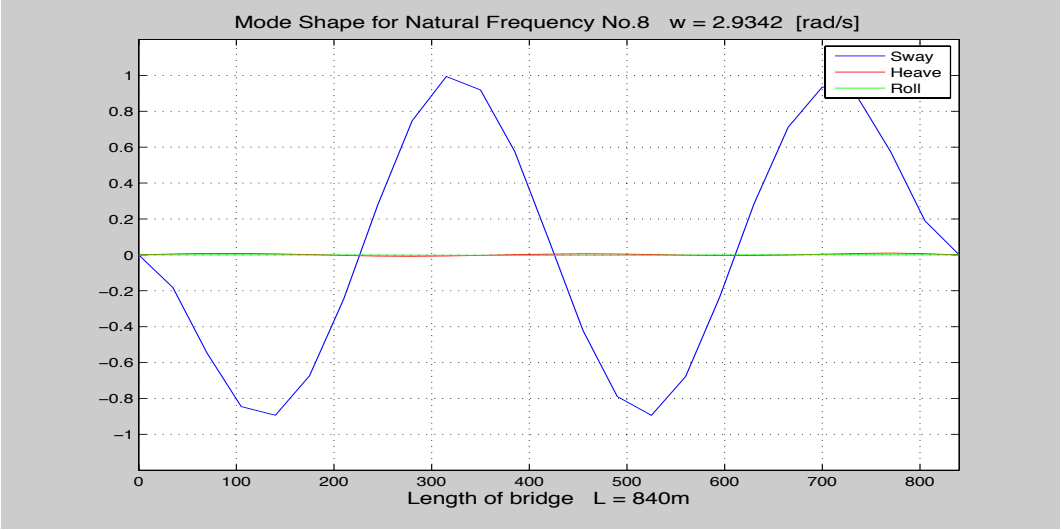
Mode Shape for Natural Frequency No.8 w = 2.9342 [rad/s]
Sway
Heave
Roll
1
0.8
0.6
0.4
0.2
0
−0.2
−0.4
−0.6
−0.8
−1
0
100
200
300
400
500
600
700
800
Length of bridge L = 840m

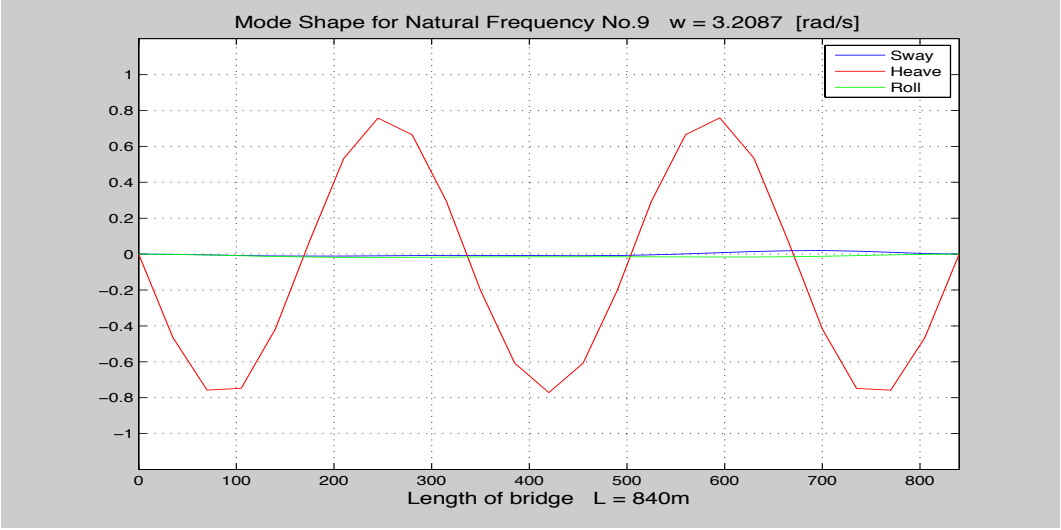
Mode Shape for Natural Frequency No.9 w = 3.2087 [rad/s]
Sway
Heave
Roll
1
0.8
0.6
0.4
0.2
0
−0.2
−0.4
−0.6
−0.8
−1
0
100
200
300
400
500
600
700
800
Length of bridge L = 840m

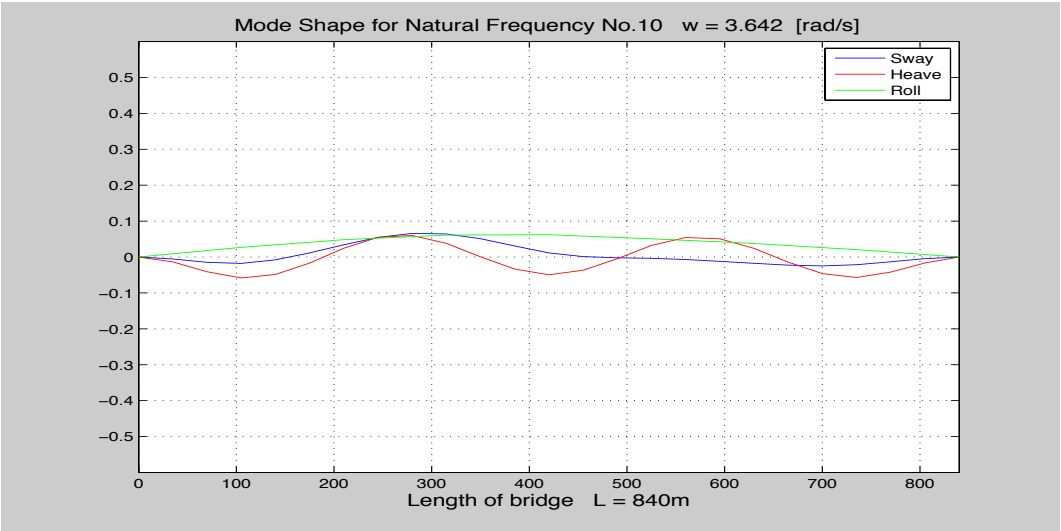
Mode Shape for Natural Frequency No.10 w = 3.642 [rad/s]
Sway
Heave
Roll
0.5
0.4
0.3
0.2
0.1
0
−0.1
−0.2
−0.3
−0.4
−0.5
0
100
200
300
400
500
600
700
800
Length of bridge L = 840m

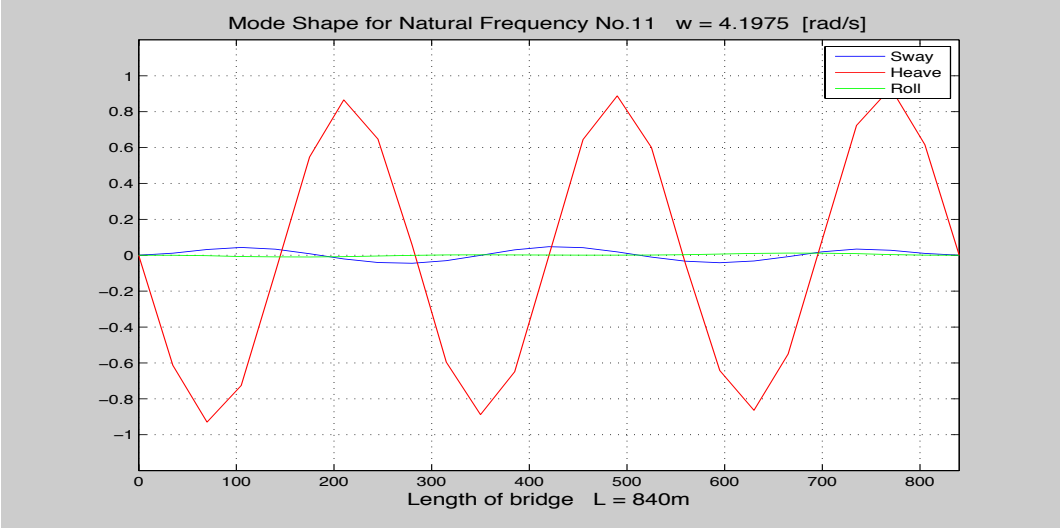
Mode Shape for Natural Frequency No.11 w = 4.1975 [rad/s]
Sway
Heave
Roll
1
0.8
0.6
0.4
0.2
0
−0.2
−0.4
−0.6
−0.8
−1
0
100
200
300
400
500
600
700
800
Length of bridge L = 840m

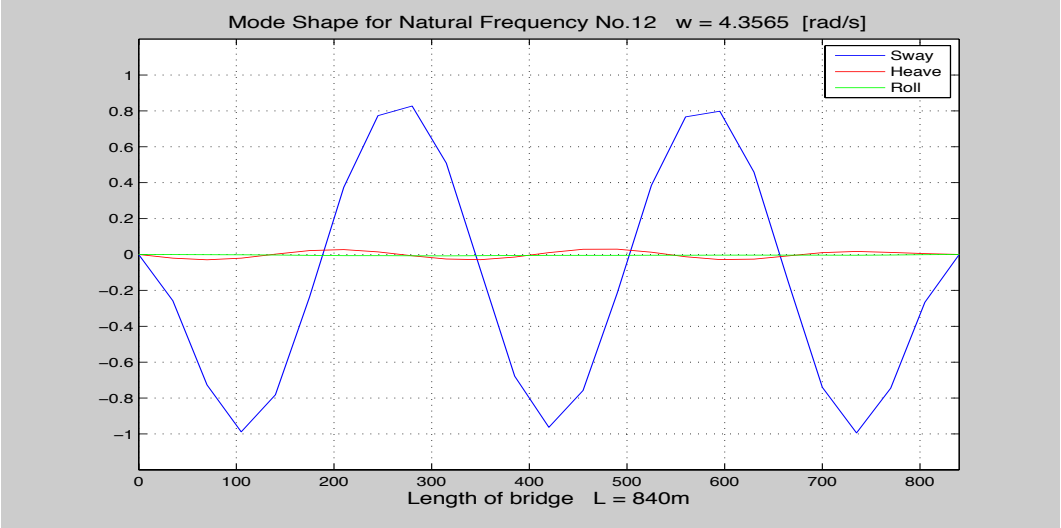
Mode Shape for Natural Frequency No.12 w = 4.3565 [rad/s]
Sway
Heave
Roll
1
0.8
0.6
0.4
0.2
0
−0.2
−0.4
−0.6
−0.8
−1
0
100
200
300
400
500
600
700
800
Length of bridge L = 840m

A.4 "DRY" EIGENVALUE ANALYSIS

An Eigenvalue analysis performed for the purely structural part of the floating bridge structure is presented herein. The hydrostatic and hydrodynamic effects on the structure are neglected in the determination of the natural frequencies and the associated mode shapes. The Eigenvalue problem is established from the non-trivial solution of the un-damped dynamic equilibrium equation for free response of the system, assuming harmonic response.

$\left[\boldsymbol{K}^{(s)} - \omega^2 \boldsymbol{M}^{(s)}\right] = \mathbf{0}$ - Eigenvalue problem structural system

The boundary conditions are assumed simply supported with respect to the vertical direction. Translational displacement in the horizontal plane, torsional displacement and the rotation about the vertical axis are assumed restrained at both supports.

The first twelve natural frequencies and mode shapes are extracted from the "dry" Eigenvalue analysis in accordance with the Eigenvalue analysis performed for the fluid-structure system. The natural frequencies and natural periods for the twelve first modes of motion are tabulated below.

No.	Natural frequency [*rad/s*]	Period [*sec*]	Mode of Motion
1	$\omega_1 = 0.1428$	$T_1 = 44.00$	Heave
2	$\omega_2 = 0.3392$	$T_2 = 18.52$	Sway
3	$\omega_3 = 0.5814$	$T_3 = 10.81$	Heave
4	$\omega_4 = 0.9125$	$T_4 = 6.89$	Sway
5	$\omega_5 = 1.3058$	$T_5 = 4.81$	Heave
6	$\omega_6 = 1.8269$	$T_6 = 3.44$	Sway
7	$\omega_7 = 2.3201$	$T_7 = 2.71$	Heave
8	$\omega_8 = 2.9342$	$T_8 = 2.14$	Sway
9	$\omega_9 = 3.5832$	$T_9 = 1.75$	Heave
10	$\omega_{10} = 3.9298$	$T_{10} = 1.60$	Sway Heave Roll
11	$\omega_{11} = 4.3589$	$T_{11} = 1.44$	Sway
12	$\omega_{12} = 5.1082$	$T_{12} = 1.23$	Heave

A.5 GENERAL FRF ANALYSIS

General frequency response functions (FRF's) are developed to study the response sensitivity of the floating bridge model. A FRF represents the frequency dependent response of a single point on the structure. As a result, the FRF's of several points along the bridge span are to be evaluated. The response at the mid-point is generally of concern when evaluating the dynamic response of a slender structure, as the largest displacements are expected to be observed at this point. Nevertheless, the dynamic responses at intermediate points between the mid-point and end-points are also evaluated. The motivation for this may be realized by studying the mode shapes from the Eigen value analysis of the dynamic system. The mode shapes of the system are generally expressed as standing sinusoidal waves in the low frequency range. Resulting in some points along the structure representing nodes of no motion for certain natural frequencies. The second mode shape associated with heave motion and natural frequency ω_4 exemplifies this. The mode shape is seen to be a complete sine wave, leaving the mid-node as a node of no motion.

The FRF's are a representation of the fluid-structure properties as expressed inversely within the $\boldsymbol{H}(\omega)$-matrix. Thus, the direct frequency response method, for determination of the general FRF's, is assembled by introducing the unit load vector, $\overline{\boldsymbol{R}}_{unit}$.

$$\bar{\boldsymbol{r}}(\omega) = \boldsymbol{H}(\omega)\, \overline{\boldsymbol{R}}_{unit}$$

Plots of the general FRF's at different points along the structure reveal the individual response sensitivities and indicate the expected mode shapes. Such a plot is presented below for the heave responses at the mid-node, the L/4-point and at the L/8-point.

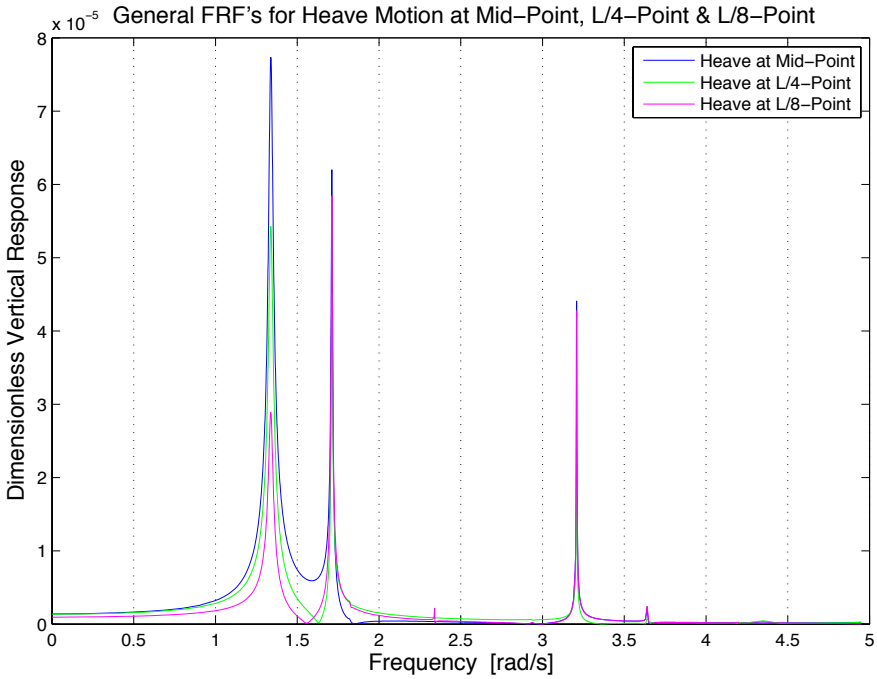

The general FRF's are further evaluated against FRF's computed for the un-damped system properties. The effect of the hydrodynamic damping becomes evident as the response peaks of the un-damped system tend towards infinity at the natural frequencies associated with heave in the mid-node.

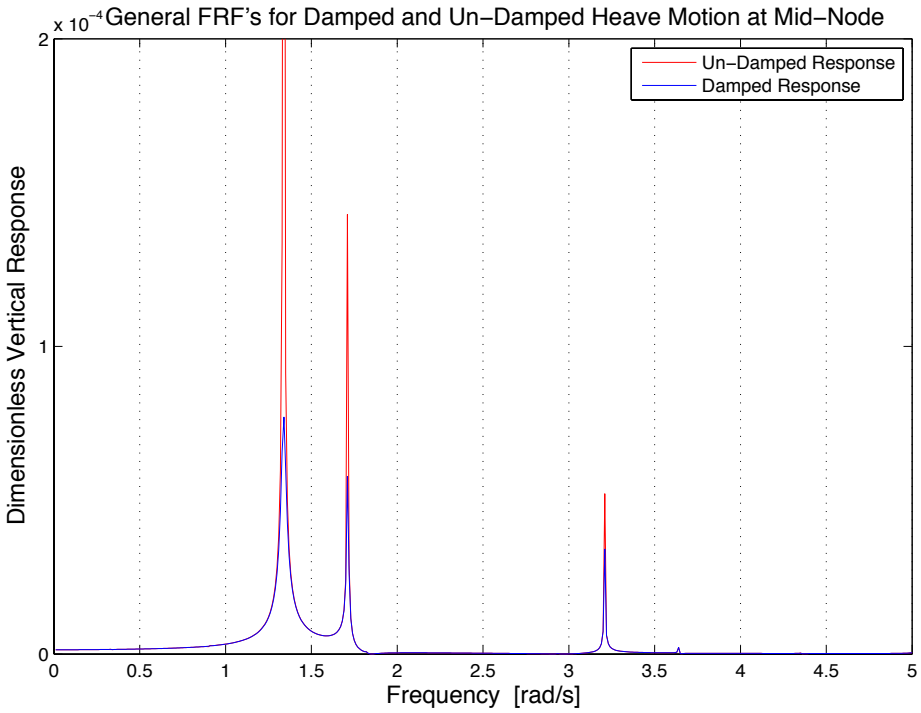

A.6 LOAD SCALED FRF ANALYSIS

In this section, the frequency response functions developed for the general case are scaled to incorporate the frequency dependent wave load transfer. The wave loading is introduced in the DOF's of the submerged pontoons and scaled according to dimensionless frequency dependent wave load transfer functions.

$\overline{\boldsymbol{q}}_0(\omega)$.

$$\bar{\boldsymbol{r}}(\omega) = \boldsymbol{H}(\omega)\,\boldsymbol{R}(\omega) = \boldsymbol{H}(\omega)\,\overline{\boldsymbol{q}}_0(\omega)\,\boldsymbol{R}_{\boldsymbol{wave}}$$

The $\boldsymbol{R}_{\boldsymbol{wave}}$-vector represents the maximum potential wave loading in the DOF's of the pontoon elements consistent with the finite element approach.

The load scaled heave response in the mid-point, the L/4-point and the L/8-point is illustrated below. The load transfer function for heave motion, $\bar{q}_{0,z}(\omega)$, has a maximum value of unity for $\omega = 0$ and decreases for higher frequencies. This effect is seen as the response peaks at high frequencies are scaled to negligible magnitudes compared with the response peaks at lower frequencies.

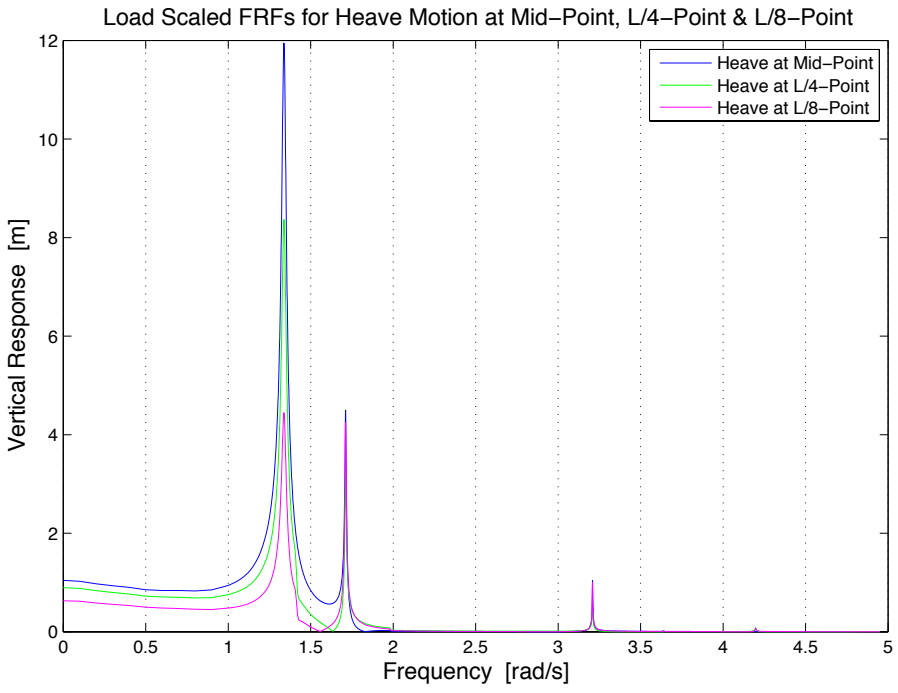

The load scaling effect is further illustrated by a plot of the response at mid-point for the damped and un-damped system.

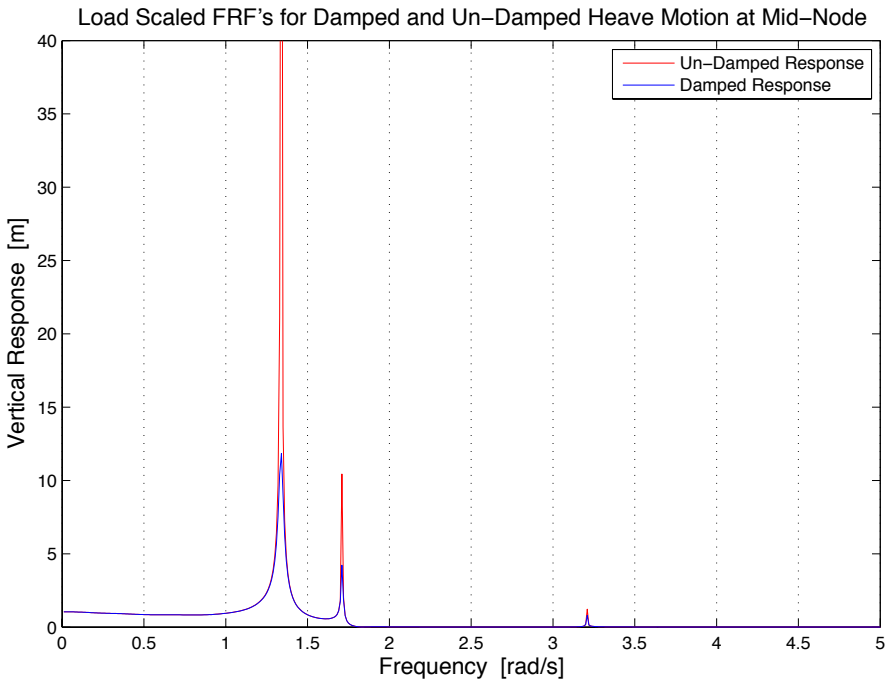

A.7 SPATIALLY SCALED FRF ANALYSIS

A dynamic response analysis of the floating bridge model is performed, taking the spatial distribution of the surface waves into consideration. The direct frequency response analysis is employed.

$$\bar{\boldsymbol{r}}(\omega) = \boldsymbol{H}(\omega)\, \bar{\boldsymbol{R}}(\omega)$$

The frequency dependent fluid-structure properties are represented within the $\boldsymbol{H}(\omega)$-matrix as determined previously. The loading on the system is now considered dependent on both frequency and the spatial location of the pontoon elements. The wave load per unit length over a submerged hydro-elastic element, *m*, is determined according to its position in the wave field. The element nodal loads and moments are developed according to the interpolation functions of the hydro-elastic elements.

$$\boldsymbol{q}_m(\omega) = \boldsymbol{q}_{Wave,m}\, \bar{\boldsymbol{q}}_0(\omega)\, q_{amp,m}$$

$$q_{amp,m} = \int N_s cos^{2s}(\theta - \bar{\theta})\; e^{-ik\left(x_m sin(\theta-\bar{\theta}) + y_m cos(\theta-\bar{\theta})\right)} d\theta$$

$$\boldsymbol{R}_m^{el}(\omega) = \int_0^{Le} \boldsymbol{N}^{\mathrm{T}}\, \boldsymbol{q}_m(\omega)\, dx$$

The analysis is performed for different combinations of the spreading index, *s*, and the mean wave angle of approach, $\bar{\theta}$. Spreading index values of $s = 3$ and $s = 15$ are chosen to represent sea states of high and low degree of multi-directionality, respectively. The mean wave angle of approach is evaluated within a range of $0 \leq \bar{\theta} \leq \pi/2$, where $\bar{\theta} = 0$ represent a mean wave angle normal to the bridge span, and $\bar{\theta} = \pi/2$ represents the somewhat fictive mean wave angle of direction along the global x-axis.

The responses at mid-point, in the L/4-point and L/8-point are evaluated during the analysis. The maximum response amplitudes at these points are tabulated below for different combinations of s and $\bar{\theta}$. Representative plots for some of these combinations are presented on the following pages to illustrate the sensitivity of the response to different sea states.

Mid-Point [m]	$\bar{\theta} = 0$	$\bar{\theta} = \pi/8$	$\bar{\theta} = \pi/4$	$\bar{\theta} = 3\pi/8$	$\bar{\theta} = \pi/2$
$s = 3$	0.4300	0.6645	0.9373	0.6771	0.4300
$s = 15$	1.8651	0.9743	1.6031	0.9840	1.8651

L/4-Point [m]	$\bar{\theta} = 0$	$\bar{\theta} = \pi/8$	$\bar{\theta} = \pi/4$	$\bar{\theta} = 3\pi/8$	$\bar{\theta} = \pi/2$
$s = 3$	0.3045	0.4892	0.6695	0.4789	0.3045
$s = 15$	1.3440	0.6826	1.1496	0.6893	1.3440

L/8-Point [m]	$\bar{\theta} = 0$	$\bar{\theta} = \pi/8$	$\bar{\theta} = \pi/4$	$\bar{\theta} = 3\pi/8$	$\bar{\theta} = \pi/2$
$s = 3$	0.3967	0.2706	0.8732	0.2556	0.3967
$s = 15$	1.7480	0.3639	1.4967	0.3656	1.7480

Plots of responses for different values of the spreading index, $s = 3$ and $s = 15$, for constant mean wave angle of approach $\bar{\theta} = 0$.

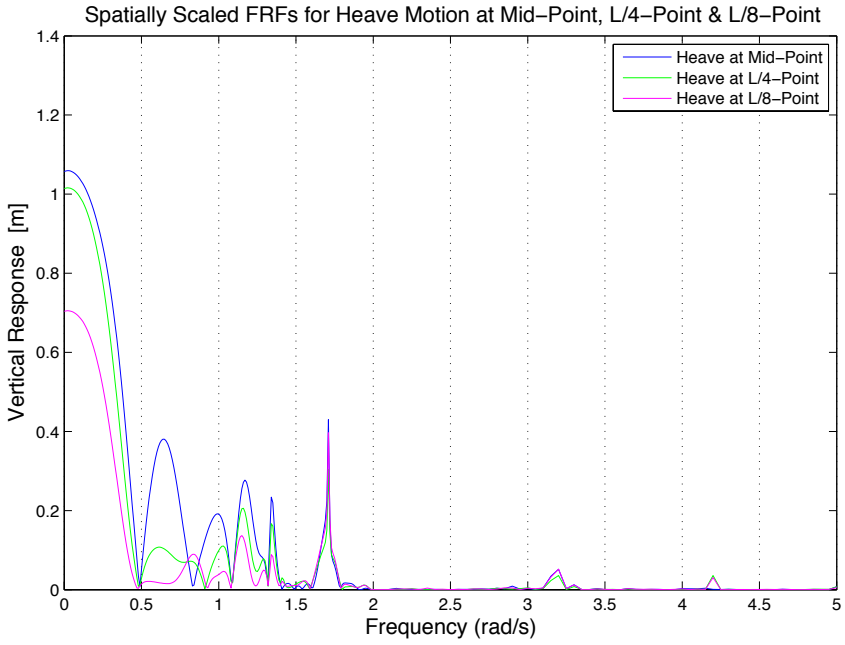

$\boldsymbol{[s = 3, \bar{\theta} = 0]}$

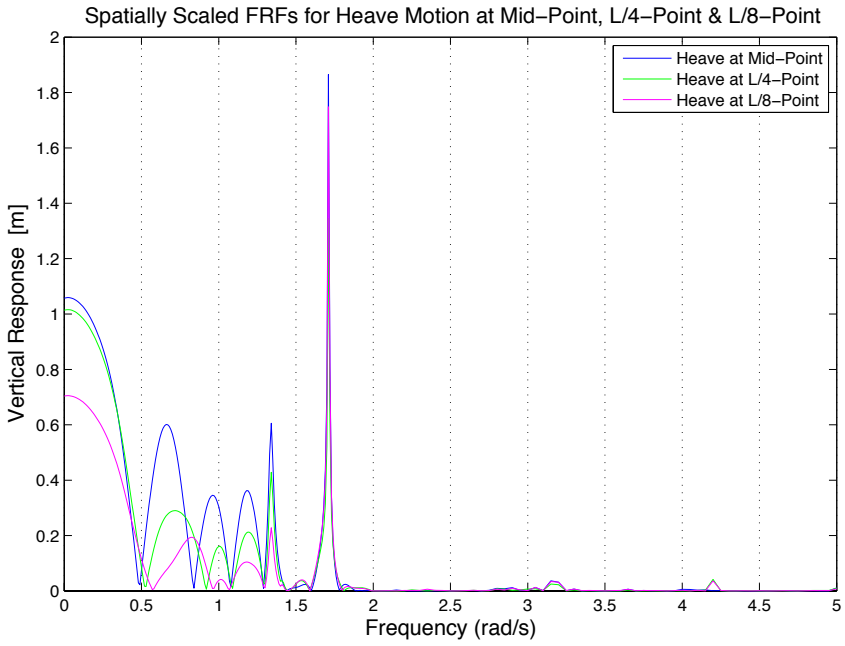

$\boldsymbol{[s = 15, \bar{\theta} = 0]}$

Plots of responses for different values of the wave angle of approach, $\bar{\theta} = \pi/8$ and $\bar{\theta} = \pi/4$, for constant value of the spreading index $s = 3$.

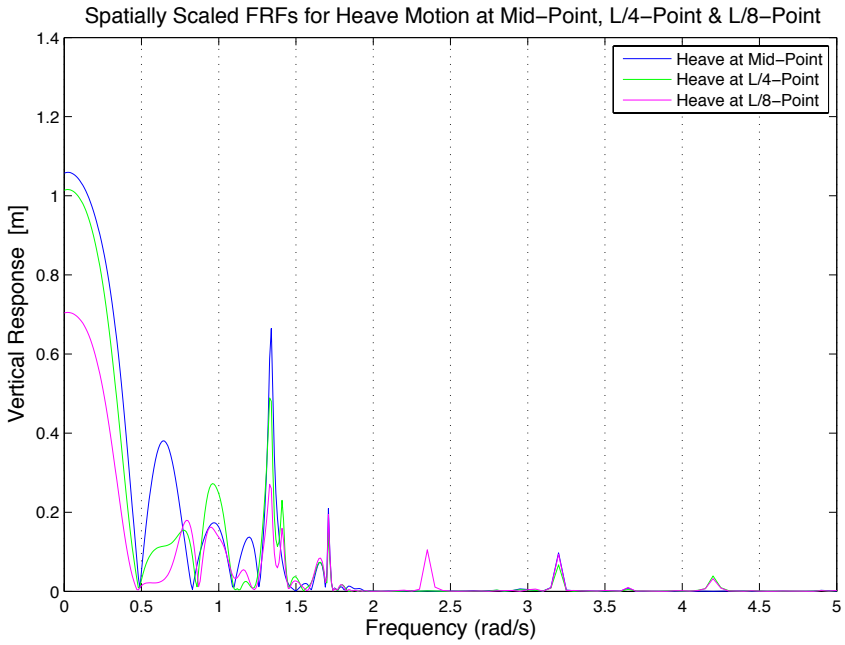

$\boldsymbol{[\bar{\theta} = \pi/8, s = 3]}$

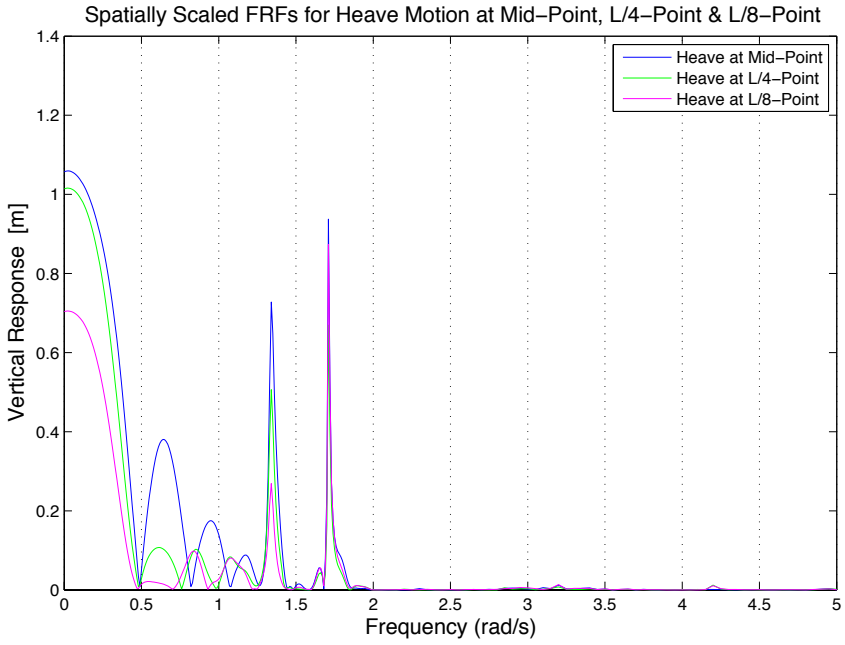

$\boldsymbol{[\bar{\theta} = \pi/4, s = 3]}$

A.8 PROBABILISTIC RESPONSE ANALYSIS

The spectral process of the dynamic response is determined by probabilistic means from the spectral process of the wave loading according to the following expression.

$$\boldsymbol{S}_r(\omega) = \boldsymbol{H}(\omega)\,\boldsymbol{\mathcal{F}}^{(h,s)}(\omega)\,\boldsymbol{H}^{*\mathrm{T}}(\omega)\,S_\eta(\omega)$$

The dynamic analysis is initially performed for two separate sea states defined by their spectral densities, $S_{\eta,i}(\omega)$. The first sea state is developed to model relatively long-crested swell waves, while the second sea state is associated with an irregular, short-crested sea state. Different values of the spreading index are introduced in the spreading function to model sea states of low and high degree of multi-directionality for the first and second sea states, respectively. Both analyses are considered over a duration of two hours for which the statistical sea state parameters are considered constant.

Sea State Parameters						
Sea State No.	s	$T_p\ [sec]$	$H_s\ [m]$	$T\ [sec]$	$E\lvert H_{max}\rvert\ [m]$	$T_{m0}\ [sec]$
1	15	10	1	7200	1.9343	7.2999
2	3	3	1	7200	2.0557	2.7666

The probabilistic response parameters obtained for various mean wave angles of approach for the two sea states are tabulated below. Also, the results from an evaluation of combined sea states are included. In the analysis of the combined sea states, two mean wave angles of approach are included for the multi-directional sea state. While the mean wave angle of approach for the more unidirectional wave field is kept constant.

The parameters tabulated are the standard deviation of the response process, σ_r, the zero crossing period, T_z, the rms bandwidth of the response process, ε, the expected maximum response, $E|r_{max}|$, the standard deviation of the expected maximum response, $\sigma|r_{max}|$, and, finally, a maximum response estimated within one standard deviation of the expected maximum response, r_{max}.

The tables are followed by plots of the auto-transfer functions and plots of the auto-density of the response for a selection of the responses.

Probabilistic Heave Response from Sea State No. 1 $\{\bar{\theta}_1 = 0\}$						
	$\sigma_r\ [m]$	$T_z\ [sec]$	ε	$E\|r_{max}\|\ [m]$	$\sigma\|r_{max}\|\ [m]$	$r_{max}\ [m]$
Mid-Point	0.2615	8.3519	0.6588	1.0026	0.0912	1.0939
L/3-Point	0.2178	8.3910	0.6628	0.8346	0.0760	0.9106
L/4-Point	0.1262	8.3121	0.6547	0.4838	0.0440	0.5278
L/8-Point	0.2550	6.5183	0.2662	0.9937	0.0873	1.0811

Probabilistic Heave Response from Sea State No. 2 $\{\bar{\theta}_2 = 0\}$						
	$\sigma_r\ [m]$	$T_z\ [sec]$	ε	$E\|r_{max}\|\ [m]$	$\sigma\|r_{max}\|\ [m]$	$r_{max}\ [m]$
Mid-Point	0.0102	3.5758	1.4452	0.0414	0.0034	0.0448
L/3-Point	0.0065	3.7718	1.3323	0.0263	0.0021	0.0284
L/4-Point	0.0074	3.6174	1.4202	0.0300	0.0024	0.0325
L/8-Point	0.0046	3.5470	1.4621	0.0187	0.0015	0.0202

Probabilistic Heave Response from Sea State No. 1 $\{\bar{\theta}_1 = \pi/8\}$						
	$\sigma_r\ [m]$	$T_z\ [sec]$	ε	$E\|r_{max}\|\ [m]$	$\sigma\|r_{max}\|\ [m]$	$r_{max}\ [m]$
Mid-Point	0.2620	8.3518	0.6588	1.0044	0.0914	1.0958
L/3-Point	0.2108	8.3910	0.6628	0.8361	0.0761	0.9122
L/4-Point	0.1264	8.3108	0.6545	0.4847	0.0441	0.5288
L/8-Point	0.2555	6.5181	0.2661	0.9956	0.0875	1.0831

Probabilistic Heave Response from Sea State No. 2 $\{\bar{\theta}_2 = \pi/8\}$						
	$\sigma_r\ [m]$	$T_z\ [sec]$	ε	$E\|r_{max}\|\ [m]$	$\sigma\|r_{max}\|\ [m]$	$r_{max}\ [m]$
Mid-Point	0.0095	3.5810	1.4417	0.0386	0.0031	0.0417
L/3-Point	0.0065	3.8015	1.3160	0.0264	0.0022	0.0286
L/4-Point	0.0073	3.6590	1.3960	0.0294	0.0024	0.0318
L/8-Point	0.0041	3.5519	1.4592	0.0168	0.0014	0.0181

Probabilistic Heave Response from Sea State No. 1 $\{\bar{\theta}_1 = \pi/4\}$						
	$\sigma_r\ [m]$	$T_z\ [sec]$	ε	$E\lvert r_{max}\rvert\ [m]$	$\sigma\lvert r_{max}\rvert\ [m]$	$r_{max}\ [m]$
Mid-Point	0.2625	8.3518	0.6588	1.0062	0.0916	1.0978
L/3-Point	0.2186	8.3910	0.6628	0.8376	0.0763	0.9139
L/4-Point	0.1266	8.3108	0.6545	0.4857	0.0442	0.5298
L/8-Point	0.2560	6.5181	0.2661	0.9976	0.0877	1.0853

Probabilistic Heave Response from Sea State No. 2 $\{\bar{\theta}_2 = \pi/4\}$						
	$\sigma_r\ [m]$	$T_z\ [sec]$	ε	$E\lvert r_{max}\rvert\ [m]$	$\sigma\lvert r_{max}\rvert\ [m]$	$r_{max}\ [m]$
Mid-Point	0.0091	3.6240	1.4163	0.0367	0.0030	0.0397
L/3-Point	0.0072	3.9386	1.2429	0.0291	0.0024	0.0315
L/4-Point	0.0078	3.7855	1.3248	0.0316	0.0026	0.0342
L/8-Point	0.0038	3.5908	1.4359	0.0155	0.0013	0.0168

Probabilistic Heave Response from Combined Sea States $\{\bar{\theta}_1 = 0, \bar{\theta}_2 = 0\}$						
	$\sigma_r\ [m]$	$T_z\ [sec]$	ε	$E\lvert r_{max}\rvert\ [m]$	$\sigma\lvert r_{max}\rvert\ [m]$	$r_{max}\ [m]$
Mid-Point	0.2617	8.3236	0.6559	1.0036	0.0913	1.0949
L/3-Point	0.2179	8.3762	0.6613	0.8350	0.0760	0.9111
L/4-Point	0.1264	8.2514	0.6482	0.4849	0.0440	0.5290
L/8-Point	0.2550	6.5158	0.2648	0.9939	0.0874	1.0813

Probabilistic Heave Response from Combined Sea States $\{\bar{\theta}_1 = 0, \bar{\theta}_2 = \pi/4\}$						
	$\sigma_r\ [m]$	$T_z\ [sec]$	ε	$E\lvert r_{max}\rvert\ [m]$	$\sigma\lvert r_{max}\rvert\ [m]$	$r_{max}\ [m]$
Mid-Point	0.2617	8.3303	0.6566	1.0034	0.0913	1.0947
L/3-Point	0.2179	8.3747	0.6611	0.8351	0.0760	0.9112
L/4-Point	0.1264	8.2518	0.6482	0.4850	0.0441	0.5291
L/8-Point	0.2550	6.5166	0.2653	0.9939	0.0874	1.0812

Auto-transfer functions for sea state 1

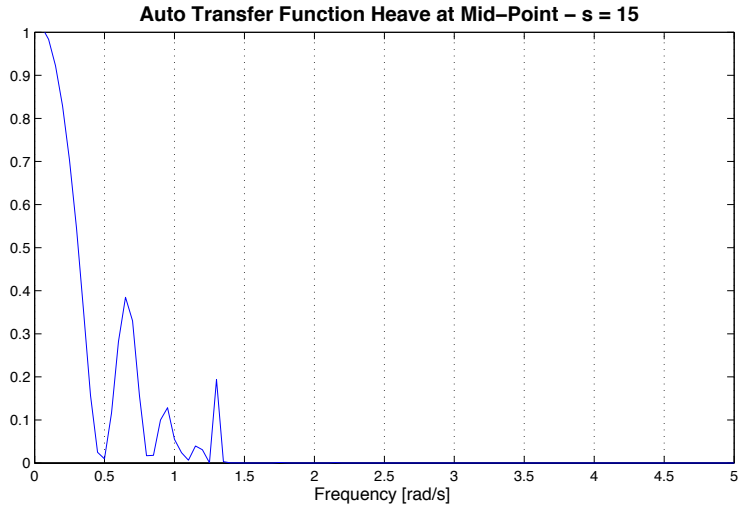

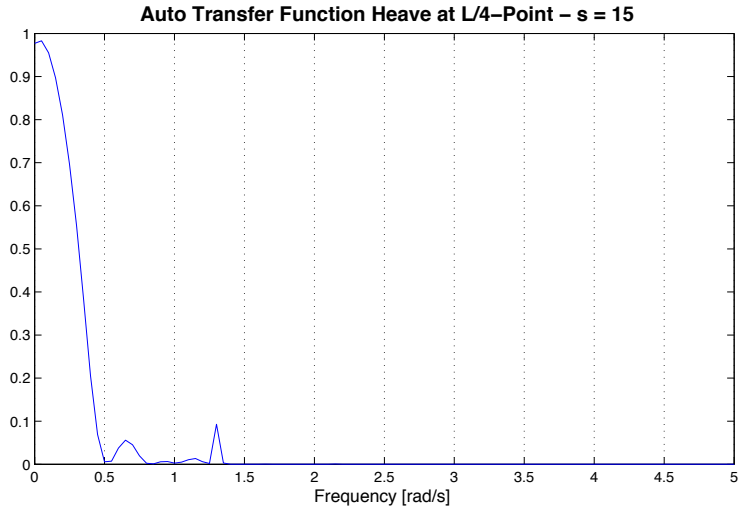

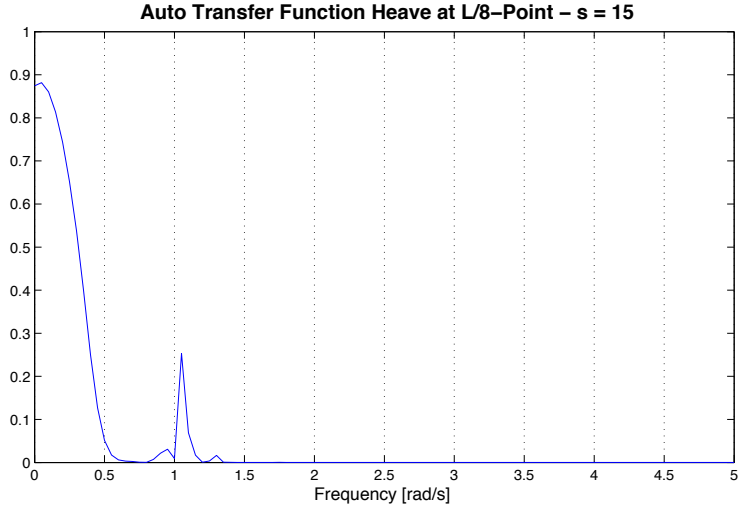

Auto-transfer functions for sea state 2

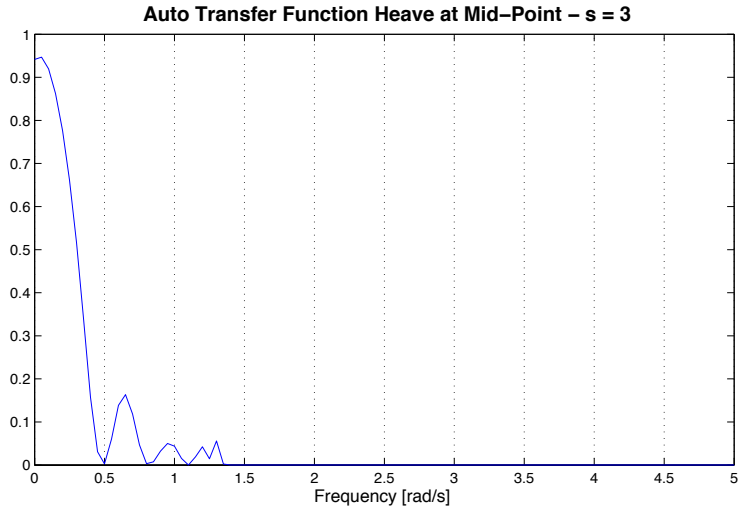

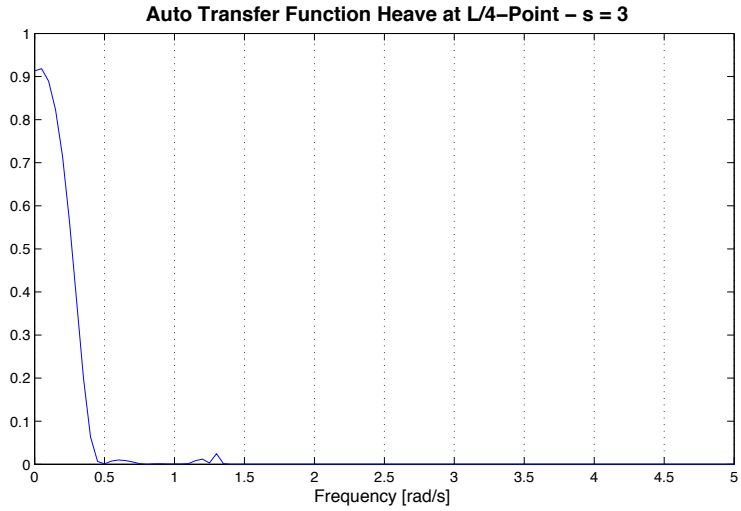

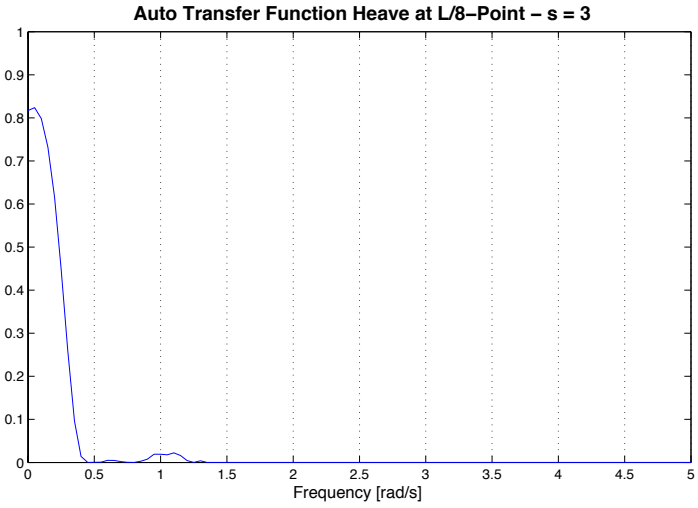

Auto spectral density of the heave response for sea state 1 for $\overline{\theta}_1 = 0$

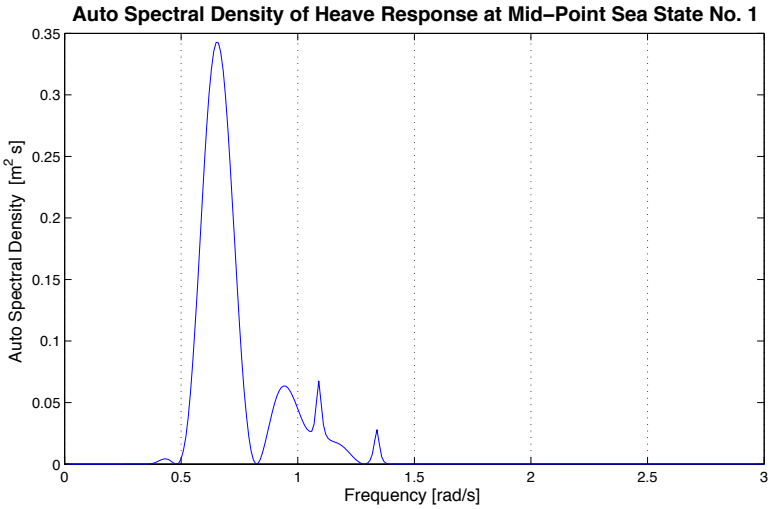

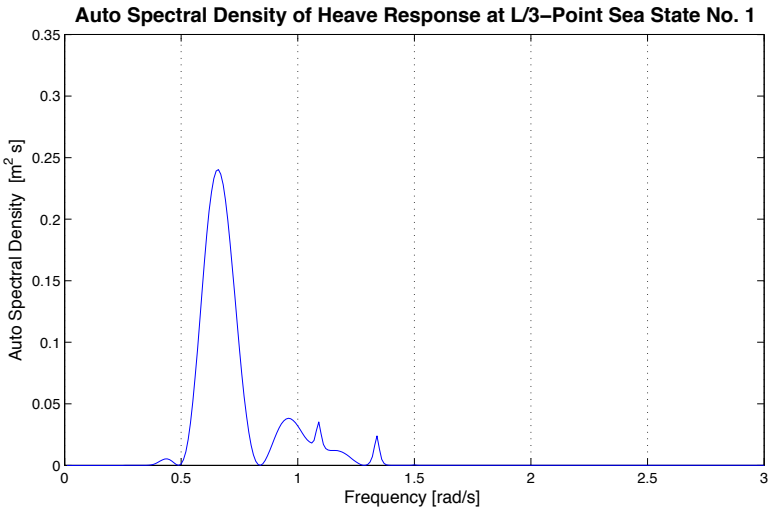

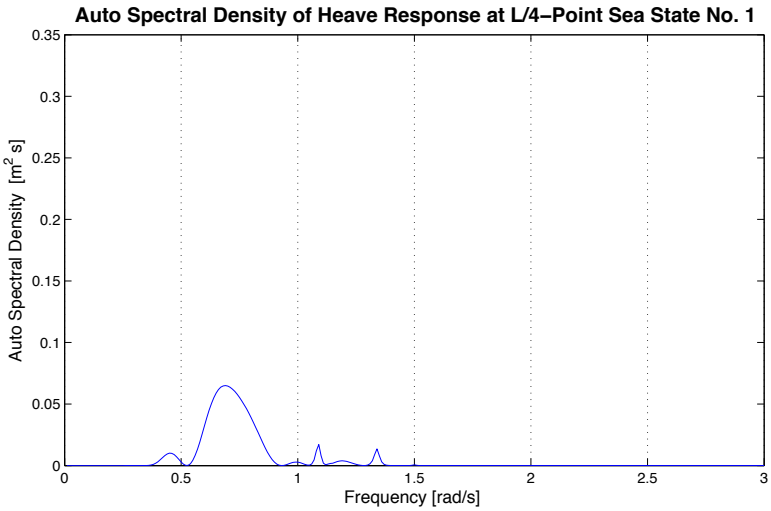

Auto spectral density of the heave response for sea state 2 for $\overline{\theta}_2 = 0$

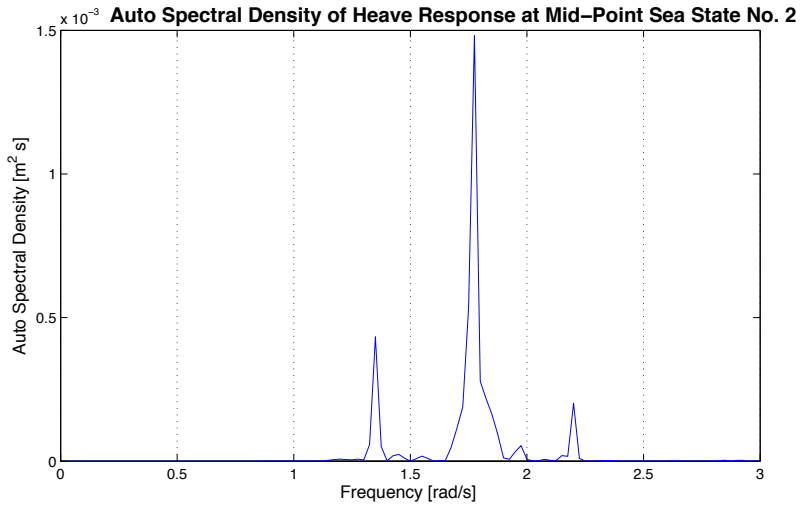

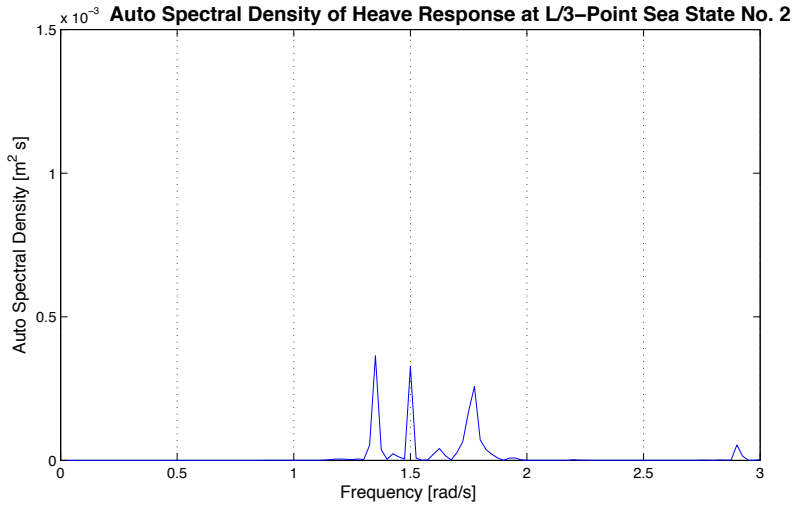

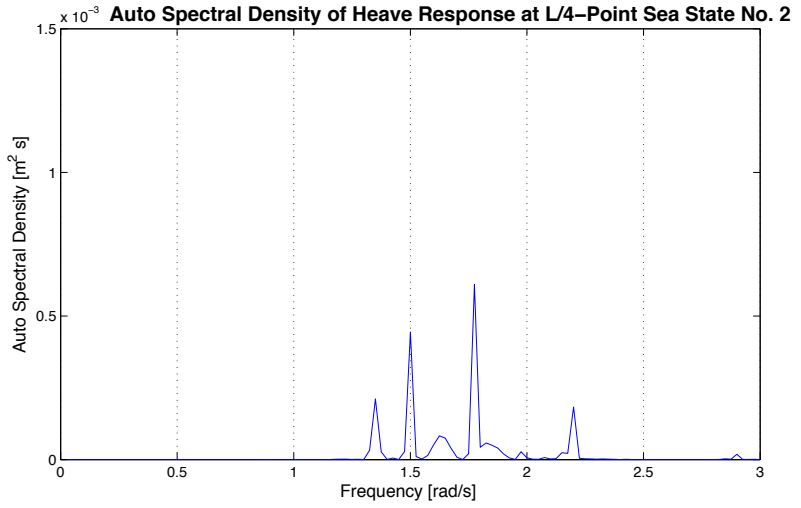

Auto spectral density of the heave response for sea state 2 for $\overline{\theta}_2 = \pi/4$

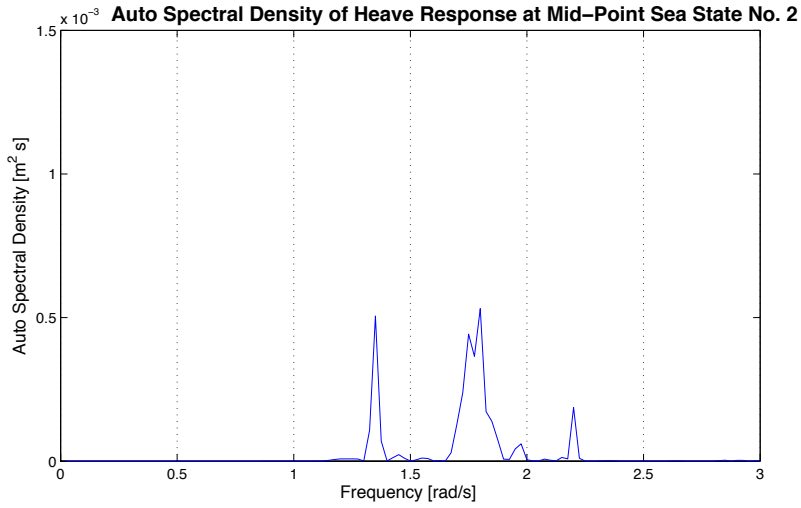

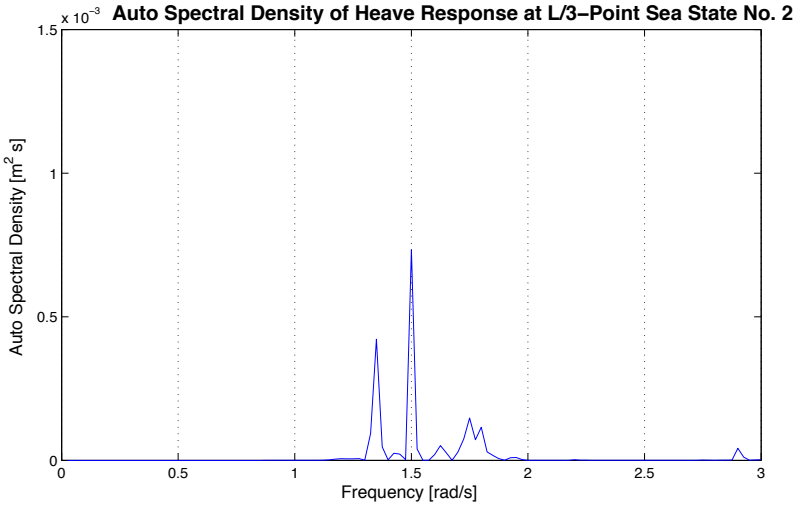

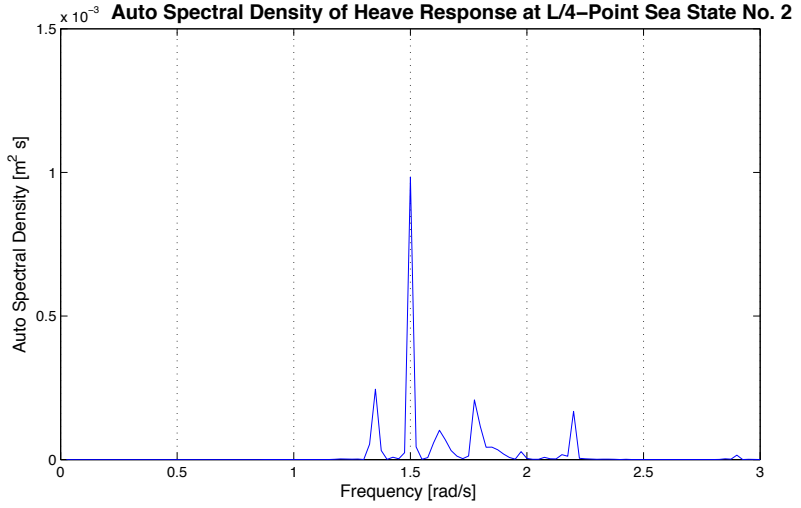

EVALUATION OF DIFFERENT SEA STATES

The first sea state is seen to complete dictate the response of the floating bridge when evaluating the combined sea states. Thus, a new set of sea states is introduced to evaluate the effect of combining more similar wave fields. Sea state number 3 is regarded as modelling close to unidirectional swell waves, whereas sea state number 4 is a short-crested, multi-directional sea state with a small increase in the wave period from sea state 2. The sea state parameters are tabulated below, and the results of the analysis follow tabulated. Plots of the auto-density of the response are presented on the following pages.

Sea State Parameters						
Sea State No.	s	$T_p\ [sec]$	$H_s\ [m]$	$T\ [sec]$	$E\lvert H_{max}\rvert\ [m]$	$T_{m0}\ [sec]$
3	12	8	1	7200	1.9610	5.9279
4	5	4	1	7200	2.0333	3.3254

Probabilistic Heave Response from Sea State No. 3 $\{\bar{\theta}_3 = 0\}$						
	$\sigma_r\ [m]$	$T_z\ [sec]$	ε	$E\lvert r_{max}\rvert\ [m]$	$\sigma\lvert r_{max}\rvert\ [m]$	$r_{max}\ [m]$
Mid-Point	0.2187	7.1338	0.4735	0.8475	0.0754	0.9229
L/3-Point	0.1777	7.1389	0.4747	0.6883	0.0613	0.7496
L/4-Point	0.1050	7.1401	0.4750	0.4069	0.0362	0.4431
L/8-Point	0.3015	6.1719	0.1908	1.1793	0.1029	1.2821

Probabilistic Heave Response from Sea State No. 4 $\{\bar{\theta}_4 = \pi/4\}$						
	$\sigma_r\ [m]$	$T_z\ [sec]$	ε	$E\lvert r_{max}\rvert\ [m]$	$\sigma\lvert r_{max}\rvert\ [m]$	$r_{max}\ [m]$
Mid-Point	0.0594	4.9267	0.7915	0.2359	0.0200	0.2559
L/3-Point	0.0522	4.8997	0.8028	0.2071	0.0175	0.2246
L/4-Point	0.0363	4.6689	0.9006	0.1444	0.0121	0.1565
L/8-Point	0.0678	5.6042	0.5070	0.2670	0.0230	0.2900

Probabilistic Heave Response from Combined Sea States $\{\bar{\theta}_3 = 0, \bar{\theta}_4 = \pi/4\}$						
	$\sigma_r\ [m]$	$T_z\ [sec]$	ε	$E\lvert r_{max}\rvert\ [m]$	$\sigma\lvert r_{max}\rvert\ [m]$	$r_{max}\ [m]$
Mid-Point	0.2267	6.8790	0.4071	0.8803	0.0780	0.9583
L/3-Point	0.1852	6.8406	0.3954	0.7194	0.0637	0.7831
L/4-Point	0.1111	6.6799	0.3395	0.4324	0.0381	0.4705
L/8-Point	0.3090	6.1404	0.2169	1.2091	0.1054	1.3145

Auto spectral density of the heave response for sea state 3 for $\overline{\theta}_3 = 0$

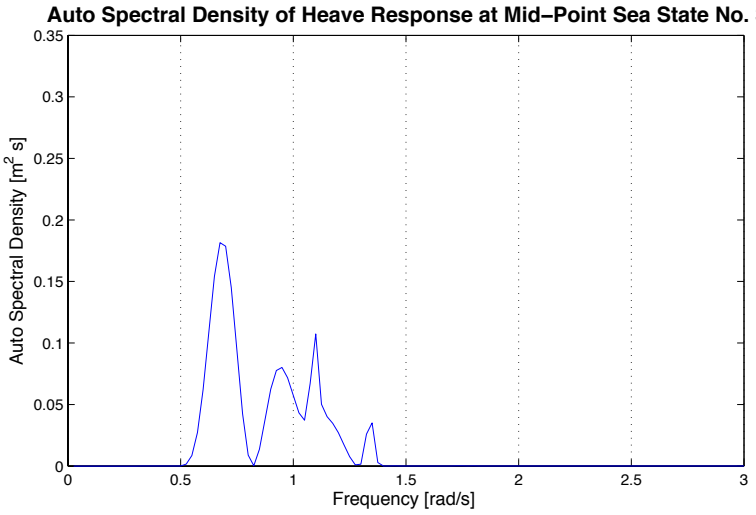

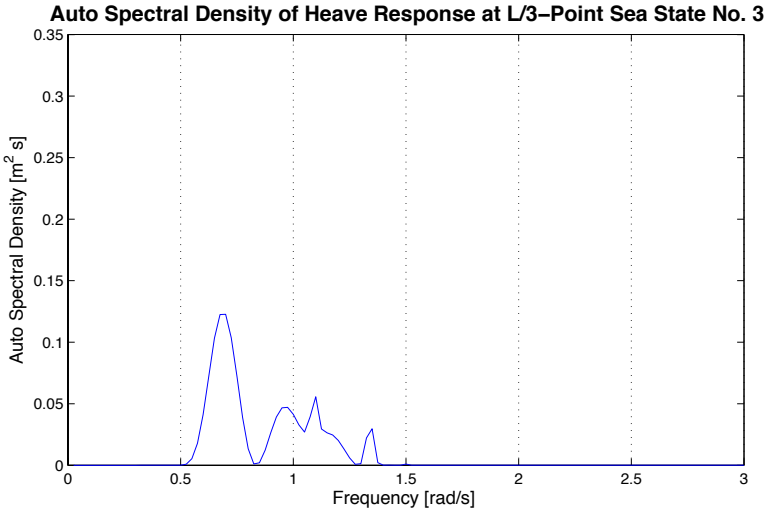

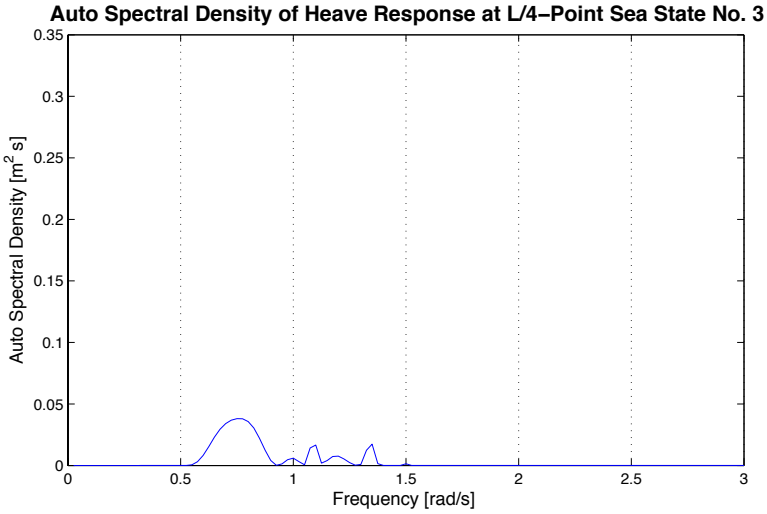

Auto spectral density of the heave response for sea state 4 for $\overline{\theta}_4 = \pi/4$

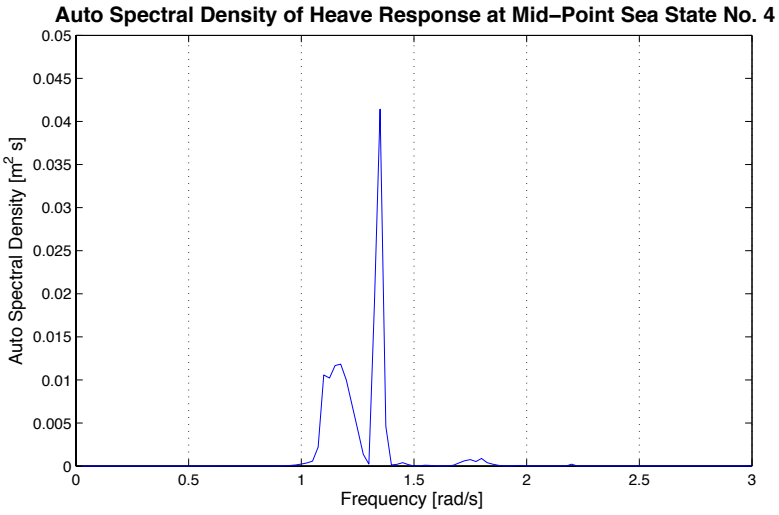

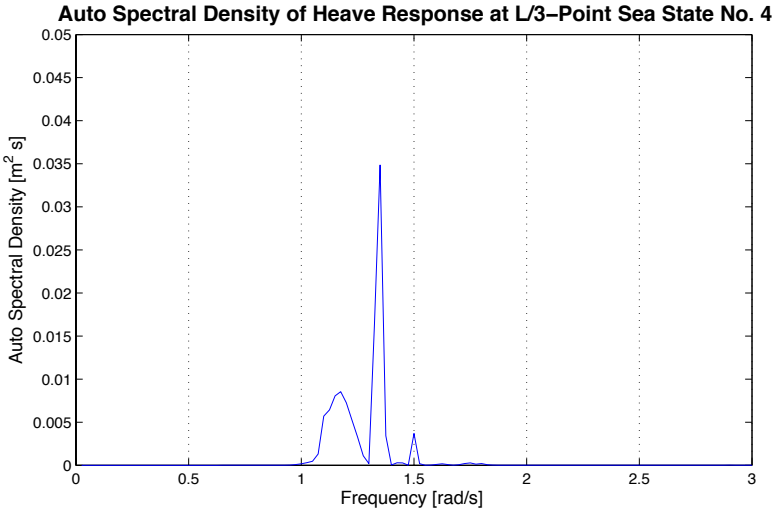

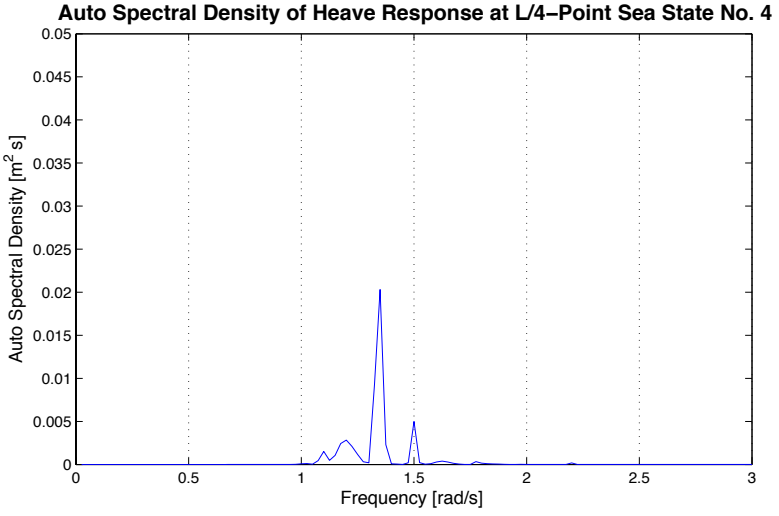

Auto spectral density of the heave response for combined sea states 3 & 4